UNIVERSITY OF OKLAHOMA

GRADUATE COLLEGE

TESTING, CHARACTERIZATION, AND ANALYSIS OF CLASS F FLY ASH GEOPOLYMERS UNDER OILFIELD TESTING CONDITIONS

A DISSERTATION

SUBMITTED TO THE GRADUATE FACULTY

in partial fulfillment of the requirements for the

Degree of

DOCTOR OF PHILOSOPHY

By

CAMERON DEVERS

Norman, Oklahoma

2024

TESTING, CHARACTERIZATION, AND ANALYSIS OF CLASS F FLY ASH GEOPOLYMERS UNDER OILFIELD TESTING CONDITIONS

A DISSERTATION APPROVED FOR THE

MEWBOURNE SCHOOL OF PETROLEUM AND GEOLOGICAL ENGINEERING

BY THE COMMITTEE CONSISTING OF

Dr. Catalin Teodoriu (Chair)

Dr. Ramadan M. Ahmed

Dr. Deepak Devegowda

Dr. Mahmood Amani

Dr. Brian P Grady

To my parents, my wife, and my future children

Acknowledgements

I would like to start by thanking Dr. Catalin Teodoriu. I have often been referred to as someone who rarely struggles to find words, but I am not sure the words exist to describe the quality of genuine care he has given not just myself, but to his entire research group. I have had the genuine pleasure of getting to work with some of the brightest people as a result of the students he has cultivated.

I would also like to sincerely thank each member of my committee. Each of you has either directly impacted my education or respect for academics in a way not many other faculty have, and for that I am forever grateful.

It would be difficult to name every positive impact among friends and colleagues who have helped along this journey, but a special thanks goes to Ian Grady for convincing me school was important and to Alex Schmidt to keeping my sanity in check after the veil of Covid began to lift.

Of course, any of what I have achieved or aim to achieve has not, would not, and will continue to not be possible without the seemingly endless support of my family. My mother, who has always been supportive; and who I am sure thought I would not have been in school so long. My father, who has been supportive in both my academic and professional pursuits. Without him I am sure this document would not exist. My sister, who has an uncanny knack for timely advice. My now wife, who has supported me since my sophomore year at the University of Oklahoma, and now continues to build a life with me. I would also like to thank my godmother, who has been a friend among family since I was very young, and has been a supporter of both myself and the life I am hopeful to build for as long as I can remember.

I would also like to thank those who have more literally made this project possible.

This work was made possible by a National Priorities Research Program grant (NPRP 11S-1126-170029) from the Qatar National Research Fund (a member of The Qatar Foundation). The statements made herein are solely the responsibility of the authors.

We also would like to thank the University of Oklahoma and Well Integrity Center for allowing access to the Cement Repository.

We also thank the Salt River Materials Group for providing materials for this work.

Abstract

The oil and gas industry relies heavily on Ordinary Portland Cement (OPC) for wellbore integrity, but the limitations of OPC in extreme environments such as high temperatures and pressures have necessitated the exploration of alternative materials. This dissertation investigates the potential of fly ash-based geopolymers as a sustainable alternative to OPC, focusing on their unconfined compressive strength (UCS) and compatibility with American Petroleum Institute (API) cement testing standards. Geopolymers are an inorganic polymer resulting from the reaction of aluminosilicate material and an alkali solution, typically comprised of potassium or sodium and hydroxides The research begins with an overview of the environmental impact of traditional cement production and the necessity for robust wellbore materials. It details the standard testing methods for OPC, including preparation, curing, and mechanical testing procedures, and extends these methods to geopolymers. The effects of various curing conditions and chemical compositions on the UCS of geopolymers are evaluated through a series of experiments. Results demonstrate significant variability in geopolymer performance, which is attributed to the inherent differences in fly ash composition and the lack of standardized testing protocols. Enhanced investigation techniques, such as Nuclear Magnetic Resonance (NMR) and Scanning Electron Microscopy (SEM), provide deeper insights into the microstructural properties of geopolymers and their correlation with mechanical performance. A comparative analysis of geopolymers and traditional API cements under similar conditions reveals that while geopolymers offer potential benefits, their inconsistent performance poses challenges for widespread adoption. The dissertation advocates for the development of standardized testing procedures specific to geopolymers to ensure reliable performance metrics. It explores the implications of using geopolymers in geothermal well completions, suggesting that with further research and standardization, geopolymers could become

a viable alternative in high-temperature applications. The study concludes with a summary of vii findings and recommendations for future research, emphasizing the need for a comprehensive understanding of geopolymer chemistry and the establishment of industry-wide standards to facilitate their adoption in oil and gas operations.

Table of Contents

List of Figures

List of Tables

List of Equations

List of Acronyms

AADE	American Association of Drilling Engineers
AASHTO	American Association of State Highways and Transportation
API	American Petroleum Institute
ASTM	American Society of Testing Materials
BTU	British Thermal Unit
CLAHE	Contrast Limited Adaptive Histogram Equalization
CNN	Convolutional Neural Network
°C	degrees Celsius
°F	degrees Fahrenheit
EJ	Exajoule (1×10^{18} Joules)
FTIR	Fourier Transform Infrared Spectroscopy
GMM	Gaussian Mixture Model
IEA	International Energy Agency
kg/m^3	kilograms per cubic meter
kN	kilonewtons
lbm/gal	pound-mass per gallon
LM	Light Microscope
mm	Millimeter
MPa	MegaPascal

NMR	Nuclear Magnetic Response
OPC	Ordinary Portland Cement
pH	potential of Hydrogen
rpm	Revolutions per Minute
SEM	Scanning Electron Microscopy
SEM-EDS	Scanning Electron Microscopy-Energy Dispersive Spectroscopy
TEM	Transmission Electron Microscopy
UCS	Unconfined Compressive Strength, also known as Uniaxial Compressive Strength
UPV	Ultrasonic Pulse Velocity
XRD	X-Ray Diffraction
XRF	X-Ray Fluorescence

Chapter 1 Introduction

The oil and gas industry is responsible for the delivery of over 250 EJ of hydrocarbon based energy across the entire globe (International Energy Agency, 2021), which **Figure 1** shows as over half of all energy delivered.

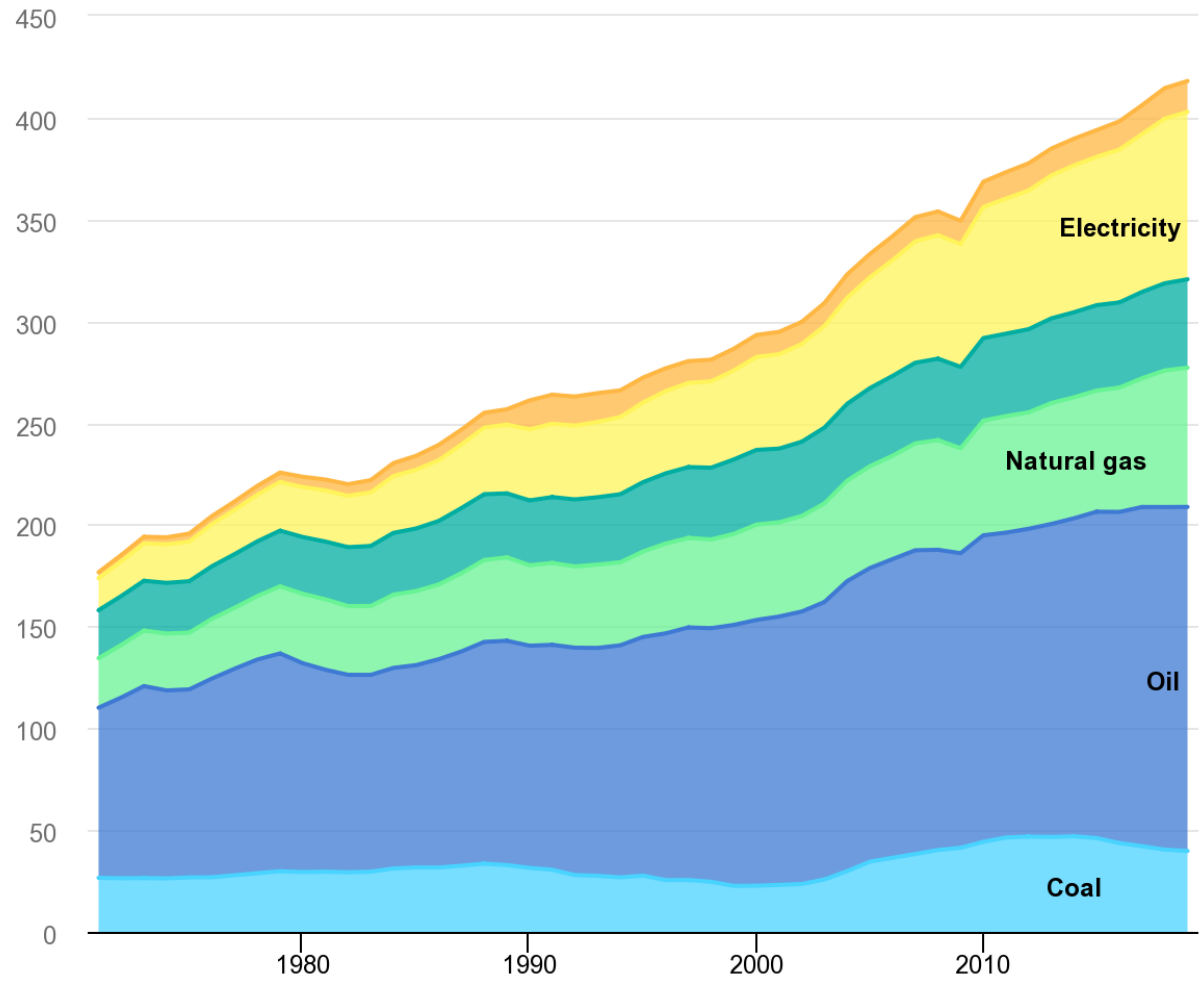

Figure 1 – Breakdown of global energy consumption by energy type, dominated by oil consumption (I.E.A. 2021)

To produce these hydrocarbons, they must first be accessed by drilling a wellbore into the subterranean environment, installing tubulars to maintain the integrity of the wellbore, and then, through varying methods of production, extracting the once trapped hydrocarbon to surface. The

process of adhering tubulars to drilled annular space is part of the wellbore completions process and secures the tubulars to provide the production environment, eliminates crossflow between the production space and the surrounding environment, and provides critical confining pressure around the wellbore (Bellabarba et al., 2008). A material called cement is used to perform this process. A cement slurry is pumped down the tubulars, past the bottom of the tubulars and back up the wellbore between the tubulars and the wellbore walls, similar to the depiction in **Figure 2** (Nelson, 2012).

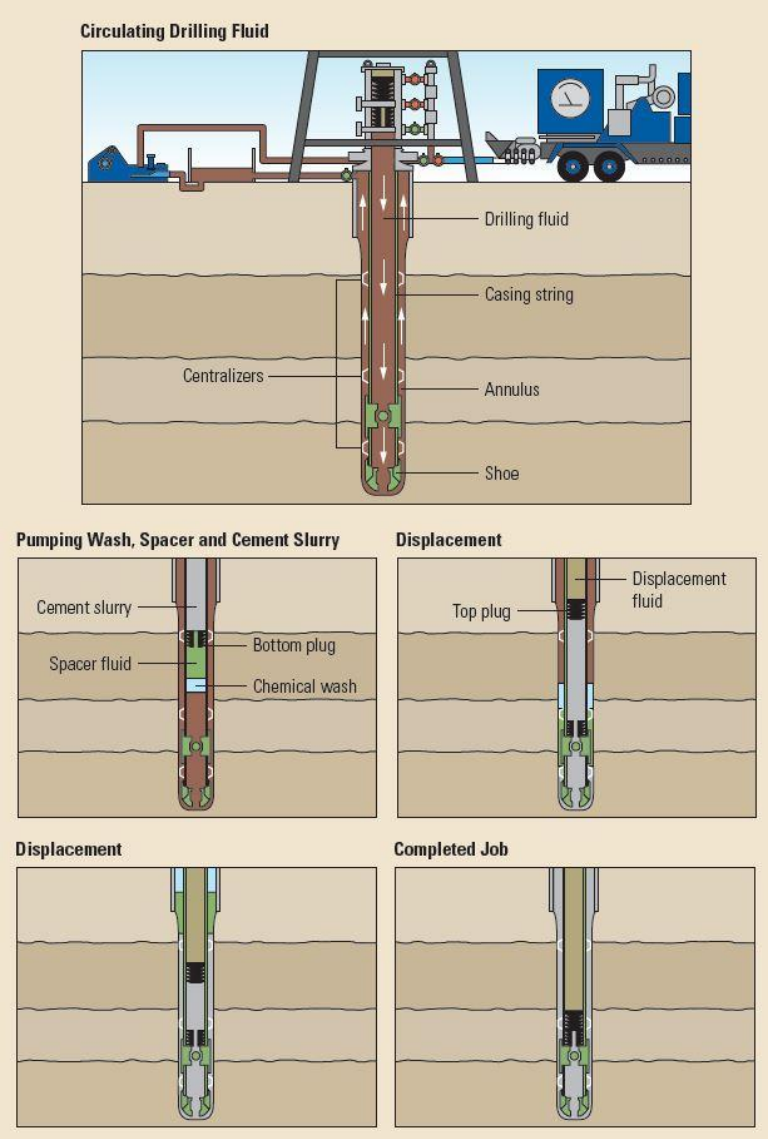

Figure 2 – Depiction of the stages of a cementing operation, from cement truck to finished operation (Nelson 2012)

As the cement cures and 'sets', reaching the designed strength and hardness, the tubulars affix to the wellbore and further operations can safely begin. While there are many stages and considerations within this process, they are all possible because of the properties cement offers.

1.1 Cement Overview

Cement is used by a multitude of industries, ranging from energy development to residential and industrial construction. Cement typically used in the oil and gas industry is a cement derivative

referred to as Portland Cement. Portland Cement is a fine, powdery substance that, when mixed with water, hardens and gains strength over time through a process called hydration. The production of Portland Cement involves five key steps: raw materials extraction, raw materials preparation, clinker production, clinker cooling, and clinker grinding.

1.1.1 Cement Manufacturing

The major raw materials needed to manufacture Portland Cement are limestone (calcium carbonate), clay, and shale. These materials are rich in compounds needed for the formation of calcium silicates and aluminates needed for the hydration process. Limestone provides calcium, while clay and shale contain aluminum, silicon, and iron oxides. Once these materials are extracted from a quarry (step 1), they are typically crushed and ground into a powder to a specified fineness (step 2). This process is critical for controlling the chemical composition of the material.

The material is then heated to 1450°C in a rotary kiln to produce a material called clinker (step 3). This heating process results in the formation of the critical materials tricalcium silicate, dicalcium silicate, tricalcium aluminate, and tetracalcium aluminoferrite. Additional insight into clinker production, captured by MacLaren and White (2003) can be seen in **Table 1**, although this is not a comprehensive listing.

Table 1 – Production of Clinker relative to C3S (MacLaren and White, 2003)

Components	Temperature of Liquid Formation /°C
$CaO–SiO_2$	2065
$CaO–SiO_2–Al_2O_3$	1455
$CaO–SiO_2–Al_2O_3–Na_2O$	1430
$CaO–SiO_2–Al_2O_3–MgO$	1375
$CaO–SiO_2–Al_2O_3–Fe_2O_3$	1340
$CaO–SiO_2–Al_2O_3–Na_2O–MgO$	1365
$CaO–SiO_2–Al_2O_3–Na_2O–Fe_2O_3$	1315
$CaO–SiO_2–Al_2O_3–MgO–Fe_2O_3$	1300
$CaO–SiO_2–Al_2O_3–Na_2O–MgO–Fe_2O_3$	1280

After the desired materials are generated, the clinker is subjected to rapid cooling to retain reactive properties, by either air or water, in a process called quenching (step 4). Once the clinker has been cooled, a small amount of gypsum is introduced to slow the setting of the material. The material is then ground into a fine powder using tools such as ball mills, vertical roller mills, or roller presses (step 5). The resultant fine powder is referred to as Portland Cement.

1.1.2 Cement Slurry Deployment

Dry cement, normally packaged in paper sacks, and any desired additives are delivered to the well site. Among other drilling equipment, wellsite equipment includes cement mixing and pumping equipment. The cement mixing equipment must be capable of completely wetting the dry cement with water, and along with any additives, mixing the components into a homogeneous mixture, or slurry, according to the slurry design. Preparation of the slurry according to the slurry design should result in a pumpable mixture, and the pumping equipment must be capable of pumping the slurry to the designed placement downhole and in a timely manner before the slurry begins to set.

Other important aspects of slurry design and testing, such as strength, cure time, and density, are further discussed later in this report.

1.1.3 Cement Hydration

Cement hydration is the chemical reaction between water and the many components which comprise cement; the result of which is the hardening and setting of the cement. Setting is defined by American Society of Testing Materials (ASTM) C125 as "the process, due to chemical reactions, occurring after the addition of mixing water, that results in a gradual development of rigidity of a cementitious mixture." This process involves the dissolution, reaction, and precipitation of various minerals and compounds. In cement chemistry, shorthand is often used to describe critical components of the hydration reaction. Cement chemistry notation represents CaO, SiO_2, Al_2O_3, and Fe_2O_3 as C, S, A, and F, respectively. Additionally, the clinker material also has a unique shorthand; tricalcium silicate, dicalcium silicate, tricalcium aluminate, and tetracalcium aluminoferrite are represented by C_3S, C_2S, C_3A, and C_4AF. **Table 2** presents this nomenclature combined with the function of each clinker material.

Table 2 – Main constitutes of Portland Cement and their function (Adams N & Charrier T, 1985)

Compound	Cement chemist notation	Purpose
Tricalcium silicate $(CaO)_3.SiO_2$	C_3S	Enhances the strength and develops early strength
Dicalcium silicate $(CaO)_2.SiO_2$	C_2S	Hydrates slowly, Strength generated over extended period of time
Tricalcium aluminate $(CaO)_3.Al_2O_3$	C_3A	Promotes rapid hydration, affects thickening time and initial setting of the cement, makes the cement susceptible to sulphate attack
Tetracalcium aluminoferrite $(CaO)_4.Al_2O_3.Fe_2O_3$	C_3AF	Responsible for slow hydration

Cement hydration can be influenced by a variety of factors, such as the clinker composition or foreign particles in the composition. Generally, the hydration reaction is given in the following equations (C. MacLaren & Anne White, 2003).

Equation 1 – Primary Hydration (1)

$$2Ca_3SiO_5 + 6H_2O \rightarrow Ca_3Si_2O_7 \cdot 3H_2O + 3Ca(OH)_2$$

Equation 2 – Primary Hydration (2)

$$2Ca_2SiO_4 + 4H_2O \rightarrow Ca_3Si_2O_7 \cdot 3H_2O + 3Ca(OH)_2$$

Equation 3 – Formation of Ettringite

$$Ca_3Al_2O_6 + 3CaSO_4 \cdot 2H_2O + 26H_2O \rightarrow Ca_6Al_2O_6(SO_4)_3 + 32H_2O$$

Equation 4 – Secondary Hydration

$$Ca(OH)_2 + SiO_2(Al_2O_3) \rightarrow C - S - H \text{ (C-A-S-H) phases}$$

Equation 1 details the hydration of tricalcium silicate to form calcium silicate hydrate (C-S-H) and calcium hydroxide (CH). The latter component is a byproduct and yields no meaningful impact to the overall cement hydration. The generation of C-S-H, however, is critical in the formation of the final cementing product as this gel-like substance contributes to both the strength and overall stiffness of the cement slurry. **Equation 2** details the hydration of dicalcium silicate, a reaction which also forms both C-S-H and CH, but the reaction is slower than the first reaction. This reaction is the reaction responsible for the continued improvement in mechanical properties of cement over longer periods of time, while the first reaction is critical in the initial setting of the cement. **Equation 3** highlights the importance of gypsum. Tricalcium aluminate typically reacts rapidly with water to generate calcium aluminate hydrates. When this material is hydrated along with gypsum, the reaction instead forms ettringite (Aft phase), which is a calcium sulfoaluminate hydrate (Brandl et al., 2011). The ettringite prevents the slurry from hardening in a way referred to as ‘flash set’, a setting method that yields near-zero workability due to how fast the slurry hardens. **Equation 4** details the hydration of tetracalcium aluminoferrite (C4AF). C4AF reacts

with water and gypsum to form hydrated calcium aluminoferrite-sulfate compounds, much like the hydration of C3A. The hydration products of C4AF contribute less to the strength development of the cement paste compared to C3S and C2S (Abid et al., 2018).

1.1.4 Cement Wellbore Application and Limits

As a critical phase in the completion of an oil and gas well is the cement stage, many considerations are made in the generation of the cement slurry (Gu & Chen, 2009). These considerations come from variations in oil and gas operations, and even oil and gas analogous operations such as geothermal drilling or storage wells. Different subterranean drilling operations will warrant distinctive characteristics from the cement, such as improved acid resistance, improved thermal resistance, or simply superior mechanical strength. Since there are multitude of methods to influence the characteristics of the cement, ranging from the initial cement selected, to the additives introduced in the slurry to alter any number of characteristics, there are multiple applications cement slurries can be designed to meet. As drilling operations continue to develop in complexity, reaching new total depths, total length, and operating in more thermally active environments, the abilities of traditional OPC based cement are pushed to the limit.

The mechanical properties of cement are thoroughly field tested for traditional, typical production land-based drilling. However, evidence has begun to accumulate that in high temperature systems such as geothermal drilling or ultradeep drilling, OPC based cement may not be sufficient. While sufficient inclusion of additives may prevent or offset many of these issues, onset of thermal microcracking and thermal degradation in high temperature environments could result in the failure of the cement sheath. Cement sheath failure, such as debonding or structural failure, can create zones of unconfined microannular space (Fu et al., 2004). This pocket of unconfined space

is subject to failures and risks the cement was intended to prevent, such as collapse failure and environmental fluid interactions. As these failures are most likely to occur in the hottest zones, they are likely to occur in the deepest parts of the well and therefore very difficult to intervene, remediate and manage. Traditional interventions to repair incomplete or damaged cement sheath bonding zones may not be adequate to engage in the extreme environments drilling operations can now reach. As a result, it has become increasingly more important to get the initial slurry and overall cementing operation correct and optimal from the beginning. Although additives can potentially improve the performance of cement in these high-risk applications, the investigation of entirely alternative bonding materials is warranted.

1.1.5 Environmental Costs

Insufficiencies in extreme conditions are not the only reason to investigate alternative solutions to OPC technology. Producing clinker, according to recent studies, costs its own weight in CO_2 emissions to generate; for every one ton of clinker produced, one ton of carbon dioxide is emitted. The poor carbon efficiency of cement generation is the primary reason the International Energy Agency (IEA) tracks the carbon cost of cement in its 'carbon net-zero by 2050' trackers. Opposed to some independent studies, the IEA reports in 2021 only a 0.59-ton CO_2 emission per ton of cement produced, but fossil fuels contributed 3.26 GJ per ton of clinker produced in a year in which 4,270 megatons of cement was produced. This resulted in 13.9 billion gigajoules, or 13.9 EJ of energy spent to produce cement. In the same year, the United States consumed just under 77.1 quadrillion BTU of energy, or approximately 81.3 EJ. Therefore, energy spent per year to produce cement is equivalent to approximately 17% of all energy consumed by the United States in a year, and more than is consumed in the United States for residential or industrial energy (International Energy Agency, 2021). Clearly, the energy demand required for cement generation

is colossal. While the oil and gas industry is not the only industry contributing to this consumption, it could suffer greatly from regulatory interference, global supply chain shift, or other unforeseen interventions making cement either unfavorable to use in the public eye or simply unavailable to get in the quantity needed.

1.1.6 Alternatives to Cement in Oil & Gas Operations

Cement application limits and cement environmental costs culminates in the conclusion that niche use cases or environmental extremes are areas where cement alternatives are of interest, and that a universal replacement material for cement in oil and gas downhole operations may be needed.

1.2 Geopolymer Overview

Conceived in the late 20th century and first brought into the academic sphere by French scientist Davidovits (2008), geopolymers are best described as a class of inorganic, amorphous, three-dimensional aluminosilicate materials. OPC could be described similarly, however, the calcium content is the defining element of the reaction. Due to the likeness these materials share with modern construction cement combined with high resistance to thermal degradation, the material has undergone expansive study in the fields of civil engineering and chemistry. As the subsets of slag and fly ash-based geopolymer tend to be the most discussed, they are often discussed as both a cement replacement and a waste product utilizer. The latter is due to the amount of fly ash which has historically been sent to landfills; some studies indicate over 70% of fly ash generated globally is sent to landfills (Ahmaruzzaman, 2010).

Geopolymers are an inorganic polymer resulting from the reaction of aluminosilicate material and an alkali solution, typically comprised of potassium or sodium and hydroxides. These are different

from a generic class of material referred to as pozzolans as they do not react with calcium hydroxide in the presence of water to generate their cementitious properties. The geopolymerization reaction instead forms a three-dimensional network of aluminate and silicate structures that result in the hardened binder that behaves similarly to OPC (Davidovits, 2008). This technology was initially conceived as a replacement in residential construction brought on due to fires decimating residential buildings in France in the 1970's (Davidovits, 2008.). The combination of geopolymerization not requiring direct consumption of energy to produce and perceived thermal resistance make the material a promising candidate as an OPC replacement.

To best formulate an approach to expanding the understanding of the potential of geopolymer material in the oil and gas industry, more about geopolymer structure and the geopolymerization reaction must be understood. A discussion of the fundamental properties known about geopolymer materials follows.

1.2.1 Geopolymer Chemistry

Geopolymers are generally composed of aluminosilicate units connected by oxygen atoms. More generally, they are 'ceramic-like inorganic polymers produced at low temperature' and 'consist of chains or networks of mineral molecules linked with covalent bonds'. As a result, the reaction results in a polymer and not a traditional ceramic material like OPC. The consequence is nomenclature is different. The clearest and most contextual example refers to the material kaolinite. Kaolinite is a clay mineral that can be used in both traditional cement applications and alkali-activated materials. In ceramics, the material is written $Al_2O_3 \cdot 2SiO_2 \cdot 2H_2O$ while in chemistry it is written as $Si_2O_5Al_2(OH)_4$. While the scope of this work is less so to break down the chemical reaction of geopolymer and more so to study the practical testing and application of the

material, it is important to maintain nomenclature clarity. According to Davidovits (2008), geopolymers are generally comprised of the following molecular units:

– Si-O-Si-O- siloxo, poly(siloxo),

– Si-O-Al-O- sialate, poly(sialate),

– Si-O-Al-O-Si-O- sialate-siloxo, poly(sialate-siloxo),

– Si-O-Al-O-Si-O-Si-O- sialate-disiloxo, poly(sialate-disiloxo),

– (R)-Si-O-Si-O-(R) organo-siloxo, poly-silicone,

– Al-O-P-O- alumino-phospho, poly(alumino-phospho),

– Fe-O-Si-O-Al-O-Si-O- ferro-sialate, poly(ferro-sialate)

While these are the general components which make up geopolymers, the exact characteristics of the geopolymer solid material are influenced by the type of geopolymer base material, reaction material, additives, and reaction environment.

1.2.2 The Geopolymerization Process

The primary building blocks of geopolymers are the $[SiO_4]_4$- and $[AlO_4]_5$- tetrahedral units, connected to form an aluminosilicate framework. The charge imbalance created by the incorporation of aluminum atoms into the structure is compensated by the presence of alkali or alkaline earth metal cations such as sodium (Na+), potassium (K+), or calcium (Ca2+). The geopolymerization process involves the dissolution of aluminosilicate source materials in a highly alkaline solution, typically composed of alkali metal hydroxides and/or silicates. This leads to the release of silicate and aluminate species, and then undergoes condensation reactions to form a three-dimensional aluminosilicate network. The geopolymerization process can be represented by three main stages: dissolution, gelation, and hardening. An example of this process is depicted in

a comparative work by Davidovits (2008) shown in **Figure 3** contrasting the process to traditional OPC hardening.

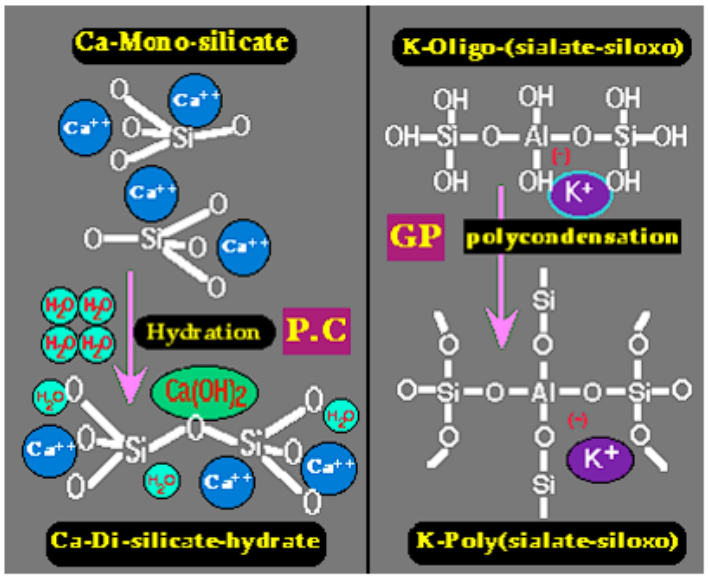

Figure 3 – Comparison between hydration and polycondensation reactions in the formation of binding material (Davidovits, 2008)

Chapter 2 Testing of Cementitious Materials

Unconfined Compressive Strength (UCS), also known as Uniaxial Compressive Strength, is closely tied to and related empirically to many other characteristics of cement. While there is room for debating if UCS is the most important property, UCS is certainly the most tested property.

Wellbore cement UCS testing, the process of uniaxially failing a material in the prescribed API method, is linked to the intended function of the cement, and not the chemistry or nature of the cement itself. The test exists to determine the strength of the cement so proper wellbore considerations can be made, particularly with regards to safety. In modern oilfield operations, the cement sheath is subject to much more than just environmental pressure. When completing wells, operations, such as hydraulic fracturing, pose serious risk to the integrity of the cement sheath. Some consider the risk to be so prevalent that the generation of microannular zones due to cement failure is unavoidable, only containable. Additionally, the risk of cement sheath failure due to cement integrity failure is of higher likelihood over time than debonding Consequently, knowledge about the strength of the deployed material is paramount in securing a controlled and safe production environment.

2.1 Cement Testing Standards

Standards for cement testing are set by the American Society of Testing Materials (ASTM) and the American Petroleum Institute (API).

ASTM standard C150-07 details the general scope of cement testing, including the eight types of ASTM specified cement, additional standard documentation, and information relating to the

composition and verification of composition of the specific Ordinary Portland Cement (OPC) types. The breakdown in composition allotments can be seen in **Table 3** below.

Table 3 – ASTM Cement Types and Compositions (ASTM)

Cement Type[A]	Applicable Test Method	I and IA	II and IIA	III and IIIA	IV	V
Aluminum oxide (Al_2O_3), max, %	C 114	...	6.0	...	...	...
Ferric oxide (Fe_2O_3), max, %	C 114	...	6.0[B,C]	...	6.5	...
Magnesium oxide (MgO), max, %	C 114	6.0	6.0	6.0	6.0	6.0
Sulfur trioxide (SO_3),[D] max, %	C 114					
When $(C_3A)^E$ is 8 % or less		3.0	3.0	3.5	2.3	2.3
When $(C_3A)^E$ is more than 8 %		3.5	[F]	4.5	[F]	[F]
Loss on ignition, max, %	C 114	3.0	3.0	3.0	2.5	3.0
Insoluble residue, max, %	C 114	0.75	0.75	0.75	0.75	0.75
Tricalcium silicate $(C_3S)^E$, max, %	See Annex A1	...	...	...	35[B]	...
Dicalcium silicate $(C_2S)^E$, min, %	See Annex A1	...	...	...	40[B]	...
Tricalcium aluminate $(C_3A)^E$, max, %	See Annex A1	...	8	15	7[B]	5[C]
Sum of $C_3S + 4.75C_3A^G$, max, %	See Annex A1	...	100[H]	...	...	...
Tetracalcium aluminoferrite plus twice the tricalcium aluminate ($C_4AF + 2(C_3A)$), or solid solution ($C_4AF + C_2F$), as applicable, max, %	See Annex A1	...	...	...	...	25[C]

While ASTM, comprised of hundreds of documents discussing testing for abrasion to sulfate resistance, dwarves API in terms of testing scope and number of standards, no ASTM tests specifically target subterranean condition testing. API standards for testing cement do not include testing cement under subterranean conditions but provide a set of standards and characteristic criteria to verify a cement mixture is viable for subterranean conditions and oilfield applications.

API 10A is the standard which "specifies requirements and gives recommendations for eight classes of well cements, including their chemical and physical requirements and procedures for physical testing" (API 10A, 2019). API 10A also establishes cement classifications and a generalized description of how each is made. API 10A includes two critical summary tables; the first, **Table 4**, establishes the chemical requirements of the cement classes in a manner similar to the ASTM table (**Table 3**). The second, **Table 5**, describes their physical and performance requirements.

Table 4 – API Cement Classes and Compositions

	Cement Class					
	A	B	C	D, E, F	G	H
ORDINARY GRADE (O)						
Magnesium oxide (MgO), maximum, %	6,0	NA	6,0	NA	NA	NA
Sulfur trioxide (SO_3), maximum, %	3,5 [a]	NA	4,5	NA	NA	NA
Loss on ignition, maximum, %	3,0	NA	3,0	NA	NA	NA
Insoluble residue, maximum, %	0,75	NA	0,75	NA	NA	NA
Tricalcium aluminate (C_3A), maximum, %	NR	NA	15	NA	NA	NA
MODERATE SULFATE-RESISTANT GRADE (MSR)						
Magnesium oxide (MgO), maximum, %	NA	6,0	6,0	6,0	6,0	6,0
Sulfur trioxide (SO_3), maximum, %	NA	3,0	3,5	3,0	3,0	3,0
Loss on ignition, maximum, %	NA	3,0	3,0	3,0	3,0	3,0
Insoluble residue, maximum, %	NA	0,75	0,75	0,75	0,75	0,75
Tricalcium silicate (C_3S) maximum, %	NA	NR	NR	NR	58 [b]	58 [b]
minimum, %	NA	NR	NR	NR	48 [b]	48 [b]
Tricalcium aluminate (C_3A), maximum % [(3)]	NA	8	8	8	8	8
Total alkali content, expressed as sodium oxide (Na_2O) equivalent, maximum, %	NA	NR	NR	NR	0,75 [c]	0,75 [c]
HIGH SULFATE-RESISTANT GRADE (HSR)						
Magnesium oxide (MgO), maximum, %	NA	6,0	6,0	6,0	6,0	6,0
Sulfur trioxide (SO_3), maximum, %	NA	3,0	3,5	3,0	3,0	3,0
Loss on ignition, maximum, %	NA	3,0	3,0	3,0	3,0	3,0
Insoluble residue, maximum, %	NA	0,75	0,75	0,75	0,75	0,75
Tricalcium silicate (C_3S) maximum, %	NA	NR	NR	NR	65 [b]	65 [b]
minimum, %	NA	NR	NR	NR	48 [b]	48 [b]
Tricalcium aluminate (C_3A), maximum, %	NA	3 [b]	3 [b]	3 [b]	3 [b]	3 [b]
Tetracalcium aluminoferrite (C_4AF) plus twice the tricalcium aluminate (C_3A), maximum, %	NA	24 [b]	24 [b]	24 [b]	24 [b]	24 [b]
Total alkali content expressed as sodium oxide (Na_2O) equivalent, maximum, %	NA	NR	NR	NR	0,75 [c]	0,75 [c]

NR = No Requirement; NA = Not Applicable

[a] When the tricalcium aluminate content (expressed as C_3A) of the cement is 8 % or less, the maximum SO_3 content shall be 3 %.

[b] The expressing of chemical limitations by means of calculated assumed compounds does not necessarily mean that the oxides are actually or entirely present as such compounds. When the ratio of the percentages of Al_2O_3 to Fe_2O_3 is 0,64 or less, the C_3A content is zero. When the Al_2O_3 to Fe_2O_3 ratio is greater than 0,64, the compounds shall be calculated as follows:

$C_3A = (2,65 \times \% Al_2O_3) - (1,69 \times \% Fe_2O_3)$

$C_4AF = 3,04 \times \% Fe_2O_3$

$C_3S = (4,07 \times \% CaO) - (7,60 \times \% SiO_2) - (6,72 \times \% Al_2O_3) - (1,43 \times \% Fe_2O_3) - (2,85 \times \% SO_3)$

When the ratio of Al_2O_3 to Fe_2O_3 is less than 0,64, the C_3S shall be calculated as follows:

$C_3S = (4,07 \times \% CaO) - (7,60 \times \% SiO_2) - (4,48 \times \% Al_2O_3) - (2,86 \times \% Fe_2O_3) - (2,85 \times \% SO_3)$

[c] The sodium oxide equivalent (expressed as Na_2O equivalent) shall be calculated by the formula:

Na_2O equivalent = $(0,658 \times \% K_2O) + (\% Na_2O)$

Table 5 – API Minimum Requirements Table

Well cement Class				**A**	**B**	**C**	**D**	**E**	**F**	**G**	**H**
Mix water, % mass fraction of cement (Table 5)				46	46	56	38	38	38	44	38
Fineness tests (alternative methods) (clause 6)											
Turbidimeter (specified surface, minimum m^2/kg)				150	160	220	NR	NR	NR	NR	NR
Air permeability (specified surface, minimum m^2/kg)				280	280	400	NR	NR	NR	NR	NR
Free fluid content, maximum % (clause 8)				NR	NR	NR	NR	NR	NR	5,9	5,9
Compressive strength test (8-h curing time) (clause 9)	**Schedule number, Table 6**	**Final curing temp.** °C (°F)	**Final curing pressure** MPa (psi)	**Minimum compressive strength** MPa (psi)							
	NA	38 (100)	atm.	1,7 (250)	1,4 (200)	2,1 (300)	NR	NR	NR	2,1 (300)	2,1 (300)
	NA	60 (140)	atm.	NR	NR	NR	NR	NR	NR	10,3 (1 500)	10,3 (1 500)
	6S	110 (230)	20,7 (3 000)	NR	NR	NR	3,4 (500)	NR	NR	NR	NR
	8S	143 (290)	20,7 (3 000)	NR	NR	NR	NR	3,4 (500)	NR	NR	NR
	9S	160 (320)	20,7 (3 000)	NR	NR	NR	NR	NR	3,4 (500)	NR	NR
Compressive strength test (24-h curing time) (clause 9)	**Schedule number, Table 6**	**Final curing temp.** °C (°F)	**Final curing pressure** MPa (psi)	**Minimum compressive strength** MPa (psi)							
	NA	38 (100)	Atm.	12,4 (1 800)	10,3 (1 500)	13,8 (2 000)	NR	NR	NR	NR	NR
	4S	77 (170)	20,7 (3 000)	NR	NR	NR	6,9 (1 000)	6,9 (1 000)	NR	NR	NR
	6S	110 (230)	20,7 (3 000)	NR	NR	NR	13,8 (2 000)	NR	6,9 (1 000)	NR	NR
	8S	143 (290)	20,7 (3 000)	NR	NR	NR	NR	13,8 (2 000)	NR	NR	NR
	9S	160 (320)	20,7 (3 000)	NR	NR	NR	NR	NR	6,9 (1 000)	NR	NR

While there are a total of seven tests (sampling, fineness, slurry preparation, free fluid, atmospheric pressure compressive strength, pressured cured compressive strength, and thickening time) not every cement class is subjected to every test. The only three ubiquitous tests are sampling, slurry preparation, and thickening time. Additionally, all eight classes of cement are subject to either the atmospheric pressure compression test or the pressured cured compressive test. Sampling and fineness refer to the source material of the cement and are not properties of either the cement slurry

or final product of the hydration reaction. These tests are by no means a comprehensive set of tests and serve primarily to establish a minimum criterion for field-bound products to ensure some level of control for safety and general regulation. More specifically, these set of tests focus on the neat product, or cement with no additives.

API 10B includes an additional set of specifications aimed to cover a more comprehensive testing than included in API 10A, primarily for testing cement and cement slurries with additives (API 10B, 2013). API 10B covers nine different tests or standard practices for the reviewing and validation of what is referred to as 'wellbore cement.' The nine sections are sampling, preparation of slurry, determination of slurry density, well-simulation compressive strength (UCS) tests, non-destructive sonic determination of compressive strength of cement, well-simulation thickening time tests, static fluid-loss tests, determination of rheological properties and gel strength using a rotational viscometer, well-simulation slurry stability tests, and compatibility of wellbore fluids.

The following discusses several of the API 10B tests.

2.2 Preparation of Slurry for Testing

The preparation of a cement slurry for oilfield testing has been refined to such a degree that API certified mixers have default settings to blend a cement slurry in accordance with the API standards. Along with this, API sets a standard for the size of the blender cup, the mixing speeds, and the mixing times. The API mixing speeds are set to 4000 revolutions per minute rpm ± 250 rpm for the first 15 seconds followed by an automatic elevation of rotary speeds to 12,000 rpm ± 250 rpm for the next 35 seconds. The blender cup itself is a 1-liter blender, but it is recommended to generate 600ml slurries as that provides sufficient volume to execute all requisite tests without overloading the blender.

Additionally, as the density of the slurry is a critical component of the cement within the oil and gas industry, API provides all the equations necessary to calculate the density of a slurry at 600ml. Determination of the relative densities of the dry components can be determined with either a gas pycnometer or a Le Chatelier flask outlined in ASTM C188-95. The relative densities of the liquid components can be determined with a hydrometer outlined in API RP 13J or the pycnometer. The determination of the relative densities of all components is critical as allotted variances in materials can result in slurry density variations up to 34kg/m^3 (.28 lbm/gal).

API stipulates all material should be mixed at field conditions, which if unknown or generalized defaults to 23°C ± 1°C (73°F ± 2°F). All liquid components are transferred to the blender cup and the solids placed in separate vessels. The blender is set to low rotary speed and the dry components are introduced into the opening on the top of the blender cup. All solids must be uniformly introduced to the blender cup, seen in **Figure 4**, and close the blender completely, all within a 15 second window, as the blender will automatically engage to high-speed mixing thereafter. At the conclusion the 35-second high shear rate mixing window, the blender stops and the preparation of the slurry is complete and is ready for transfer to curing molds.

Figure 4 – API certified mixer and blender cup

The slurry preparation for API cement introduces two different chemical process concerns. The first is API selected the rotary speeds based on OPC and field research. As cement is a hydration reaction, it is unlikely the same mixing conditions are optimal for the geopolymerization reaction. Investigations into the effects of mixing, both length of mixing time and mixing speeds, have indicated the traditional API conditions are suboptimal for geopolymer reactions.

The second concern is density. Calculating density of the resultant slurry based on desired output is not the issue, but achieving the target density might be. Using fly ash geopolymers as a reference point, there are literature debates about two key factors of the alkali-activator. The first factor, or consideration, is whether to distribute the sodium or potassium hydroxide into the solid, dry components or to preemptively prepare an aqueous sodium hydroxide solution. The second consideration is what molarity of alkali activator to use. Regardless of whether the hydroxide component is dry or aqueous or the molarity, the mass quantity is determinable, so in both cases

the provided approach to density calculations is compatible. The API equations, however, cannot be used as they reference industry specific measurements for quantities and weights of cement. As the industry has no ‘standard packaging’ for geopolymers in the same way a sack of cement is 94 pounds. Because of this, auxiliary information for the calculation of slurry density will need to be conceived, likely using a generic weight total such as 100 pounds.

Mohd Ali et al., (2020) indicates preparing an aqueous solution yields a higher slurry performance and helps to mitigate the heat produced by the reaction. Both the preparation of aqueous sodium hydroxide and geopolymerization reaction generate heat, which could be a concern for certain applications. The downside is Kabir et al., (2015) also suggests a high molarity of hydroxide solution must be utilized. Therefore, it may be a deterrent in the adoption of the material at the field level. While the handling of high-molar sodium hydroxide or potassium hydroxide will need to be considered for the adoption of geopolymer in the field, that discussion falls well outside the scope of cement testing.

The final portion of the sample preparation includes test fluid condition, which is a process by which the slurry is subjected to wellbore conditions. By use of a consistometer, the slurry can be subjected to testing at either atmospheric or downhole pressures. While the general viability of this test is already debated for additive-rich cement, the test is not incompatible with the geopolymer slurry. As the consistometer is utilized in other tests, the exact details regarding the differences between the slurries are discussed in the relevant tests. For the scope of slurry preparation, the intent of this portion of the testing is to verify ‘pumpability’ to ensure the fluid can be moved downhole and back up the annular space.

2.3 Slurry Sampling

Sampling, as a test, is the most straightforward in both approach and intent. As oilfield cement slurries are comprised of dry ingredients, wet ingredients, and mixing water; there are a multitude of acceptable ways to harvest a representative portion of those ingredients for validation. The extraction of these materials can happen anywhere along the traveling path of the ingredients, from the manufacture all the way to the field location. This level of testing is important as API classified OPC has rigid chemical requirements, and this rigidity garners confidence in the use of testing standards. The intent of testing additives serves much of the same purpose. As additives begin to establish purpose and practical functionality, they achieve a wider range of adoption. Once this happens, to mitigate operational complacency, monitoring the additives for the slurry helps to ensure the intended slurry is generated without contamination. Contamination is a real risk at the field level, not just of additives or cement, but the water for mixing the cement as well. Dirty water containing contaminants, like salt, could greatly impact the set time of the cement during the cementing operation. Specific tools, such as those depicted in **Figure 5**, are used to acquire material for testing.

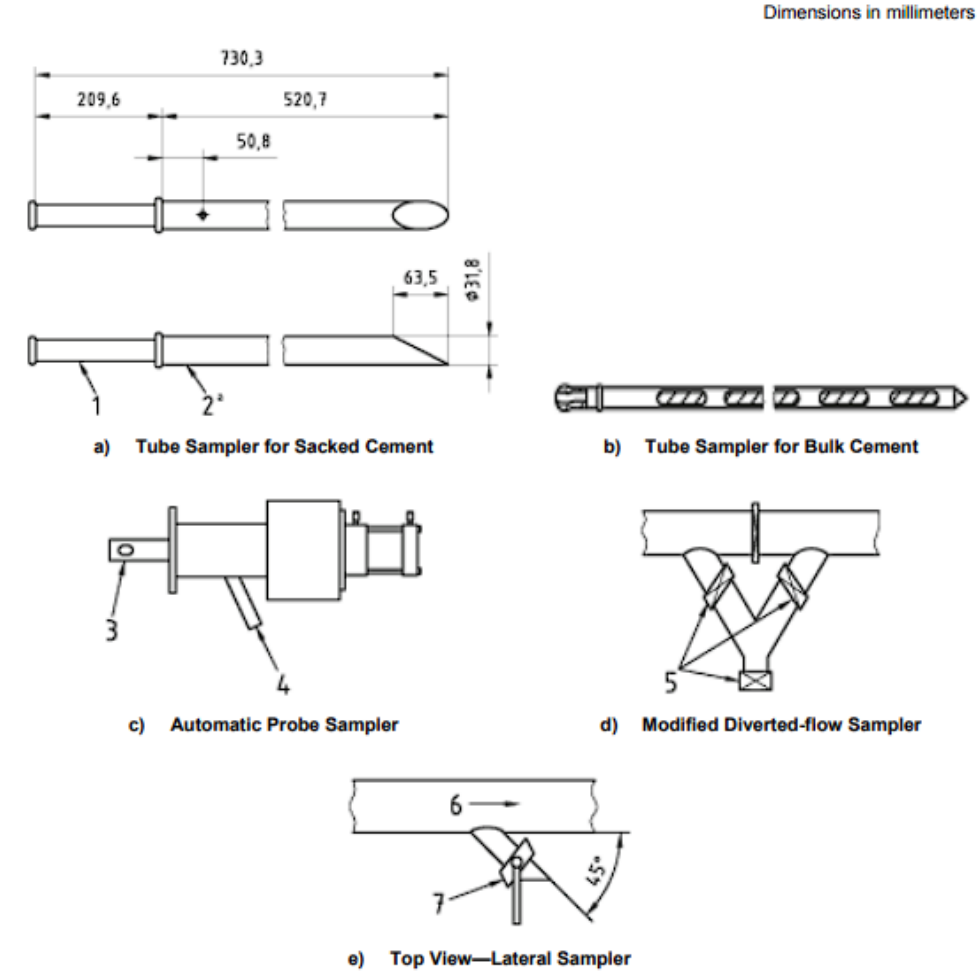

Key

1 handle
2 dragg tubing
3 sample tube, extended
4 product discharge
5 valve
6 flow direction
7 valve

[a] Approximate volume = 320 ml.

Figure 5 – Examples of traditional sampling equipment (API 10B, 2013)

Acquiring the sample is only the first step, however. The resultant material must be tested for composition; the most common method for determining the cement composition is X-Ray Fluorescence (Suchorski, n.d.). Most commonly, results are reported in the form of metal oxides, such as those in **Table 6**.

Table 6 – Metal Oxides potentially present in ASTM tested OPC (Suchorski, n.d.)

Constituent	Comments
SiO_2	No specified limit
Al_2O_3	Specified maximum 6% for Type II cements for sulfate resistance
Fe_2O_3	Specified limit may apply for sulfate resistance
CaO	No specified limit
MgO	Specified maximum of 6% for portland cements. Excessive amounts of free MgO can cause expansion in concrete
SO_3	Specified limit depends on cement type. SO_3 (typically in the form of gypsum) is used to control the C_3A reactions and is optimized for setting time and strength
Loss on ignition (LOI)	Specified limit depends on cement type. A high LOI can indicate partial prehydration of the cement
Na_2O	Optional maximum limit of 0.60% on equivalent Na_2O for low-alkali cements. Alkalis accelerate the hydration of the cement and any SCMs present
K_2O	
Insoluble residue	Specified limit depends on cement type. Insoluble residue is material that cannot be dissolved in a strong acid or alkali solution. Excessive amounts of insoluble residue may indicate contamination or high amounts of siliceous or argillaceous materials in the cement
CO_2	No specified limit
Limestone	Up to 5% limestone may be added to portland cement during finish grinding
$CaCO_3$ in limestone	Specified minimum of 70% for portland cements. This information is needed for calculation of the chemical compounds
Inorganic processing addition	In addition to limestone, up to 5% inorganic processing additions may be added to portland cement during finish grinding

The final mill test report may be slightly different than shown based on the provider of the material being used, but an excerpt of a report can be seen in **Figure 6**.

ASTM C595 and AASHTO M 240

CHEMICAL ANALYSIS

Item	Spec limit	Test Result
Rapid Method, X-Ray *(C114)*		
SiO_2 (%)	---	18.4
Al_2O_3 (%)	---	4.5
Fe_2O_3 (%)	---	3.2
CaO (%)	---	63.3
MgO (%)	---	1.1
SO_3 (%)	3.0 max *	2.5
Loss on ignition (%)	10.0 max	5.8
Insoluble residue (%)	---	
Na_2O_{Eq} (%)	---	0.36
CO_2 (%)	---	4.6
Limestone (%)	15.0 max	8.3
$CaCO_3$ in Limestone (%)	70 min	95
Inorganic Process Addition (Baghouse Dust)	---	3.0

PHYSICAL ANALYSIS

Item	Spec limit	Test Result
Air content of mortar (%) *(C185)*	12 max	7.3
Blaine Fineness (m^2/kg) *(C204)*	---	484
-325 (%) (C430)	---	98.9
Autoclave expansion (%) *(C151)*	0.80 max	0.01
Density of Cement (g/cm^3) (C188) **	---	3.1
Compressive strength (MPa, [PSI]) *(C109)*		
1 day	---	15.4 [2230]
3 days	13.0 [1890] min	27.2 [3940]
7 days	20.0 [2900] min	35.2 [5100]
28 days	25.0 [3620] min	45.4 [6580]
Time of setting (minutes)		
Vicat Initial (C191)	45 - 420	139
3 Days Heat of Hydration (KJ/Kg, [cal/g]) *(C1702)*		289 [69]
Mortar Bar Expansion (%) *(C1038)*	0.020 max	0.002

* May exceed 3.0% SO3 maximum based on our Test Method C1038 results of < 0.020 % expansion at 14 days.

** Average of 12 month data

We certify that the above described cement, at the time of shipment, meets the chemical and physical requirements of ASTM C595 and AASHTO M 240.

§ Please refer to ASTM C1778 for guidance on reducing the risk of alkali aggregate reaction in concrete

This product also meets the requirements of ASTM C1157 Type GU and Type MS

Figure 6 – Mill Run Report indicating requisite parameters falling within critical standardization criterion from Argos USA, Newberry Plant

This process, however, draws out one of the largest impedances to geopolymer adoption. The importance of sampling and subsequent chemical verification of cement is due to the specific chemical make-up of each class of cement set by the API. Each of the classes has a variance allotment and clear chemical breakdown, all provided by API. Each class of cement is designed to benchmark and perform in the field a particular way. Solid geopolymer material, by its nature, is not produced in the same controlled manor as is cement clinker. Fly ash, the most reviewed subclass of geopolymer for oilfield use, is a poorly classified material. Fly ash, classified into Class F and Class C, was divided only based on a specific reactivity based on the percentage of calcium oxide. Class F, the subtype most investigated for oilfield usage, is low in its calcium oxide content; less than 10% by mass. Class C Fly Ash, however, ranges in calcium oxide content from 10% to 30%. While this variance alone is considerably larger than any variance in an API OPC class, the

allotted variance of Class F Fly Ash silica dioxide ranges from 40% to 70%. This variance does not make the material unsamplable but defeats the point of sampling in the first place. Consider the work of Duxson where it is bluntly stated the natural chemical variation of fly ash is so extreme that to better understand the material one is better off artificially constructing the material (Duxson, Fernández-Jiménez, et al., 2007; Duxson, Mallicoat, et al., 2007).

Fly ash is the main sub-component of coal ash, the byproduct of the burning of coal. Coal composition, while primarily carbon and hydrogen, varies greatly by source location. This, combined with different combustion conditions coal is subjected to can result in significant variance in coal ash composition. A report of chemical analysis conducted on material sampled from a quantity of gathered fly ash is called a mill report. This report typically contains the composition of the primary components (silicon dioxide, aluminum oxide, iron oxide, calcium oxide) and information critical to control and for documentation regarding ASTM standard C618. While there is not an ASTM standard for the use of fly ash for the generation of geopolymer, ASTM C618 discusses the specifications for the use of fly ash in concrete. In conjunction with the American Association of State Highway and Transportation (AASHTO) standard AASHTO-M295 (2023) “Standard Specification for Coal Fly Ash and Raw or Calcined Natural Pozzolan for Use in Concrete”, these two documents are the documents utilized by United States federal and state industries to regulate fly ash concrete (Suraneni et al., 2021). These two standards have considerable overlap regarding much of the documents and are considered by many reviewers to be functionally the same. When compared to global considerations regarding fly ash usage, discussions about both the chemical composition variance allotments and concrete tests – both their validity and appropriateness – are debated. Even in the primary use industry the material usage is debated not for its benefit, but for its appropriate testing and regulation.

Fortunately for oilfield considerations, especially given the established precedent that API references ASTM for foundational considerations, the only reason to engage in this debate is if API will develop oilfield specific fly ash compositions. Currently, this seems unlikely and unreasonable due to how fly ash is sourced. Additionally, the refinement of fly ash classifications and their respective chemical compositions will only help to refine expectations of testing results, not the validity of the tests themselves.

As such, current API cement methods are in line with ASTM sampling methods for fly ash material. The major problem is with classification and chemical composition, not with the act of classification itself.

Problems with the standards aside, methods for generating a composition of the base material for a geopolymer material exist. The primary methods of determination outside a mill report are Fourier Transform Infrared Spectroscopy (FTIR), X-Ray Diffraction (XRD), X-ray Fluorescence (XRF), and even Scanning Electron Microscopy (Alterary & Marei, 2021). Fortunately, these are methods which have undergone some level of discussion by ASTM and even have some level of standards. XRF, for example is standardized by ASTM D4326 (ASTM, 2014). However, these reports appear far less standardized towards industry standards and rather, are presented in ways more attuned to research. Additionally, as the complexity of the geopolymer source material is larger, there is typically more analysis required to generate the report. A good example is exhibited in **Figure 7** and the subsequent results in **Table 7** (Mahima Kumar et al., 2020).

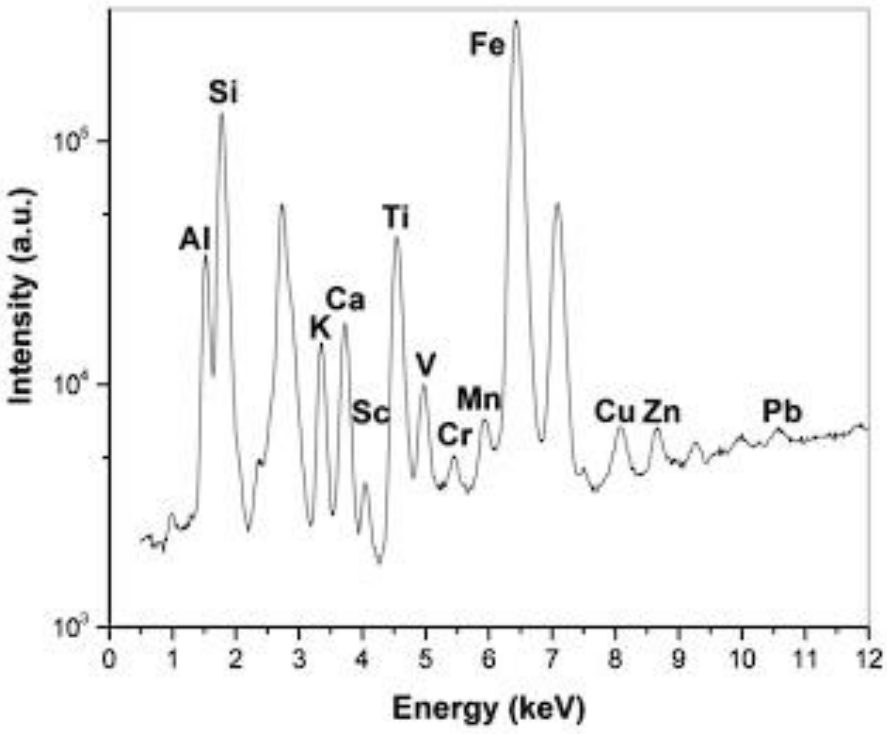

Figure 7 – EDS-XRF Graph of the source material from Mahima Kumar et al., (2020)

Table 7 – Resultant critical information from converting the information from Figure 7 (Mahima Kumar et al., 2020)

Element	ppm	wt%	Conversion factor	Oxide %
Al*	147,000 ± 2000	14.7	1.8895	27.77565
As	8.0 ± 0.4	$8*10^{-4}$	1.3203	0.00011
Ba	510 ± 50	0.051	1.1165	0.05694
Ca*	7200 ± 200	0.72	1.3992	1.00742
Ce	200 ± 10	0.02	1.2284	0.02568
Co	26.6 ± 0.6	0.0027	1.2715	0.00343
Cr	197 ± 9	0.0197	1.4615	0.02879
Cs	10.8 ± 0.6	0.0010	1.0602	0.00106
Eu	2.34 ± 0.14	0.0002	1.1579	0.00023
Fe	35,800 ± 900	3.5	1.4297	5.00395
Hf	9.0 ± 0.8	0.0009	1.1793	0.00161
K	11,950 ± 170	1.195	1.2046	1.43949
La	117 ± 2	0.0117	1.1728	0.01372
Lu	0.92 ± 0.11	0.00009	1.1371	0.00010
Mn	390 ± 40	$3.69*10^{-6}$	1.5825	0.000006
Na	790 ± 10	$7.9*10^{-6}$	1.3480	0.00001
Nd	95.7 ± 18.8	0.00957	1.1664	0.01116
Pb*	28.9 ± 1.9	0.00289	1.1544	0.00333
Rb	90.1 ± 19.6	0.00901	1.0936	0.00985
Sb	1.71 ± 0.35	0.00017	1.3284	0.00022
Sc	31.7 ± 0.2	0.0031	1.5338	0.00474
Si*	222,000 ± 1000	22.2	2.1393	47.4924
Sm	15.4 ± 0.2	0.00154	1.1596	0.00174
Ta	3.58 ± 1.0	0.00035	1.2211	0.00043
Tb	2.2 ± 0.4	0.00022	1.1510	0.00025
Th	39.8 ± 1.5	0.0039	1.1379	0.00443
U	8.3 ± 0.7	0.0008	1.1344(+4)	0.00094
W	8.4 ± 1.2	0.0008	1.2610	0.00105
Yb	6.6 ± 0.4	0.0006	1.1387	0.00068
Zn	162 ± 17	0.0167	1.2448	0.02078
LOI				1.2%

Unlike the cement mill report, the analysis for many geopolymer experiments report element, not compound. If this is due to the lack of knowledge about the material is typically dependent on the paper and additional investigative capabilities of the research laboratory.

2.4 Determination of Slurry Density

While density calculations in slurry preparation are designed to ensure a proper slurry is assembled, the experimental determination of the density serves to verify the real density. To do this, a tool called a pressurized fluid density balance is utilized. This tool works by pressuring the cup in which the slurry is transferred to, expelling the entrained air. The apparatus is comprised of two major pieces, the syringe like pump (**Figure 8**) that pressurizes the cup and the balance (**Figure 9**).

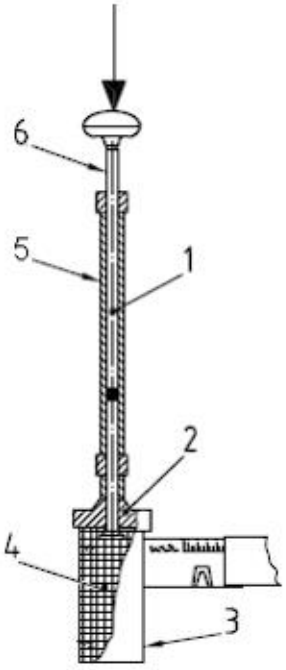

Key

1 pressurizing pump
2 pressurizing valve
3 sample cup
4 slurry sample with entrained air
5 cylinder housing
6 piston rod

Figure 8 – Pressuring pump for cement slurry density determination (API 10B, 2013)

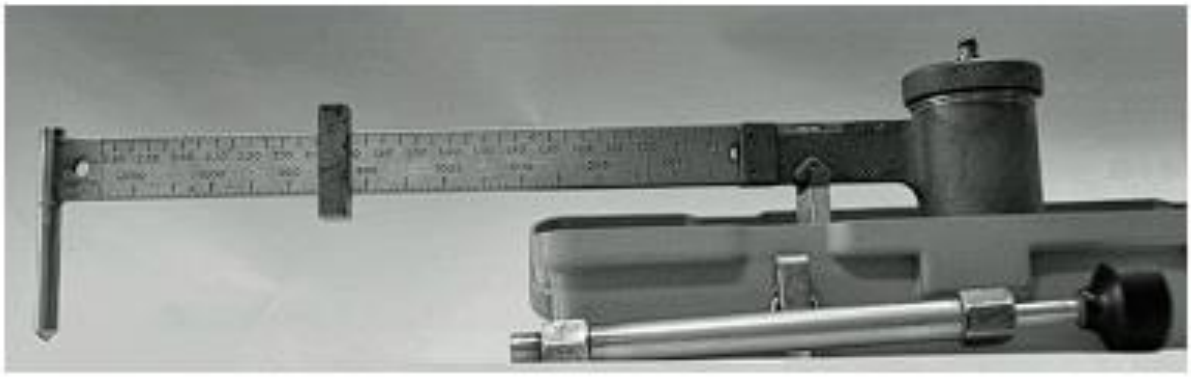

Figure 9 – Common pressurized fluid density balance (API 10B, 2013)

Once the slurry cup is filled, and the entrained air expunged, the counterbalance weight of the slide portion of the balance is used to level out the tool. Once the indicator bubble indicates the balance is level, the markings on the slide are recorded for balance. There are other ways to indicate the sample density; the balance is a suggested apparatus and not a requisite. Additionally, the sample cup on the balance is small, only using a small amount of the sample slurry to determine the density of the entire slurry. This process assumes the slurry is homogenous. For this assumption to be valid, the general slurry preparation process must be valid. Assuming this is true, this test is compatible with the geopolymer reaction, as neither minor pressurization fluctuations nor air removal have been shown to impact the characteristics of the slurry or the hardened sample.

2.5 Compressive-Strength (UCS) Tests

Compressive strength testing is the first of the tests that require the sample to undergo a meaningful amount of curing time to form a hardened sample. One of the most practiced tests for determining the compressive strength of a cement sample is by failing the sample mechanically under uniaxial pressure. To conduct this test under API regulations, not only does the method of testing need to follow standard practices, but so does the curing process of the slurry and the shape of the samples generated. Once again, API invokes an ASTM standard, ASTM C109/C109M-07, as the

foundation of the testing. The primary indicated differences between the tests are the bearing block surface dimension requirement, the bearing block Rockwell hardness requirement, and that the molds can be separated into more than two chambers. API also clarifies that the sample should be placed with surfaces parallel to the loading frame without any titling, and be cured in molds of corrosive resistant metals, although glass is also acceptable in certain applications.

The general process of curing cement samples once the slurry is generated is to transfer the sample into curing molds which generate 2 inch or 50mm sample cubes, such as in **Figure 10**. These molds are then placed into the curing environment. The standard for API cement is for samples to be cured in an aqueous environment, such as a water bath (**Figure 11**).

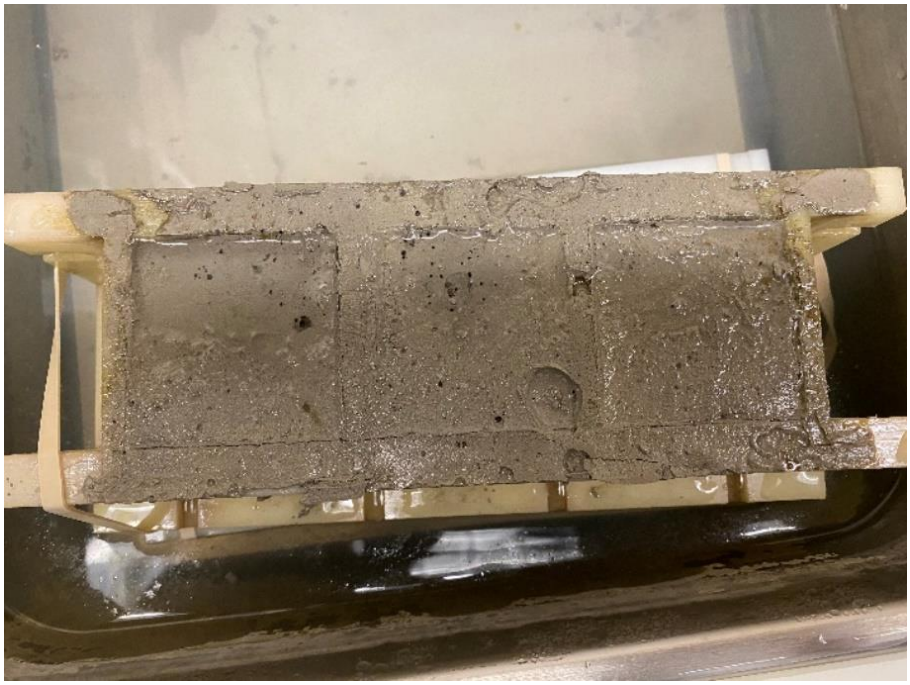

Figure 10 – Geopolymer slurry poured into API regulation sized molds

Figure 11 – Example of a thermally active aqueous curing environment

A water bath is a more representative of an environment than open air curing, as much of the surface area of the slurry will be in direct contact with either the material of the tubular, typically steel, or the subterranean wall. Subterranean earth is a permeable body, with water-enriched pores a reasonable possibility in any given drilling operations.

There are two main parts of the compressive testing section: the sample generation, and the sample testing. ASTM C109/C109M-07 is the primary reference document for these steps, which dictate samples should be cubes of two inches in length. The molds used for this process, in practice, are typically triplicate cubical molds. These molds are often coated in a non-reactive grease, per API recommendations, to ensure the molds are properly sealed and cement does not bond to the mold during the curing process. The molds are typically assembled from multiple parts that lock together in groves, and the grease aids in ensuring the grooves do not allow fluid exchange. The molds are typically assembled and prepared for sample transfer before the slurry is generated to ensure minimal resting time in the wrong environment. To transfer the slurry from the blender cup to the cubical molds, the compartments of the molds are first filled half-way with the slurry. Once half-

full, a spatula is used to gently stir the slurry to remove the trapped air. Once this is done, the remainder of the compartments are filled past the lip of the mold to overflow. Then, the residual slurry is scrapped off with the spatula. Finally, the cover is placed onto the top of the sample mold.

Once the molds are properly filled with the generated slurry, the molds are transferred to the proper curing environment. The curing enviorment will either be an atmospheric water bath or a pressurized water bath. For atmospheric water baths, if the curing temperature is considerably above room temperature, samples should be removed from the heated environment, the samples extracted from the molds, and transferred to a cooling bath approximately 45 minutes before desired cure time is reached to ensure the samples are engageable. For pressurized curing, the process of testing samples cured at elevated temperatures is the same, extracting and transferring the samples 45 minutes prior to the testing window. The major difference with the pressurized testing procedure is the adherence to the testing schedule. While API provides schedule recommendations, there are limits to the considered thermal gradients and depths. Consequently, API indicates user defined testing schedules are allowed if they are outlined. Regardless of the testing schedule, once the samples have reached target curing times under target conditions, the samples are extracted from their molds and curing environments and moved to sample testing.

Sample testing is straight forward. The sample should be loaded at a rate of 18 kN ± 2 kN for samples with an expected strength of 3.5 MPa, or at a rate of 72 kN ± 7 kN for samples with a strength expectation greater than 3.5 MPa, and this is typically done by a programmable device like the one in **Figure 12**. While these rates are only a recommendation and not a requirement, they should be heeded as the rapid overloading of the sample will result in inaccurate test results. The test is completed once the sample has been totally failed, and the strength is to be reported to the nearest .3 MPa along with all relevant testing conditions.

Figure 12 – Crush test apparatus for determining the UCS of target material

2.6 Curing and UCS Relationship

Cement sample test results are strongly related to the hardening process of the binder. One key example of this is the relationship between the curing environment temperature and the resultant UCS of the sample. Research suggests cement strength, as a function of curing time, greatly improves when cured under elevated temperatures - but not necessarily the final maximum strength of the cement.

Geopolymer samples, by comparison, do not demonstrate such uniform behaviors. Works comparing the impact of short-term temperature-elevated curing conditions on the long-term effects on geopolymer strength show that at lower temperatures OPC yields higher UCS at all

testing curing times. Other test results, from both this Work and in the literature review conducted, show indications that elevated curing temperature may positively influence geopolymer UCS. However, these results are problematic to accept as much of the literature's experimental methods are diluted by large variances in mixing and curing procedures. Additionally, presented evidence indicates elevated curing temperatures can also be detrimental to the mechanical strength of the materials.

Further, few works in the reviewed literature have varied both additive inclusions and temperature concurrently. There is conflicting discussion regarding geopolymers which include additives; indicating that while an elevated temperature is beneficial, there is a limit to that benefit before negative impacts begin to influence the strength.

Because of the varying impacts of not only temperature but pressure as well on geopolymer curing behavior, the existing test schedule tables are irrelevant. While API has already considered this, API is unclear on the extent additives to the slurry need to be declared.

Although API standards do not address this, it is common practice to test cement samples at 3, 7, and 28 days. If the experiments are even longer term, the gap between testing intervals often elongates as well. The UCS gain of cement with respect to time seems to constantly exhibit a logarithmic trend as can be seen in **Figure 13**.

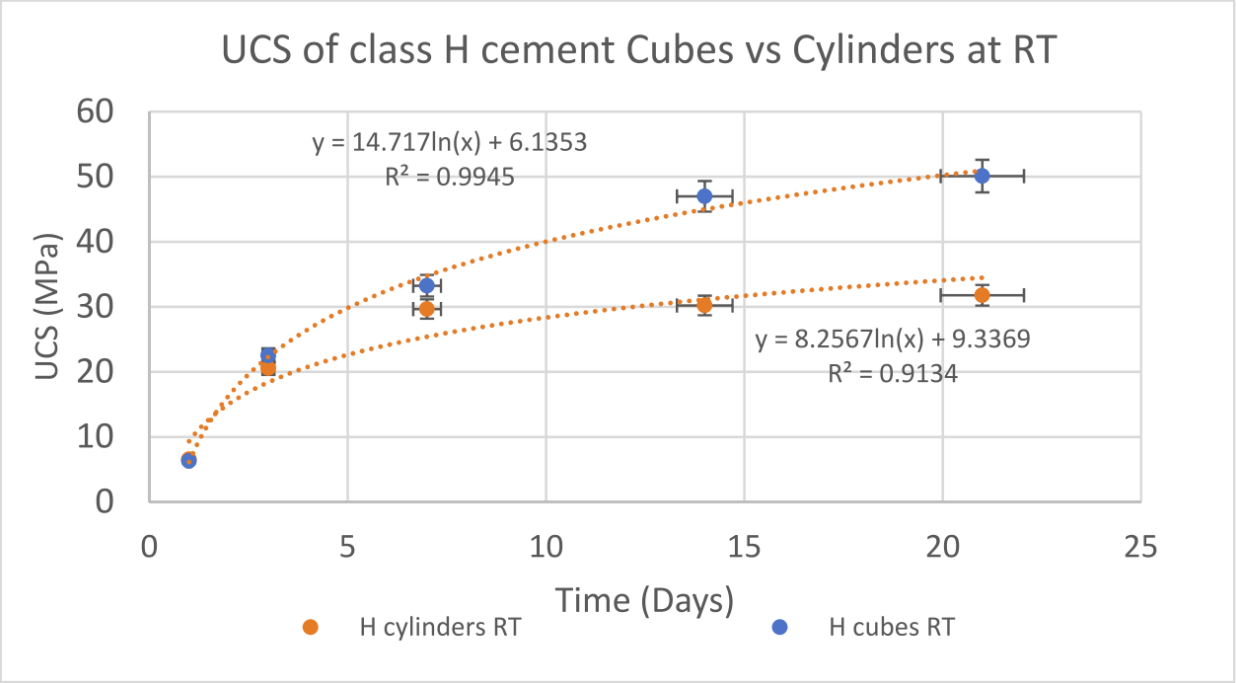

Figure 13 – Class H Cement UCS Gain as a Function of Time, Rincon et al., (2022)

Although a multi-day cure time testing process is not API standard, it is prevalently observed in literature (Figure 13Figure 13 – Class H Cement UCS Gain as a Function of Time, Rincon et al., (2022) regarding oilfield cement. The UCS at key times are important to acknowledge because the strength requirements cement must meet at the prescribed times exist because of the understanding of how cement will continue to gain strength as a function of time. Fortunately, geopolymer samples do continue to improve as a function of time, however, the completeness of understanding of that relationship, especially as it relates to exact geopolymer recipe considerations, is not well established.

In summary, while the API testing approach may be used for geopolymers, the interpretation and expectations of the data must be analyzed only within the lens of geopolymerization, and not hydration or other binder reactions.

2.7 Nondestructive Sonic Determination of Compressive Strength of Cement

Sonic compressional travel time, or ultrasonic pulse velocity (UPV), is a used and accepted standard cement test for non-destructive determination of the compressive strength of a sample. The relationship between UCS and UPV is often observed to have a strong correlation and often a linear one. These relationships are observed under a multitude of cement recipes and testing schedules, so reporting on both the non-destructive UPV testing and the destructive UCS testing is commonplace. While the relationship is strong, API notes UPV should not be reported as the actual compressive strength because sample geometry can greatly impact the observed strength of the sample. So, while the trend between UCS and UPV is historically reliable, they are not substitutes for each other.

The method for UPV testing of a sample is comprised of equipment which can measure the temperature, pressure, and the sonic travel time. Additionally, a device is needed to emit the signal which is being measured. API recommends using the manufacturers specifications for testing and collecting the data. As most testing of cement occurs at atmospheric conditions, a device such as the one shown in **Figure 14** can be used, whereby the transducers of the tool are coated in a gel to generate good contact with the sample. Once the device has been calibrated with a control sample, the transducers are attached to opposite sides of the sample and the signal is passed through the sample. The resultant travel time can be used to compute sonic strength using known correlations between the travel time and strength. The testing schedule for the UPV should be the same as the testing schedule used for the destructive testing.

Figure 14 – UPV indicator screen connected to transducers

The operating principle of acoustic impedance is valid for all solid body porous media. The benefit of the test is the correlation to empirically determined compressive strength, primarily that determined from the uniaxial compressive test. This is why it is important to match testing conditions to generate accurate correlations. The test and test data results data are only useful if there is relevant and available reference data to use to compare. As literature continues to develop and establish the mechanical behavior of geopolymer recipes, the information gained from sonic travel time will be more applicable. Additionally, if API were to adapt its 10B standards to include geopolymer samples, or create an entirely new standard, researchers would have a reference from which to compare information. Subsequently, a need would arise for larger-scale engagement in both UPV and UCS testing of geopolymer samples in oilfield tailored research. Without meaningful compressive strengths to compare UPV values to, they will only be values without beneficial physical interpretation. If all relevant information is recorded, however, the slurries can be reformulated, and appropriate tests can be conducted to give UPV values meaning.

2.8 Additional API Tests

API 10B includes four more standard tests. These tests test for thickening time, static fluid loss, rheological properties including gel strength, and slurry stability tests. All these tests apply to the slurry and involve either a well test schedule or a consistometer. Therefore, the same problems from the slurry density tests arise from these tests. These tests, while conducted in field testing environments equipped with a consistometer, are typically only conducted when the experimental scope covers understanding the slurry and not the solid-body binder. Often, these experiments are either investigating the influence of downhole conditions or the influence of additives. As there are no standards for downhole well test schedules for geopolymer testing schema nor are there standards for reporting on the workability, pumpability, or general fluid properties of geopolymers, the experiments will exist without applicable context. Testing of fluids under these API recommendations have not been conducted under this scope of work.

Chapter 3 Testing of Geopolymer Materials

When considering geopolymers as a potential substitute for cement in oil and gas applications, the geopolymer UCS is equally of critical importance as it is for cement. At the time of this writing, no industry standards for geopolymer manufacturing and testing have been published. Therefore, both literature reviews and experiments were conducted to better understand geopolymer testing for geopolymer use in the oil and gas industry. Several experiments were performed, varying the geopolymer composition, curing times and curing environments to study the results, make comparisons, and develop conclusions and recommendations.

The following discusses a literature review of geopolymer testing, the use of API cement standards to test geopolymers, and several experiments that were performed.

3.1 Literature Review of Geopolymer Testing

As the development of geopolymer research continues, it does so without a baseline for testing, standardization of information reporting, or general regulation. The lack of standard practice combined with positive perception of the material have led to the amassing of literature which is difficult to cross-compare. A brief study focusing on oil and gas-oriented application research of geopolymers was conducted to explore the large variance among studied geopolymers. The overview of this study is seen in **Table 8**.

Table 8 – Review of Oilfield Relevant Geopolymer Research

Author	Sample Type	Aging Times (Days)	UCS (MPa) 2	Curing Temperature (°C)	Sample Shape	Mix time (s)	API Mixing
Salehi et al., 2018	Class F Fly Ash	1 3 7 14	10.3 12.4 22.8 43.4	120	cylinder	N/A	no
Salehi et al., 2017a	Class F Fly Ash	1 3 7 14	9.6 12.8 17.9 34.2	65 80 93	N/A	0, 1200, 2400	no
Paiva et al., 2018	Class F Fly Ash	14	37.4	49	cylinder	N/A	no
Ahdaya & Imqam, 2019a	Class F Fly Ash	1 3 7	7.6 15.1 21.37	24	cube	50	no
Bu et al., 2020	Class F Fly Ash	24	18	75	cube	>120	no
Giasuddin et al., 2013	Class F Fly Ash	28	92	23	cylinder	300	no
Rickard et al., 2016	Class F Fly Ash	56	70.2	23	cylinder, cube	480	no
Jani & Imqam, 2021	Class C Fly Ash	N/A	N/A	N/A	cylinder	N/A	no

Table 8 – Review of Oilfield Relevant Geopolymer Research

Author	Sample Type	Aging Times (Days)	UCS (MPa) 2	Curing Temperature (°C)	Sample Shape	Mix time (s)	API Mixing
Ahdaya & Imqam, 2019b	Class C Fly Ash	1	8.5	24	cylinder	50	no
Lee & Van Deventer, 2002	Class F Fly Ash	7	27.4	23	cylinder	600, 900	no
		21	38.4				
		90	52.3				
		180	62.3				
		270	65.3				
Igbojekwe et al., 2015	Class F Fly Ash	1	28	66	cylinder	720	no
				93			
				121			
				149			
Thirumakal et al., 2020	Class F Fly Ash	45	37.1	50	cylinder	N/A	no
Palomo et al., 1999	Metakaolin	7	N/A	N/A	Rectangular prism	180	no
		28					
		56					
		90					
		180					
		270					
Patel & Shah, 2018	Class F Fly Ash	3	35.33	23	cylinder, cube	330	no
		7	38.27				
		28	42.6				

Table 8 – Review of Oilfield Relevant Geopolymer Research

Author	Sample Type	Aging Times (Days)	UCS (MPa) 2	Curing Temperature (°C)	Sample Shape	Mix time (s)	API Mixing
Rahman et al., 2020	Class F Fly Ash	Up to 40	17.7	60	cylinder	50	yes
Nasvi et al., 2014	Class F Fly Ash	1	N/A	50	cylinder	180	no
Heah et al., 2011	Metakaolin	1 3 7 28	3.25 5.9 9.4 6.8	23 40 60 80 100	cube	>60	no
Mehta & Siddique, 2017	Class F Fly Ash	3 7 28 90	63 64 64.5 65	80* 23	cylinder, cube	900	no
Xie & Kayali, 2014	Class F Fly Ash	7 14	42.07 N/A	23 60	cube	300	no
Soutsos et al., 2016	Class F Fly Ash	28	80	70	cube	900	no
Aliabdo et al., 2016	Class F Fly Ash	7 28	45 46	28 50 70 90	cylinder, cube	300	no

Table 8 – Review of Oilfield Relevant Geopolymer Research

Author	Sample Type	Aging Times (Days)	UCS (MPa) 2	Curing Temperature (°C)	Sample Shape	Mix time (s)	API Mixing
Nath et al., 2016	Class F Fly Ash	28	N/A	27 45 60	cylinder	N/A	no

While there is much more literature than **Table 8** presents, this sampling is representative of the more foundational investigations. Studies are not overly reliant nor focused on niche applications or specialty additives. While a portion of these studies do include additives such as sodium silicate or rice husk ash, these are common inclusions in geopolymer studies.

The two most common parameters studied among this literature sample are the sample shape and the type of geopolymer cured. Although usage of cylinder-shaped samples is not API recommended, this shape is more commonly utilized in civil engineering practices. Another reason the shape is popular in these studies is the samples were not API standard cures. Many of these studies utilized cured samples and cored cylinders out of a larger body, instead of using a sample mold. Additionally, while most of the work did use Class F Fly Ash, due to the wide variance of Class F Fly Ash combined with the underreported unique composition used in the experiments, there is high likelihood the variation in results between the experiments is significant. Variability is compounded since mixing times range from the API regulated 50 seconds total to well over 10 minutes. While some works, such as by Duxson (2017b), suggest longer times are appropriate, the influence of compositional variance and mixing variance is understudied and no correlative relationships exist to draw comparisons of different compositions, mix times, and UCS. If an attempt were made, using these studies, to generate that trend; it would look like **Figure 15**.

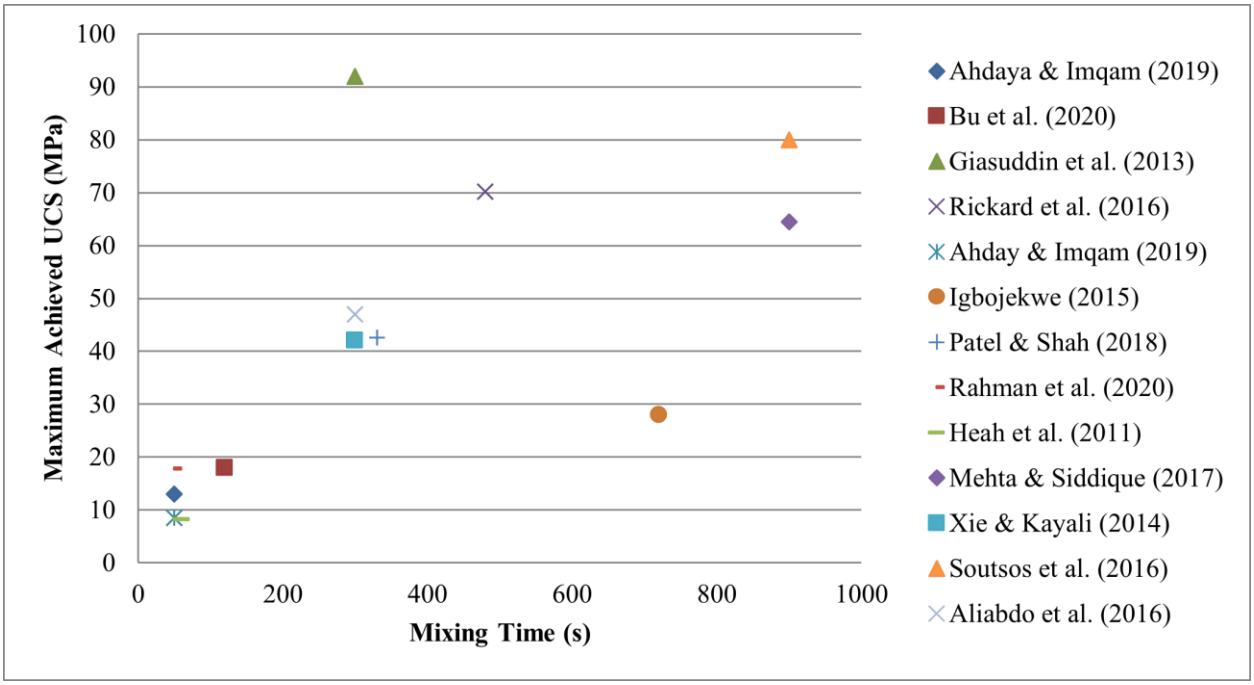

Figure 15 – Analysis of Mixing time and achieved UCS in geopolymer literature

This plot generally supports the conclusions drawn by Duxson that mixing time improves UCS (Duxson, Fernández-Jiménez, et al., 2007; Duxson, Mallicoat, et al., 2007). Omitting the work by Igbojewe et al., (2015) and Giasuddin et al., (2013) the trend suggests a logarithmic improvement in UCS as a function of mixing time. This graphic is problematic, however; because the sample cure times do not match, which is likely the reason for the outliers mentioned. The lack of standard practice, such as standard sample cure time test intervals or mix times, continues to be an issue for cross literature examinations as can be seen in **Figure 16**, which discusses the maximum achieved UCS by cure time of some of the works from **Table 8**.

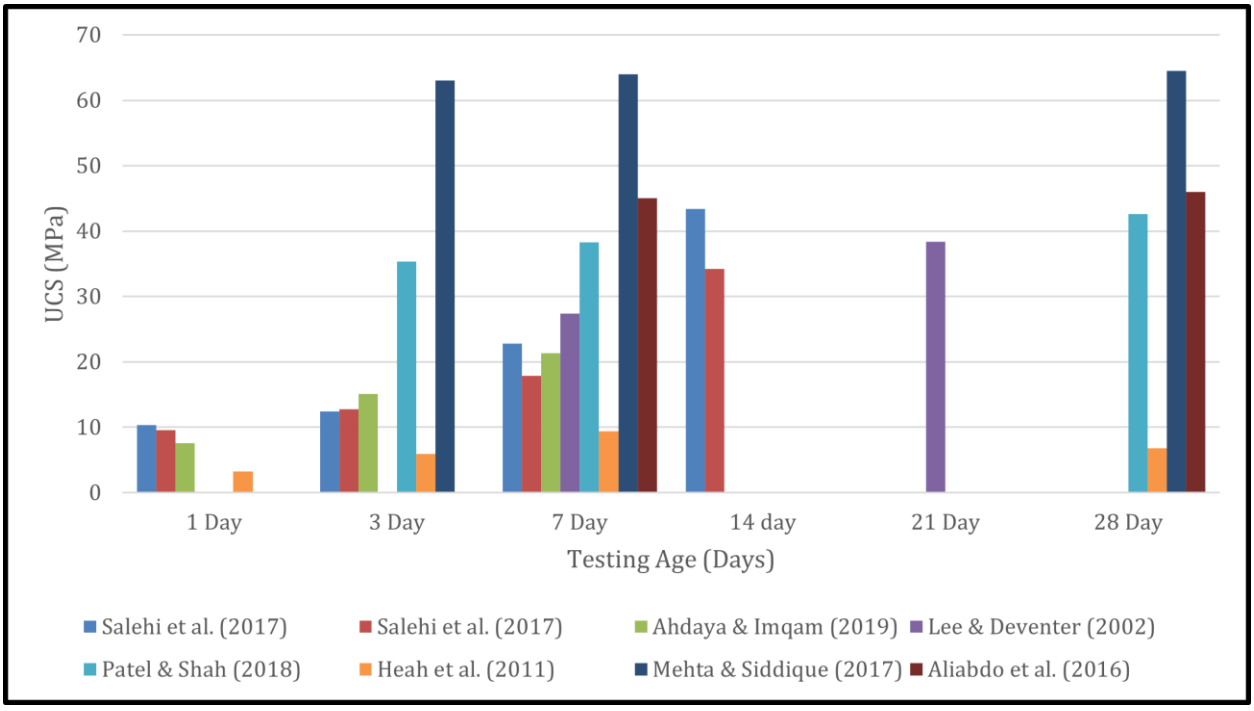

Figure 16 – Analysis of UCS grouping relating to curing time from geopolymer literature

The works were selected for highlighting as they had the largest diversity of curing times. These results are generally in line with standard oilfield cement testing practices. The data shows the logarithmic relationship often observed between curing time and UCS of OPC. Salehi et al., (2017a) almost suggests an exponential trend, almost doubling in UCS between the 7- and 14-day mark. Mehta & Siddique (2017) data show hardly any UCS development after day 3. The only work which seems to indicate logarithmic UCS growth is the work by Heah et al., (2011), which is interestingly one of the works which most closely mirrored API testing conditions without matching them exactly. While a definitive conclusion is difficult to draw from this sampling of work, the question does present itself as to what truly determines the UCS of a geopolymer compared to how geopolymer samples are cured and tested. These works may suggest certain additive inclusions result in significant impacts in strength development, both in rate of growth and total achieved UCS.

While there is little consistency among the general testing practices involving the fly ash, this inconsistency doesn't discredit the proof there is some combination of mixing parameters, mixing ratios, and additives which greatly improve the UCS.. For example, the work of Mehta & Siddique (2017) stabilized the UCS as a function of time while simultaneously bringing the UCS to above 60 MPa across a month of testing intervals. Several works all show a stronger, positive-linear time dependence of UCS of geopolymer samples (Ahdaya and Imqam 2019a; Salehi, Khattak, Bwala, et al., 2017b; Salehi, Khattak, Rizvi, et al., 2017a). One work was even able to maximize the UCS of Class F Fly Ash geopolymer at 90 MPa within a month of curing (Giasuddin et al., 2013). All this literature clearly indicates the material can achieve equal or superior UCS required to replace API cement, or at least justify additional experiments needed to fully understand the mechanical strength of the geopolymer material. Visibility of this is improved when grouping all the tests from **Figure 17** into two groups: API tested groups and all others, shown as **Figure 18**. From the review, only one of the experiments adhered to the API testing, and that was the work done by Rahman et al., (2020). The previously mentioned work was grouped with this experimental work and plotted against the other works. **Figure 18** clearly indicates the strength of samples evaluated under non-API conditions are superior to API tested samples, and the relational dependence on time is much more pronounced. The nature of this comparison does not confirm or disprove that it is the API mixing is causing the inferiority, but instead establishes evidence for a need to investigate optimal baseline testing for fly ash geopolymers.

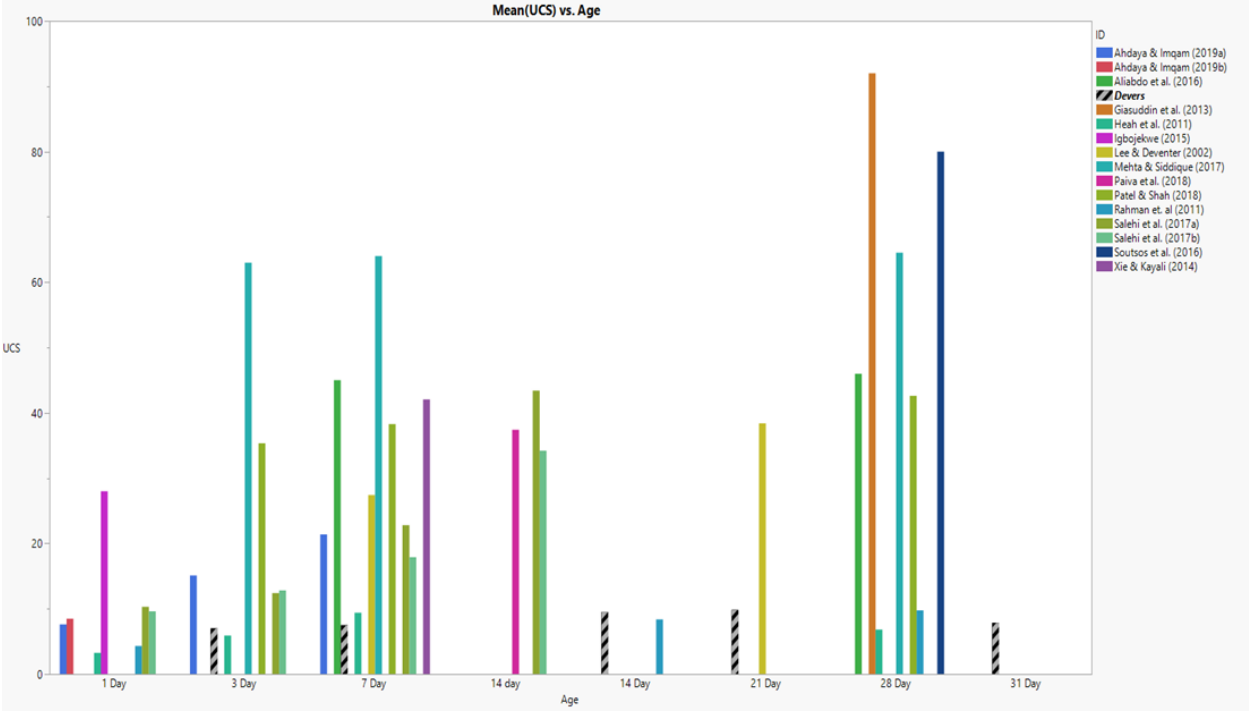

Figure 17 – A collection of literature that tests geopolymers under a variety of different mixing practices. The testing ranges from mixing times, mixing speeds, sample shape, materials ratio, etc.

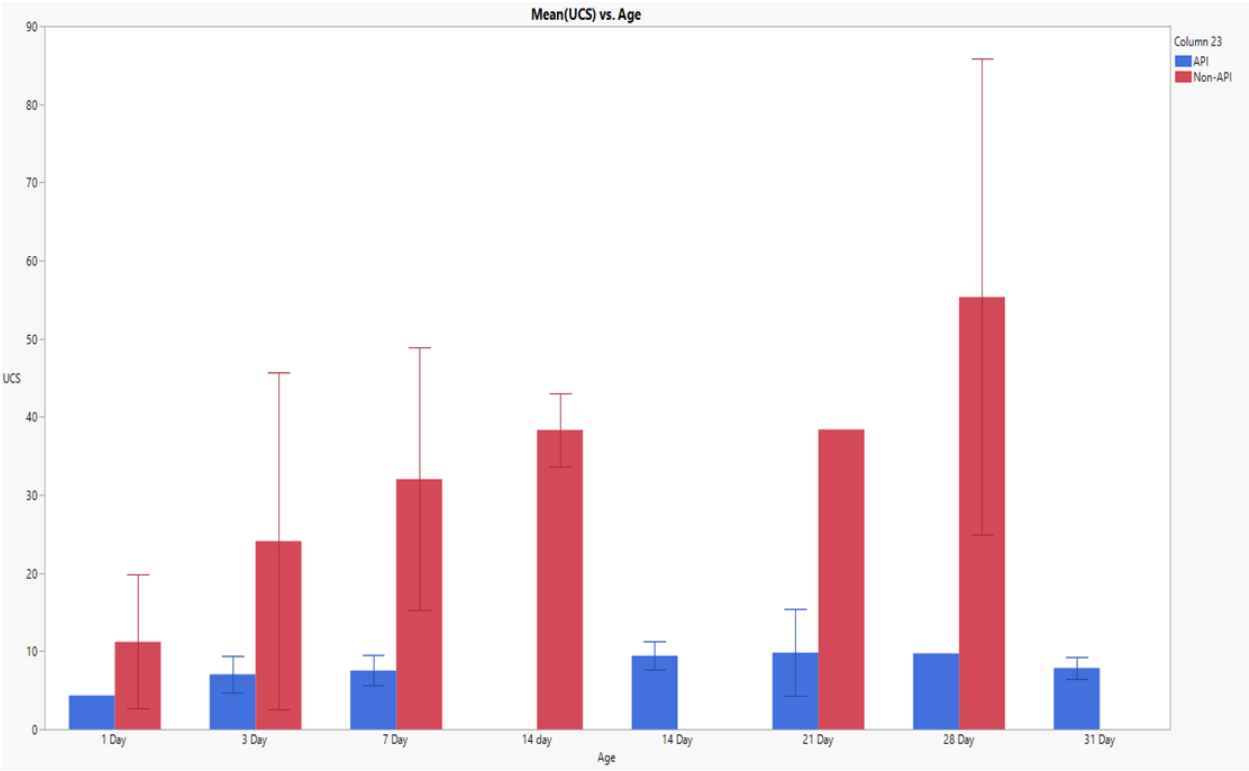

Figure 18 – Comparison of Geopolymer samples tested under API conditions versus all non-standardized testing.

Until a standard of testing and reporting is adopted, large variations in characteristic data of surface-level similar geopolymer will likely continue and cause concern for geopolymer stability and consistency.

3.1.1 Literature Review Focused on Geopolymer UCS

A thorough review of existing literature was also conducted to obtain a more comprehensive understanding of the mechanical performance and variability of geopolymers. This review focused on studies that investigated the UCS of fly ash-based geopolymers, with particular attention to those using Class F Fly Ash. The review revealed a substantial variance in UCS results, underscoring the heterogeneity in testing methodologies, material compositions, and curing conditions employed across different studies.

The high variability in UCS results observed in the literature can be attributed to several factors. Firstly, the source and chemical composition of fly ash used in geopolymer synthesis play a crucial role in determining the final mechanical properties of the material. Fly ash, a byproduct of coal combustion, can vary significantly in its content of silica, alumina, iron oxides, and other trace elements depending on the source of the coal and combustion conditions. These variations influence the reactivity of the fly ash and, consequently, the extent of geopolymerization and the mechanical properties of the resulting geopolymer.

Secondly, the choice and concentration of alkali activators, such as sodium hydroxide (NaOH) or potassium hydroxide (KOH), significantly impact the geopolymerization process. Higher concentrations of alkali activators can enhance the dissolution of alumino-silicate precursors, leading to a more extensive network of alumino-silicate gel and improved mechanical properties. However, excessive concentrations can also lead to the formation of efflorescence and reduced

long-term durability. The literature review indicates that the optimal concentration of alkali activators varies widely among studies, contributing to the observed variability in UCS results.

Curing conditions, including temperature, humidity, and duration, are also critical factors influencing the mechanical performance of geopolymers. Elevated curing temperatures can accelerate the geopolymerization process and enhance early-age strength, but they may also induce thermal stresses and microcracking, adversely affecting long-term strength and durability. The reviewed studies employed a range of curing conditions, from ambient temperature curing to high-temperature steam curing, further contributing to the variability in UCS results.

In addition to these factors, the mixing ratios of fly ash to alkali activator, the inclusion of supplementary materials such as slag or silica fume, and the presence of additives like superplasticizers or retarders can significantly influence the mechanical properties of geopolymers.

The literature review highlights the lack of standardized protocols for geopolymer synthesis and testing, leading to a wide range of experimental conditions and, consequently, highly variable UCS results. The review also identified several studies that achieved high UCS values through optimized material formulations and curing regimes. For instance, the work of Mehta & Siddique (2017) demonstrated that by carefully controlling the alkali activator concentration and curing conditions, fly ash-based geopolymers could achieve UCS values exceeding 60 MPa within a month of curing. Similarly, Giasuddin et al., (2013) reported UCS values of up to 90 MPa for geopolymers cured under specific conditions. These studies highlight the potential of geopolymers to achieve mechanical properties comparable to or even superior to traditional Portland cement when optimized synthesis and curing protocols are employed.

In conclusion, the review of geopolymer testing literature reveals significant variability in UCS results, primarily due to differences in fly ash composition, alkali activator concentration, curing conditions, and material formulations, resulting in much difficulty in comparing published testing results. This variability highlights the critical need for developing standardized testing protocols for geopolymers to ensure meaningful comparisons and reproducibility of results. By addressing these challenges, the scientific community can advance the understanding and practical application of geopolymers, contributing to the development of sustainable cementitious materials for the oil and gas industry.

3.2 Use of API Cement Standards to Test Geopolymers

API provides comprehensive cement manufacturing and testing standards but lacks inclusion of geopolymer manufacturing and testing criteria. API cement standards are tailored to optimize the performance of Portland cement. API has incorporated considerations for pozzolanic materials. Geopolymers are designed to be analogous in function to OPC. For these reasons, API testing procedures may be a fair approach to geopolymer testing.

The mixing, curing, and testing protocols specified in API standards were developed based on the hydration kinetics and mechanical behavior of Portland cement. Geopolymers, however, exhibit different setting times, curing behaviors, and long-term strength development profiles. For instance, the initial setting time of geopolymers can be significantly influenced by the concentration and type of alkali activator used, as well as the curing temperature and humidity conditions. The API standard curing conditions, typically involving high temperatures and specific humidity controls, may not be optimal for geopolymer systems, potentially leading to suboptimal mechanical performance. Therefore, several experiments were performed using the API 10B

standard as a frame of reference to better understand the use of API standards for geopolymer testing.

3.3 Curing Time Variation Effect on UCS

Investigative experiments were conducted to compare the experiment results of UCS testing at varying curing durations of controlled geopolymer samples to comparable API grade cement.

3.3.1 Experimental Procedure

To ensure a fair comparison between controlled geopolymer samples and API grade cement samples, all curing and testing was performed in accordance with 10B using Class F Fly Ash having the same fly ash source from recipe aggregated recipe from the literature review and traditional API OPC.

API standards call for the mixing of solids into liquids. Best practice is that the required 10M sodium hydroxide component be prepared in solution form rather than introduced with the solids. This solution was prepared by introducing the sodium hydroxide dry powder to deionized water and allowed to cool back to room temperature before being utilized as the fluid component of the solution. Once the material reached ambient temperature and samples ready to be prepared, 500 grams of Class F Fly Ash was measured out and set aside. Then, 250 grams of the sodium hydroxide solution was transferred from the original container to the API standard blender. This material ratio was determined and rationalized from several experimental works and geopolymer material reviews (Adjei et al., 2022; Salehi et al., 2017a; Salehi et al., 2017b; Salehi et al., 2018).

These materials were then mixed into a slurry per API standards. At the conclusion of the mixing, the slurry was placed into curing molds and transferred into an aquatic environment heated to

75°C, for a minimum of 3 days, at which point the material was removed from their molds and either transferred to the mechanical testing stations or returned to the heating environment for the duration of their prescribed curing period. All material samples are removed at the 3-day mark to ensure the samples do not overly bond to the material of the mold itself.

The samples of API Class C cement used for the offset comparisons were prepared in the same manner, per API standards.

Once samples reached their prescribed curing period and transferred from their curing environment to the testing area, length, width, and height measurements of all samples were taken in triplicate and averaged and recorded. Samples were also weighed in water and air. Finally, samples were tested for their UPV before being subjected to a uniaxial crush test to determine UCS: the primary metric of observation in this study. Results were recorded for all samples in both a laboratory book and a digital repository. The results were graphed, to best relay trends and other phenomenon, and included in the following experiment results section.

3.3.2 Experimental Results

The experimental results were compared to a selection of geopolymer literature, highlighting performance inconsistency in literature, which show UCS results far more variant than classic API class G, C, or H cement, with many samples failing to show strengths superior to traditional cement classes. Further investigation suggests that these variances are observed across samples from the same fly ash source and also vary with setting environmental temperature.

Additionally, it is strongly suggested by this Work that there are methods of formulating, mixing, and curing geopolymer which yield stronger UCS results than the Work here.

The box-and-whisker chart (**Figure 19**) shows clearly that there is little time-based difference between the curing age of the geopolymer samples. This observation is contrary to the expected behavior of classical neat, Portland-based cement products, which typically show a logarithmic increase in strength over time.

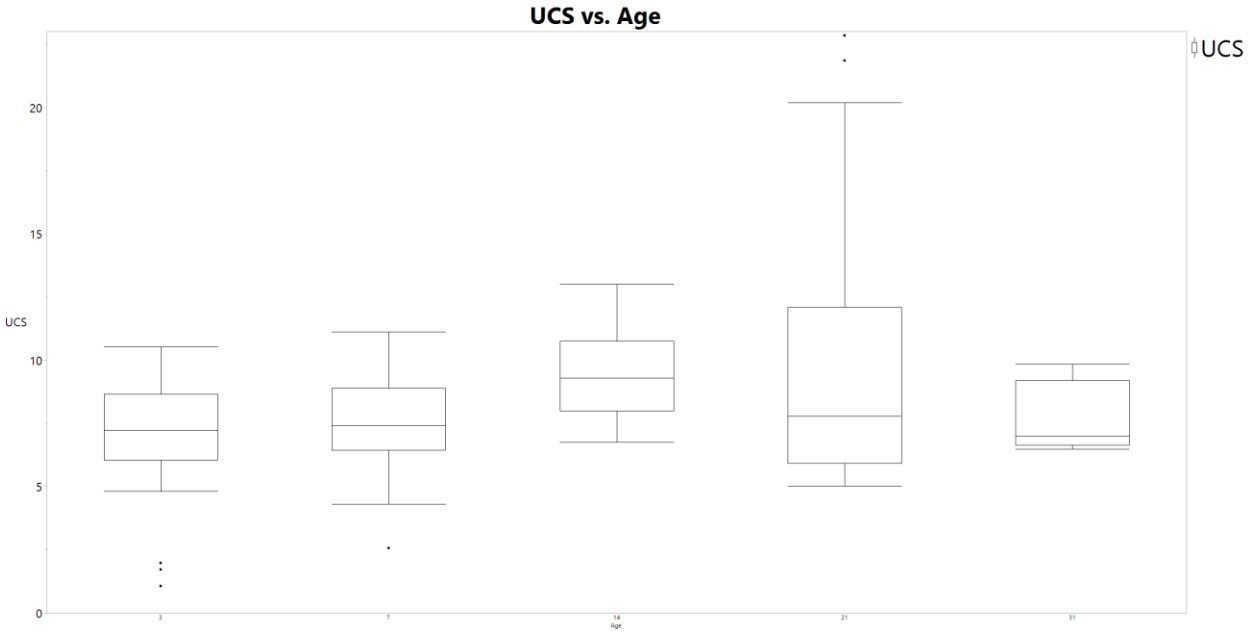

Figure 19 – Box and Whisker chart for UCS of tested Samples by Age

Both **Figure 19** and **Figure 20** reveal similar averages in geopolymer UCS across different testing ages, with considerable variation within the same age group. This variability in UCS results suggests that the factors influencing the strength development of geopolymer cements are more complex and less predictable compared to traditional Portland cement. The UCS results are more aligned with the work done by Salehi et al., (2018), which also reported significant variability in UCS results for geopolymer samples. However, it contrasts with studies that incorporate substantial amounts of additional liquid glass, which typically report higher and more consistent UCS values. For instance, Mehta & Siddique (2017) observed much higher UCS values in their study of the influence of additional additives on geopolymer cements.

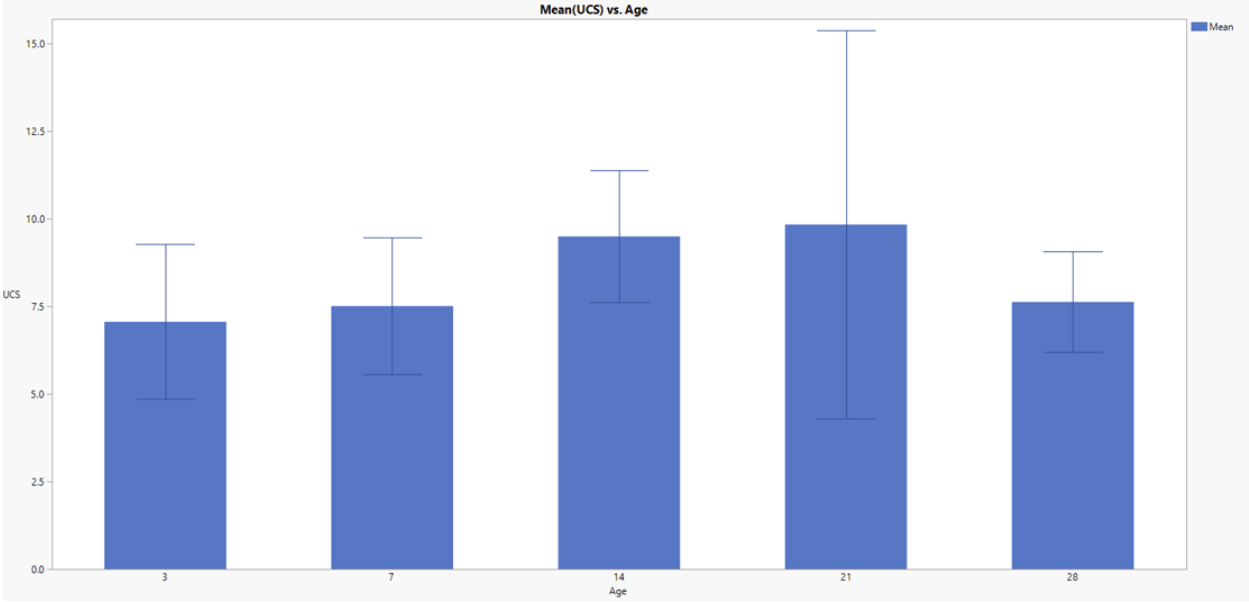

Figure 20 – UCS over time of the Class F Fly Ash, standard deviation error bar included

The observed negative parabolic trend in UCS with time (**Figure 21**) further underscores the fundamental differences in the strength development mechanisms between geopolymers and Portland cement. Note, this observed negative parabolic trend was not observed in the literature review .

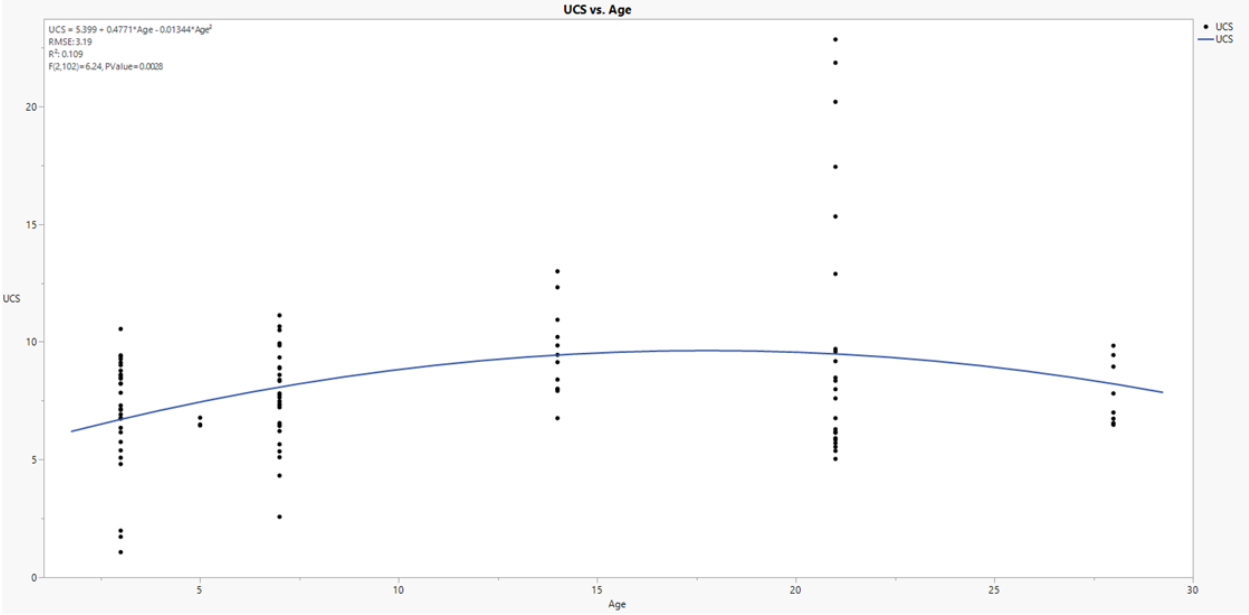

Figure 21 – The UCS of the Class F Fly plotted as a function of time, with regression statistics. Note the very low correlative value.

The extensive range in UCS results raises questions about the reproducibility and reliability of geopolymer cements in practical applications. OPC must meet defined mechanical strengths at defined testing windows to be considered valid use materials (API 10B, 2013). It suggests that the underlying chemical and physical processes governing the strength development in geopolymers are not fully understood and are highly sensitive to variations in the composition and curing conditions. This inconsistency poses a significant challenge for the adoption of geopolymers as a reliable alternative to traditional cements in geothermal well applications, where consistent and predictable material properties are crucial for ensuring long-term structural integrity and zonal isolation.

Moreover, the trend in UCS observed in this study is indicative of a different hydration or polymerization mechanism in geopolymers compared to the well-established cement hydration in Portland cement. Portland cement undergoes a complex set of reactions involving the formation of calcium-silicate-hydrate (C-S-H) gel, which contributes to its logarithmic strength development over time. Geopolymers, on the other hand, involve the formation of an alumino-silicate network,

the kinetics of which may be influenced by various factors such as the source of fly ash, activator solution concentration, and curing conditions. The observed linear trend suggests a steady, but less pronounced, increase in strength, which may be due to the continuous dissolution and re-polymerization processes occurring within the geopolymer matrix.

The significant variability in UCS results also highlights the importance of stringent quality control measures during the preparation and curing of geopolymer samples. The consistency of the mixing process, the purity of the raw materials, and the uniformity of curing conditions are critical factors that need to be carefully controlled to achieve reproducible results. The lack of standardization in these aspects can lead to discrepancies in the mechanical properties of geopolymer cements, making it challenging to draw definitive conclusions about their performance.

However, the UCS was much higher. **Figure 21** shows a slight increase of UCS with age, but the trend is more linear, unlike Portland cement where a logarithmic tendency is noted. The range of this issue is made apparent when the data is broken out into binned histograms, as is done in **Figure 22**, **Figure 23**, **Figure 24** and **Figure 25**. For clarity, the histograms are binned in a range of .5 MPa, with the number of included samples denoted in the top right of the graphs.

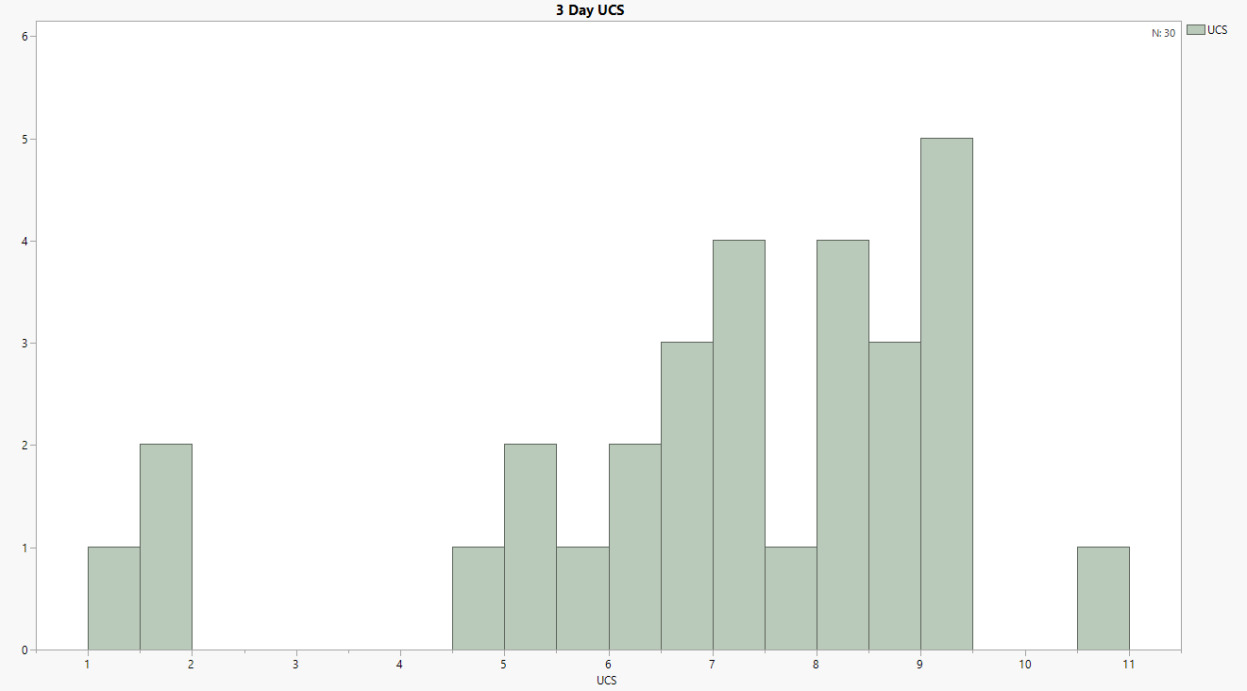

Figure 22 – 3 Day UCS Histogram

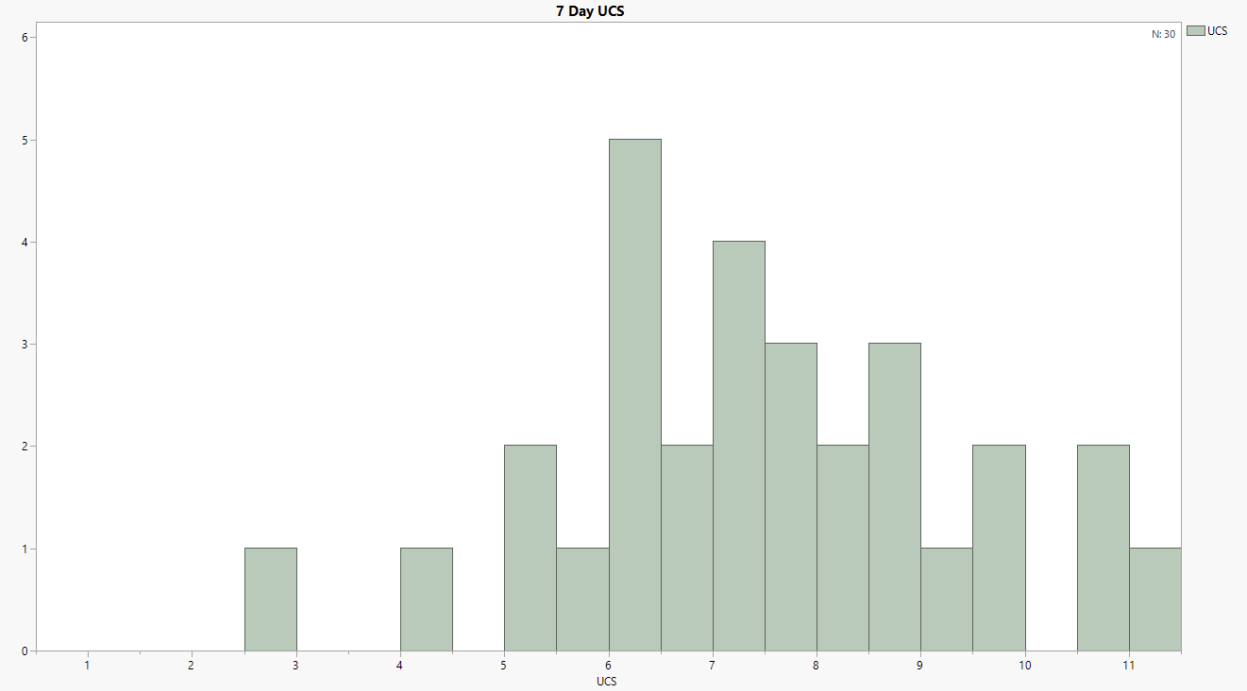

Figure 23 – 7 Day UCS Histogram

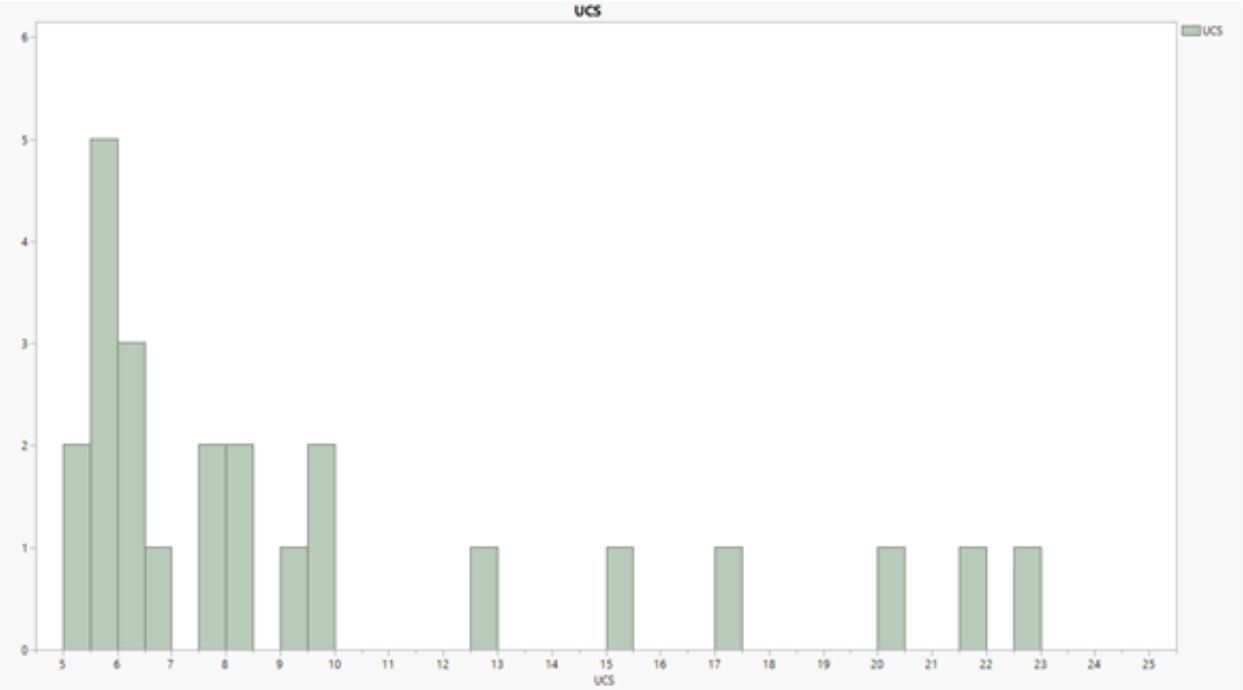

Figure 24 – 21 Day UCS Histogram

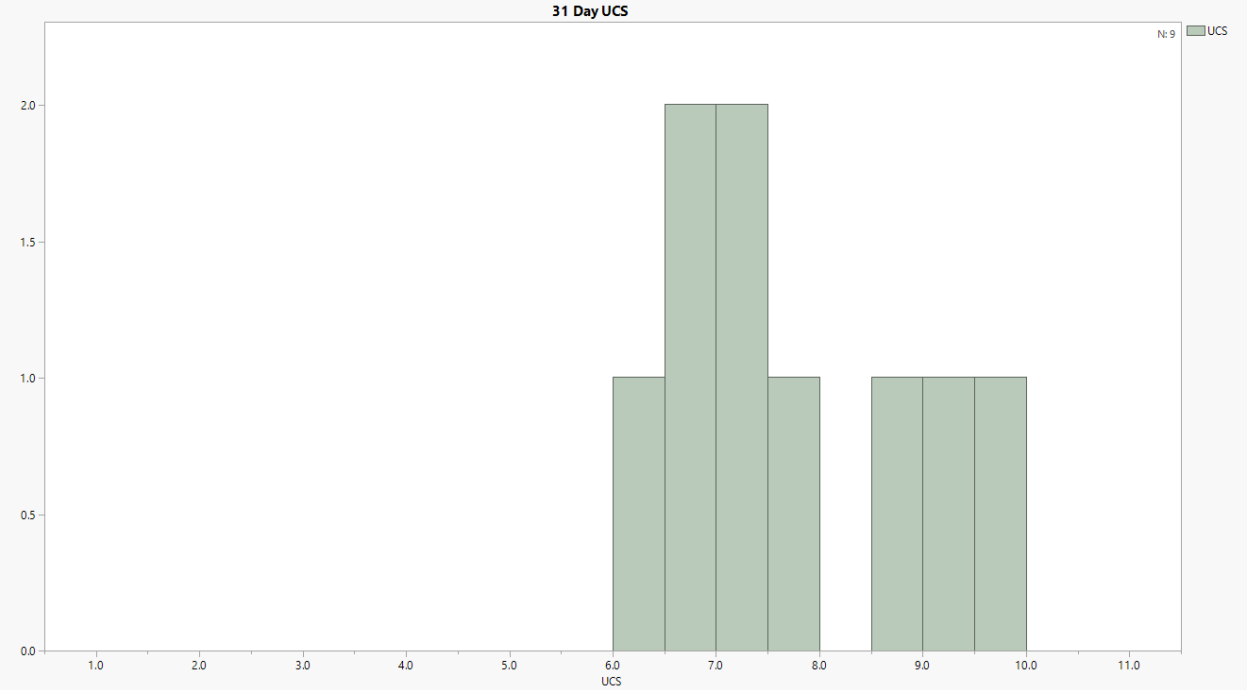

Figure 25 – 31 Day UCS Histogram

From this breakdown, it is observed that the samples not only have a large range in UCS but have no ‘normal’ distributive behaviors. First addressing the samples that were tested after the 7-day mark, it is seen that 31-day testing times has the tightest grouping of material, both displaying 7 subgroups across 12 tests. The 21-day mark has a better bins-to-samples ratio, having 8 subgroups across 24 samples, however, the grouping is far worse. The 21-day mark is the best bins to samples ratio. Both the 3- and 7-day tests are comprised of 30 samples but have 13 and 14 bins, respectively. While UCS poorly functions with time, UPV shows a much stronger correlation with time, displaying a quadratic trend between the two with an R2 of .51, which still is lower than anticipated. The interesting piece of note here is that UPV has a moderate trend with time while UCS has no discernable relationship. One reason for this could be due to the relationship between density and UPV, while UCS has a higher dependence on the internal bonding of the material, however the work of Rahman et al., (2020) suggests the density of the slurry has a notable level of influence on the UCS.

Below are the UCS testing results for the traditional API OPC.

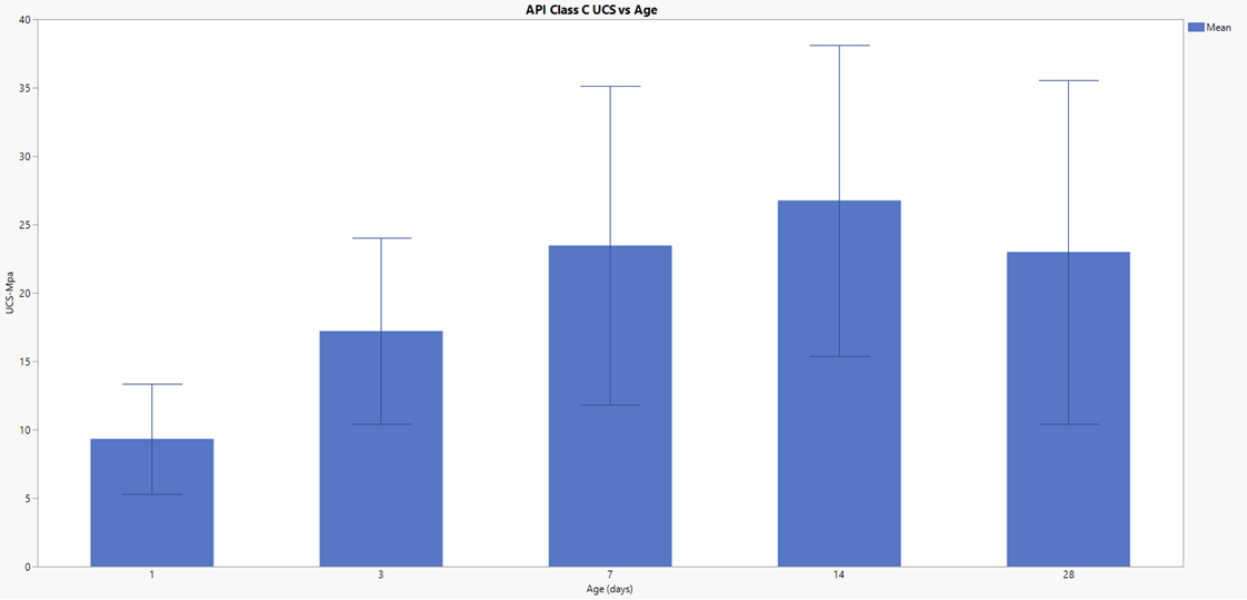

Figure 26 – UCS of API Class C comparison samples that were tested under equivalent conditions.

To best obtain a clear understanding of the practical functional difference between the API Class C cement and the Class F Fly Ash alternative, the two datasets are plotted together on a histogram, shown in **Figure 27**. This look gives clear insight to the UCS superiority of the Class C cement over the Class F Fly Ash. At every tested time interval, the Class C cement outperformed the Class F Fly Ash geopolymer by at least 200%. It is possible that the primary reason for the UCS disparity between the two materials is the nature of testing between the two.

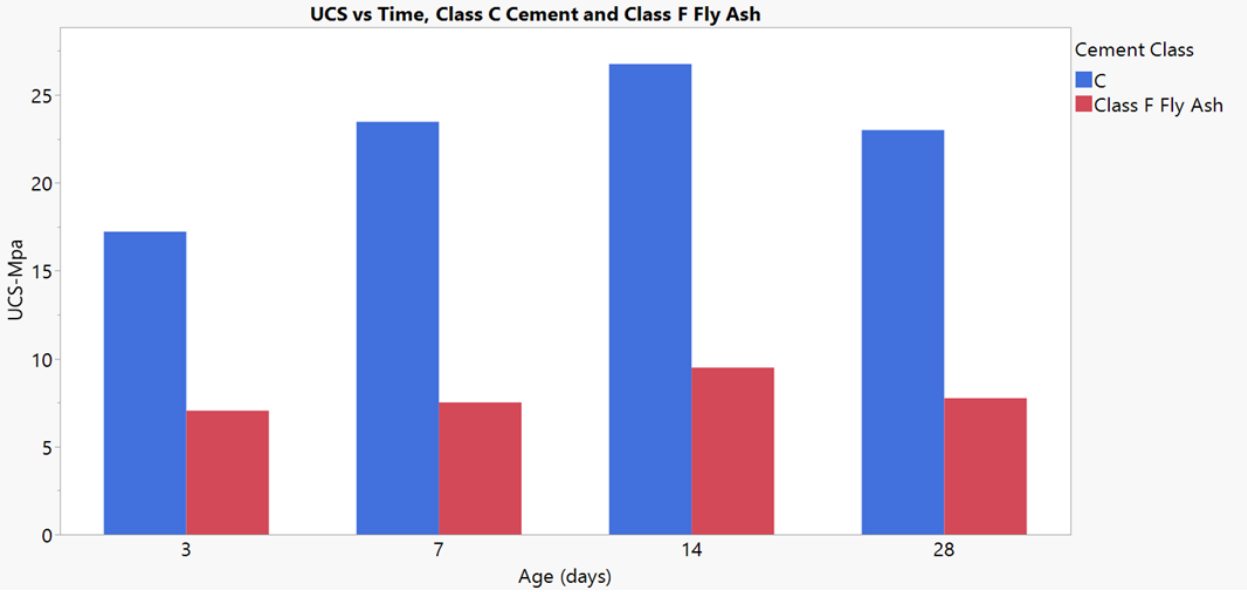

Figure 27 – Direct Comparison of API Cement Class C to Class F Fly Ash Geopolymers

3.4 Geopolymer Composition Variation Effect on UCS

This experiment focused on geopolymer compositional variation effect on UCS. Geopolymer samples were tested in accordance with API standards, maintaining constant mixing conditions. Class F Fly Ash of varying composition were used and tested at variable cure times. Additionally, results were compared to API-grade cement under identical testing conditions for offset comparison.

3.4.1 Experimental Procedure

Samples and testing were performed according to API standards. Four unique pozzolan formulations were studied. Two sets of OPC, neat Class H and neat Class G, were taken from archival data and generated at elevated curing conditions in a water bath across the same curing intervals. Two sets of geopolymers were also generated for this analysis. The geopolymer recipes, determined through literature review and selected for their common investigation and typical performance, comprised a 2:1 solid-to-liquid ratio by mass, with the liquid component being a

10M sodium hydroxide solution (250 grams) and the solid component being Class F Fly Ash (500 grams). The only difference between the two geopolymer sets was the fly ash sourcing, with compositions determined by XRF.

3.4.2 Experimental Results

The results section of this study presents a detailed analysis of the UCS of the tested materials over a one-month span, as well as the raw XRF output from the materials used to generate cementing material.

3.4.2.1. UCS Results

UCS results are depicted in **Figure 28**, depicting the performance of four tested materials over a one-month period.

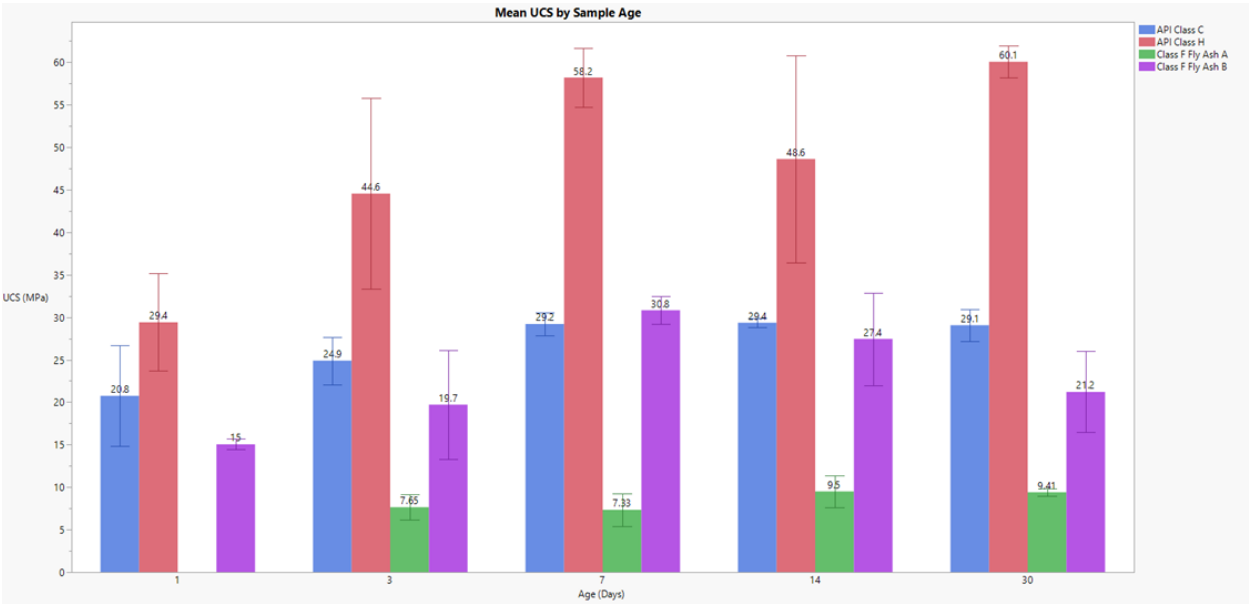

Figure 28 – UCS of the four tested materials across a one-month span. Note that in this experiment that Class F Fly Ash A failed to generate a 1-day test

API Class H cement consistently outperformed all other materials at every time interval. Class F Fly Ash A geopolymer performed the poorest, failing to generate a 1-day test sample and displaying no clear trend in UCS over time. While there was a 30% increase in UCS from 7 to 14 days, changes between other intervals were negligible.

Class F Fly Ash B geopolymer and API Class C cement exhibited intermediate performance. While Class C cement started stronger on day 1, Fly Ash B achieved a higher UCS by day 7 but then began to deteriorate, falling by 33% from its peak UCS of 30.8 MPa.

3.4.2.2. Chemical Composition Analysis Results

XRF output (**Figure 29**) provided an elemental breakdown of the materials. Due to the nature of XRF testing, the raw data did not perfectly represent the true component composition. Despite this, an effort was made to determine the compositional breakdown.

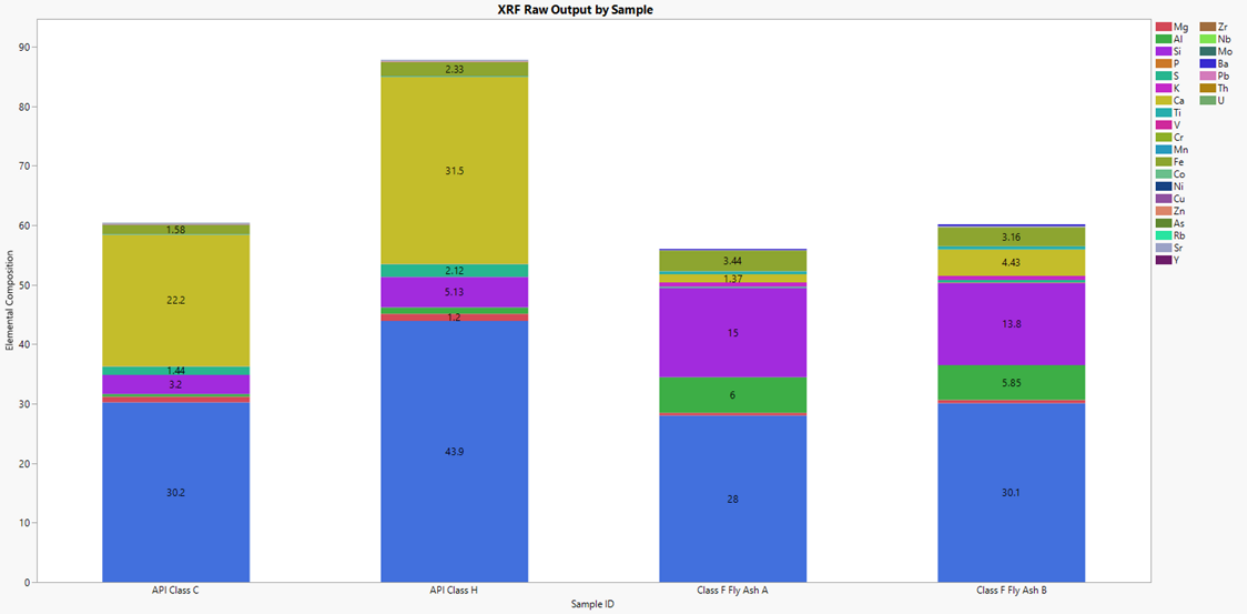

Figure 29 – Raw XRF output from the testing of the four materials used to generate cementing material, note that due to the nature of XRF the totals are not 100, nor the same across materials.

The totals for materials in both Class F Fly Ash samples were similar, differing by only 2%. Notably, Fly Ash A had 15% silica dioxide and 0.9% calcium oxide, while Fly Ash B had 14% and 2.9%, respectively. These small differences in composition appear to significantly impact UCS, with Fly Ash B performing better likely due to its higher calcium content.

3.4.3 Experimental Results Analysis and Conclusions

3.4.3.1. UCS Trends and Material Performance

UCS trends observed in this study offer critical insights into the mechanical performance of geopolymers and their comparison with traditional API-grade cement. The primary finding was that API Class H cement consistently demonstrated superior performance across all time intervals, with a strong upward trend in UCS over time. This indicates that, under the specified curing conditions, Class H cement is exceptionally reliable in terms of mechanical strength. This reliability is crucial for its application in securing tubulars in wellbores, where high compressive strength is necessary to ensure zonal isolation and pressure control.

In stark contrast, Class F Fly Ash A geopolymer failed to produce a 1-day sample and exhibited poor UCS across all tested intervals. The lack of a clear trend and the negligible changes in UCS suggest that the composition of Fly Ash A is not conducive to forming a geopolymer with adequate mechanical properties under the tested conditions. This poor performance underscores the variability and unpredictability associated with geopolymers derived from different fly ash sources.

Class F Fly Ash B geopolymer performed better than Class F Fly Ash A geopolymer, achieving a higher UCS by day 7. However, its performance declined significantly over time, dropping by

33% from its peak value. This decline suggests that while Fly Ash B initially forms a geopolymer with reasonable strength, its long-term stability is compromised. This could be due to several factors, including the incomplete polymerization of the alumino-silicate network or the destabilization of the geopolymer matrix over time.

The API Class C cement, while not as strong as Class H, showed more consistent performance compared to the geopolymers. It started stronger than Fly Ash B on day 1 and maintained a relatively stable UCS, indicating that traditional cement formulations still offer more predictable and reliable mechanical properties under the specified conditions.

3.4.3.2. Chemical Composition and Its Impact

The chemical composition analysis, particularly the XRF results, highlighted significant differences between the materials tested. Despite the raw data not perfectly representing the component composition, the differences in silica dioxide and calcium oxide content were notable. Fly Ash A, with 15% silica dioxide and 0.9% calcium oxide, performed poorly in UCS tests. In contrast, Fly Ash B, with 14% silica dioxide and 2.9% calcium oxide, showed better initial performance.

The higher calcium content in Fly Ash B likely contributes to its better performance, as calcium plays a crucial role in the geopolymerization process. The formation of calcium silicate hydrate (C-S-H) phases can enhance the mechanical strength of the geopolymer matrix. However, the long-term stability of these phases in a geopolymer matrix remains a concern, as evidenced by the decline in UCS over time for Fly Ash B.

3.5 Moisture and Temperature Curing Environment Variation and Slurry Additive Effect on UCS

The presence of water is near-certain in oil & gas wellbores and cannot reasonably be removed (but can be reasonably introduced). Therefore, understanding the impact to UCS of curing in a water-abundant (wet) environment versus a dry curing environment is of significant interest. Further, the effect on UCS of varying curing temperatures and slurry additives are also of interest. Experiments to study the UCS effects of applying these variables were performed. Test results were recorded and analyzed.

3.5.1 Experimental Procedure

Samples were generated and tested according to API standards. The Class F Fly Ash geopolymer recipe utilized for this experiment was taken from popularity among other works, prepared in accordance with API standards for the preparation of cement. One recipe contained no additive, and the other recipe included the additive sodium silicate (colloquially known as water glass). The testing times were 1, 3, 7, and 14 days. The heating temperatures were 75°C and 85°C degrees Celsius. All points of testing had 3 samples cured in each of the experimental conditions. The testing results of UPV and UCS were compared as a function of time across wet and dry testing environments, and across testing environments at same time curing intervals. The sample testing matrix is included as **Table 9**.

Table 9 – Sample Testing Matrix for Moisture, Temperature and Recipe Variation Testing (Devers et al., 2022a)

Experiment Number	Recipe	Curing Environment	Age (Days)	Temperature (C)
1	A	Oven	1	75
2	A	Water Bath	1	75
3	B	Oven	1	75
4	B	Water Bath	1	75
5	A	Oven	3	75
6	A	Water Bath	3	75
7	B	Oven	3	75
8	B	Water Bath	3	75
9	A	Oven	7	75
10	A	Water Bath	7	75
11	B	Oven	7	75
12	B	Water Bath	7	75
13	A	Oven	14	75
14	A	Water Bath	14	75
15	B	Oven	14	75
16	B	Water Bath	14	75
17	A	Oven	1	85
18	A	Water Bath	1	85
19	B	Oven	1	85
20	B	Water Bath	1	85
21	A	Oven	3	85
22	A	Water Bath	3	85
23	B	Oven	3	85
24	B	Water Bath	3	85
25	A	Oven	7	85
26	A	Water Bath	7	85
27	B	Oven	7	85
28	B	Water Bath	7	85
29	A	Oven	14	85
30	A	Water Bath	14	85
31	B	Oven	14	85
32	B	Water Bath	14	85

3.5.2 Experimental Results

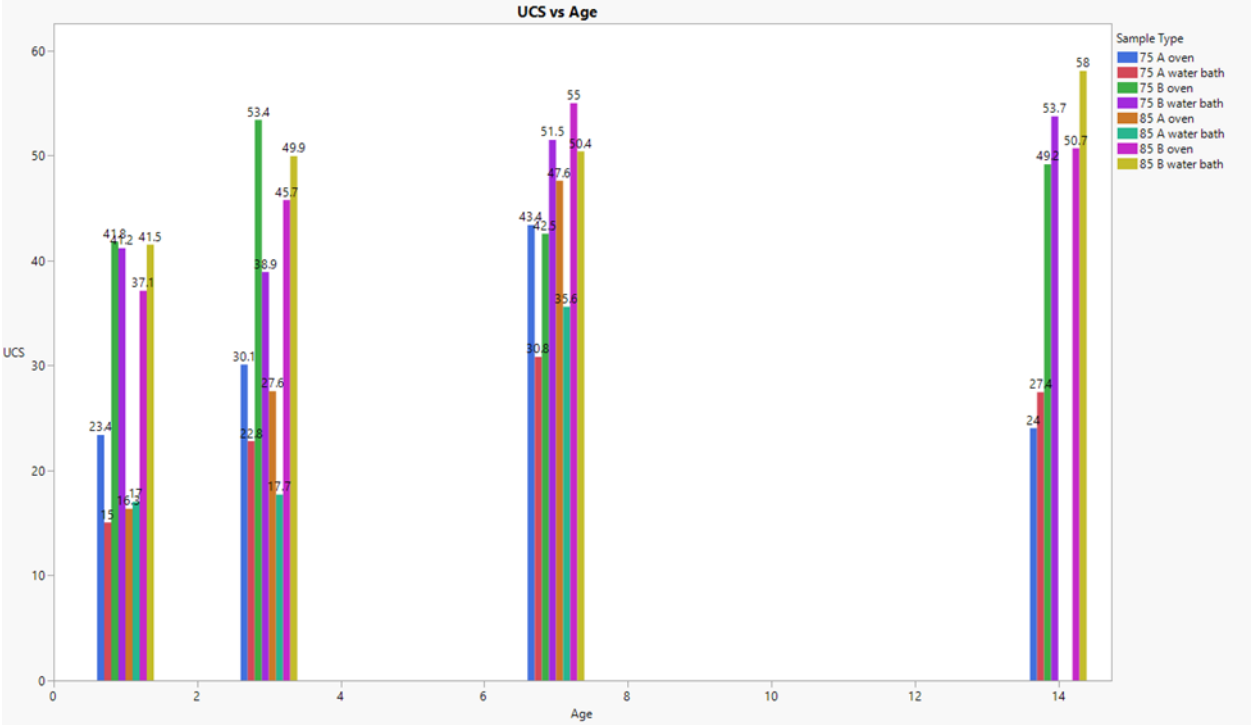

Figure 30 – Bar Chart mean UCS breakdown (Devers et al., 2022a)

Some of the samples listed in **Table 9** do not appear in the **Figure 30** data. Namely, the samples tested under the '85 A' subset of tests at the 14-day mark. The samples cured under those conditions were not able to develop a stable geopolymerization or failed during the curing process: the latter more common with the oven environment and the former more occurrent in the water bath.

Figure 30 displays the mean UCS for every cure time tested for every sample set. The gap caused by the failed-to-cure samples from the '85 A' testing block are apparent on the 14-day block. Additionally, on that same block, it's seen that the '75 A' block of samples show considerably weaker UCS than the previous testing period of 7 days. This could be evidence of thermal degradation and possibly explains why the samples at the higher temperatures are failing in-situ. In fact, the only samples that show no decrease at any point in time are the 'B water bath' block

of samples, both at 75ºC and 85 ºC. Furthermore, for all 3 sample sets that tested successfully on all 4 cure times, UCS decreased at the 14-day mark from the 7-day mark but showed improvement leading up to the 7-day mark. This suggests that potentially it is a combination of the lack of atmospheric, or free water, in the oven environment that is notably contributing to the degradation of all samples, as is made abundantly clear in **Figure 31**, **Figure 32**,and **Figure 33**.

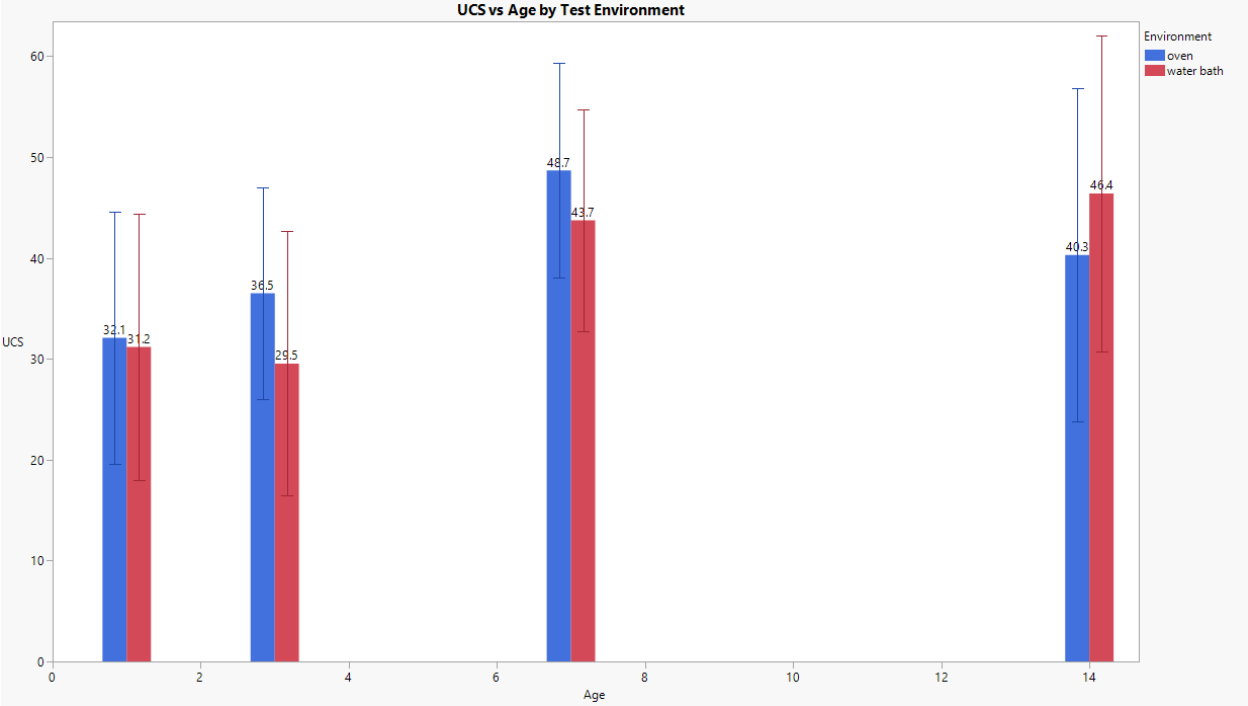

Figure 31 – UCS vs Age of sample sets grouped by environment only (Devers et al., 2022a)

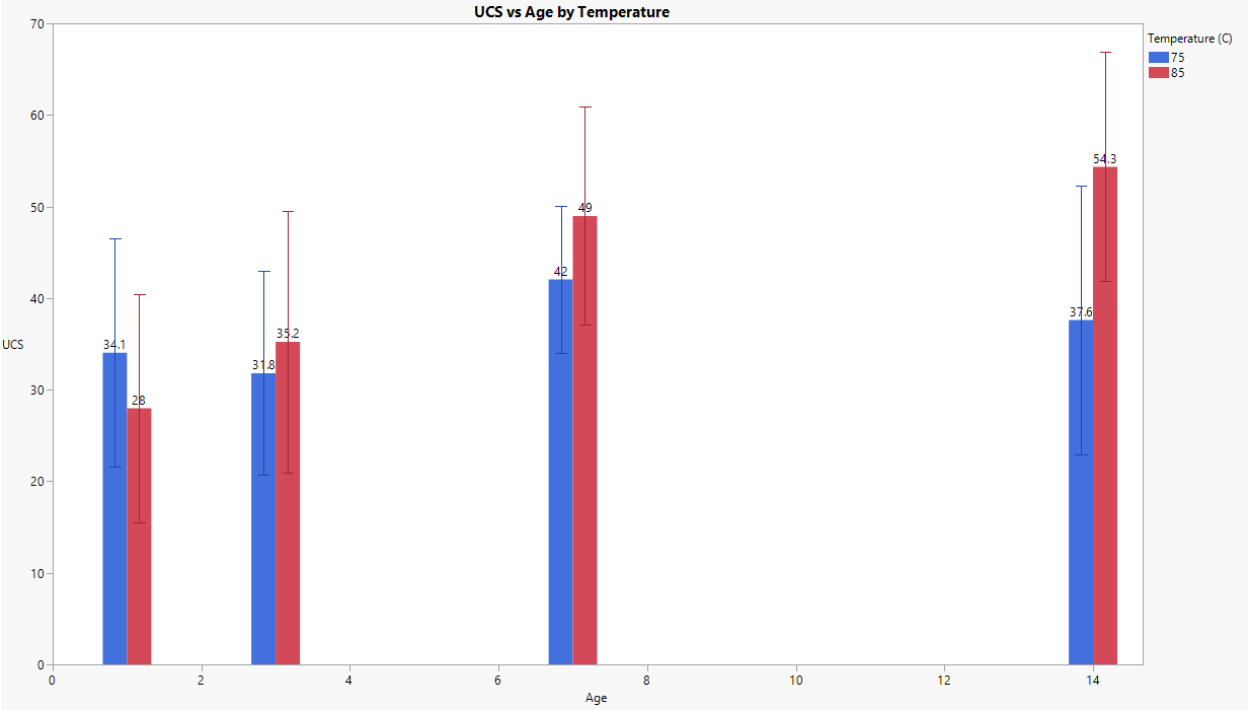

Figure 32 – UCS vs Age of sample sets grouped by temperature only (Devers et al., 2022a)

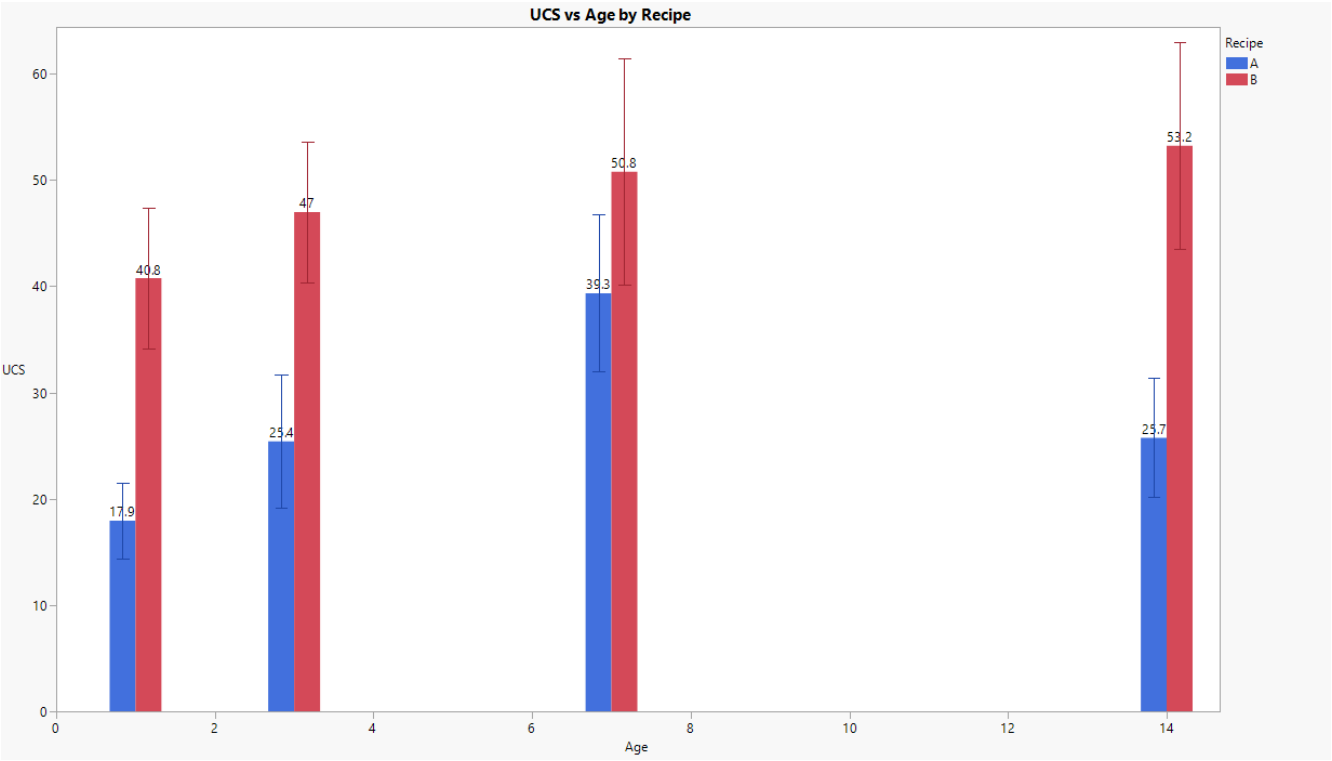

Figure 33 – UCS vs Age of sample sets grouped by recipe only (Devers et al., 2022a)

In this breakdown, the isolation of one parameter at a time more clearly depicts which parameters, and by potentially how much each parameter, may be influencing the resultant UCS. Again, the data does not account for sample failure at the 14-day mark, there is simply no contributing value at all. Even considering that, recipe B outclasses recipe A on average by over 100% at 14 days.

The least difference in UCS by binary parameter variation is in the testing environment itself, only displaying 6 MPa differential at the 14-day mark, however; the water bath increased 3 MPa while the oven decreased 8 MPa, again without considering the in-situ sample failure. This means the gap is larger than the tested 6 MPa variation, like the recipe difference since only recipe A failed. Finally, curing the sample at a higher temperature suggests a roughly 16.7 MPa increase in UCS at 14 days. This gap, however; is likely smaller as samples only failed at 85^{o}C.

3.5.2.1. UPV Results Analysis (Temperature and Moisture Variance)

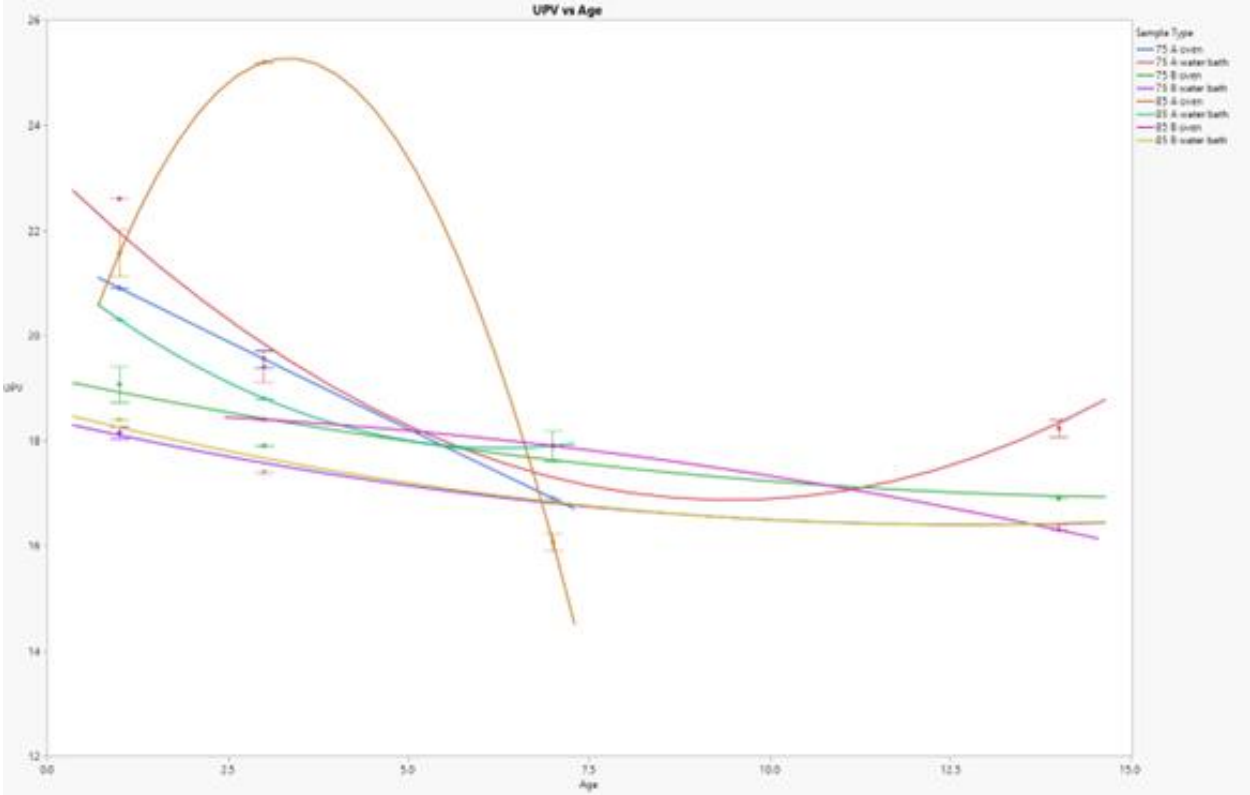

Figure 34 – UPV Trend line break out of sample set, quadratic line of fit (Devers et al., 2022a)

Figure 34 shows the results in the UPV as trends along age for each sample set. Trend analysis is investigated here as geopolymer UPV is under reported and the suggested trends are physically reasonable. Every sample set achieves both an acceptable R^2 and F-test, however; 3 of the sample sets have an R^2 value of .99 or higher. While .99 is not necessarily impossible, the presence of a value of 1 suggests the model is perfectly fit, which is highly unlikely to occur in experimental practice. Inspection of the data reveals the measurements were identically taken on the 3 samples that make up each of the 3 data points in both cases of the perfect correlative coefficient, and since there are only 3 points on the 2 of those plots, the quadratic model generates a perfect fit. This continues back to the previously discussed samples that failed prematurely during the curing process. The presence of those testing intervals would help to correct the trend away from being

overfit. Additionally, it is worthy to note that the sample set with the worst R^2 in UPV is also the worst in UCS, ’75 B Oven’.

UPV results showed that samples in water-rich environments had higher velocities. This indicates better internal structure and integrity. Samples cured at 85°C showed higher UPV values than those at 75°C.

UPV measurements provide valuable insights into the internal structure and integrity of materials. In this study, UPV was used as a non-destructive test to evaluate the quality and consistency of fly ash-based geopolymer samples cured under different conditions.

The UPV results revealed that samples cured in water-abundant environments exhibited higher velocities compared to those cured in dry environments. Higher UPV values indicate better internal structure and integrity, suggesting that water plays a crucial role in enhancing the geopolymerization process. In water-rich environments, the dissolution of fly ash particles is facilitated, leading to the formation of a denser and more cohesive matrix. This observation aligns with the UCS results, which also showed superior mechanical properties for samples cured in water-abundant environments.

The UPV results also indicated that samples cured at 85°C exhibited higher velocities compared to those cured at 75°C. Higher UPV values at elevated temperatures suggest a more extensive and robust geopolymer matrix. This finding is consistent with the UCS results, which also showed enhanced mechanical properties for samples cured at higher temperatures. The relationship between UPV and UCS underscores the reliability of UPV as a non-destructive indicator of material integrity.

The use of UPV as a non-destructive test offers several advantages. It allows for the assessment of internal structure and consistency without damaging the sample, providing valuable information on the quality and integrity of the material. UPV measurements can be used to identify defects, such as microcracks and voids, which may compromise the material's performance. In this study, the correlation between UPV and UCS results demonstrates the effectiveness of UPV in evaluating the internal structure and mechanical properties of fly ash-based geopolymers.

The UPV results also provide insights into the potential risks of thermal degradation. Samples cured at 85°C exhibited higher UPV values initially, but some samples failed during the 14-day curing period. The initial high UPV values suggest a strong and cohesive matrix, but the subsequent failures indicate potential thermal stability issues. This observation highlights the importance of monitoring both UPV and UCS to ensure the long-term performance of geopolymers.

In summary, UPV is a reliable non-destructive test that provides valuable insights into the internal structure and integrity of fly ash-based geopolymers. Higher UPV values indicate better internal structure and consistency, which correlate with superior mechanical properties. The use of UPV in conjunction with UCS measurements allows for a comprehensive assessment of material quality and performance. However, the potential risks of thermal degradation at higher temperatures warrant further investigation to ensure the long-term stability and integrity of geopolymers in geothermal applications.

3.5.2.2. UCS Results Analysis (Moisture, Additives and Temperature Variance)

UCS results revealed that samples in water-rich environments retained more strength. Samples containing the addition of sodium silicate exhibited significantly improved UCS. Samples cured

at 85°C exhibited higher UCS values compared to those cured at 75°C. However, some samples at 85°C failed during the 14-day curing period.

The UCS results indicate that the moisture content of the curing environment has a profound impact on the mechanical properties of fly ash-based geopolymers. Samples cured in water-abundant environments exhibited significantly higher UCS values compared to those cured in dry environments. This finding suggests that the presence of water plays a crucial role in enhancing the geopolymerization process, leading to improved mechanical strength.

Water facilitates the dissolution of fly ash particles and the subsequent formation of a gel-like structure that contributes to the overall strength of the material. In dry environments, the lack of sufficient moisture can hinder this process, resulting in lower UCS values. This observation aligns with previous studies that have highlighted the importance of water in the geopolymerization process (Fernández-Jiménez et al., 2005).

Moreover, the addition of sodium silicate in Recipe B improved the UCS by over 100% at 14 days compared to Recipe A, which did not contain an additive. This heavily suggests that the presence of sodium silicate either strengthens the base material past the normal reaction as a function of time, offsets thermal degradation as a function of time, or a combination of both. Many of the previously discussed works, such as those by Salehi et al., (2017a, 2017b, 2018) also show evidence that the inclusion of the sodium silicate material yields considerable UCS advantage, and this phenomenon is well documented. Sodium silicate acts as an additional source of silicate ions, which enhances the formation of the geopolymer matrix. This additive accelerates the dissolution of fly ash particles and promotes the formation of a denser and more cohesive matrix. The superior

performance of samples containing added sodium silicate indicates sodium silicate can significantly enhance the mechanical properties of fly ash-based geopolymers.

The influence of curing time on UCS was also evident in the results. Samples cured for longer periods generally exhibited higher UCS values. This trend suggests that the geopolymerization process continues to develop over time, leading to a stronger material. The 14-day curing period resulted in the highest UCS values, indicating that prolonged curing can enhance the mechanical properties of geopolymers. However, it is important to note that samples cured at 85°C experienced failures during the 14-day curing period. This observation suggests a potential thermal stability limit for fly ash-based geopolymers. At higher temperatures, the accelerated geopolymerization process may lead to the formation of microcracks and other structural defects, which can compromise the material's integrity. Therefore, while elevated temperatures can enhance the initial strength of geopolymers, they may also pose a risk of long-term degradation.

In summary, the UCS results highlight the critical role of the curing environment, additives, and curing time in determining the mechanical properties of fly ash-based geopolymers. Water-abundant environments and the inclusion of sodium silicate significantly enhance the material's strength, while prolonged curing periods contribute to the development of a robust geopolymer matrix. However, the potential thermal stability limit at higher temperatures warrants further investigation to ensure the long-term performance of geopolymers in geothermal applications.

3.5.2.3. Influence of Temperature on Geopolymerization

Temperature plays a critical role in the geopolymerization process and significantly impacts the mechanical properties of the resulting material. Samples were cured at two different temperatures,

75°C and 85°C, to evaluate the influence of thermal conditions on the performance of fly ash-based geopolymers.

The UCS results revealed that samples cured at 85°C exhibited higher UCS values compared to those cured at 75°C. This observation is consistent with the understanding that elevated temperatures accelerate the geopolymerization process, leading to the formation of a denser and more cohesive matrix. At higher temperatures, the dissolution of fly ash particles is enhanced, resulting in a more extensive and robust geopolymer matrix.

The enhanced UCS values at 85°C suggest that higher curing temperatures can significantly improve the mechanical properties of fly ash-based geopolymers. However, it is important to note that samples cured at 85°C also experienced failures during the 14-day curing period. This finding indicates that while elevated temperatures can enhance the initial strength of geopolymers, they may also pose a risk of long-term degradation.

The failures observed at 85°C suggest a potential thermal stability limit for fly ash-based geopolymers. The accelerated geopolymerization process at higher temperatures may lead to the formation of microcracks and other structural defects, which can compromise the material's integrity. Therefore, while elevated temperatures can enhance the mechanical properties of geopolymers, they may also introduce risks of thermal degradation over extended curing periods.

The influence of temperature on the geopolymerization process is further corroborated by the UPV results. Samples cured at 85°C exhibited higher UPV values compared to those cured at 75°C, indicating better internal structure and integrity. Higher UPV values suggest a denser and more cohesive matrix, which contributes to the overall strength of the material.

The relationship between temperature and geopolymerization is complex and multifaceted. While higher temperatures can accelerate the geopolymerization process and enhance the material's mechanical properties, they may also introduce risks of thermal degradation and structural defects. Therefore, it is crucial to carefully balance the benefits and risks associated with elevated curing temperatures to ensure the long-term performance of geopolymers in geothermal applications.

In summary, the influence of temperature on the geopolymerization process is evident from the UCS and UPV results. Higher curing temperatures enhance the mechanical properties of fly ash-based geopolymers by accelerating the geopolymerization process and promoting the formation of a denser and more cohesive matrix. However, the potential risks of thermal degradation and structural defects at higher temperatures warrant further investigation to ensure the long-term performance and stability of geopolymers in geothermal applications.

3.6 Influence of pH on UCS

The potential influence of the pH of the curing environment on the UCS of geopolymer samples was investigated, particularly to determine if the testing environment's pH might adversely affect the final UCS of the samples. To verify this, samples were cured in both fresh deionized water and reused water from previous tests. The results, shown in **Figure 35**, **Figure 36**, and **Figure 37**, indicate a clear improvement in UCS for samples cured in fresh water compared to those cured in reused water.

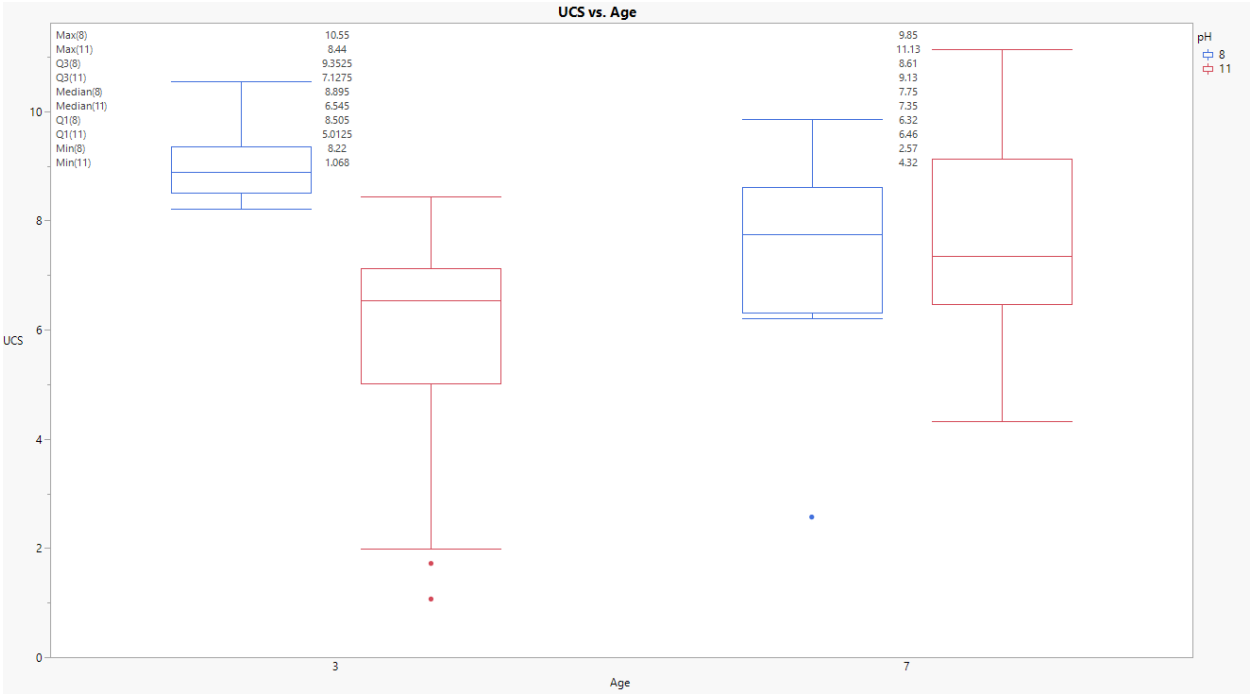

Figure 35 – Box and Whisker of 3- and 7-day tests by pH (Devers et al., 2022b)

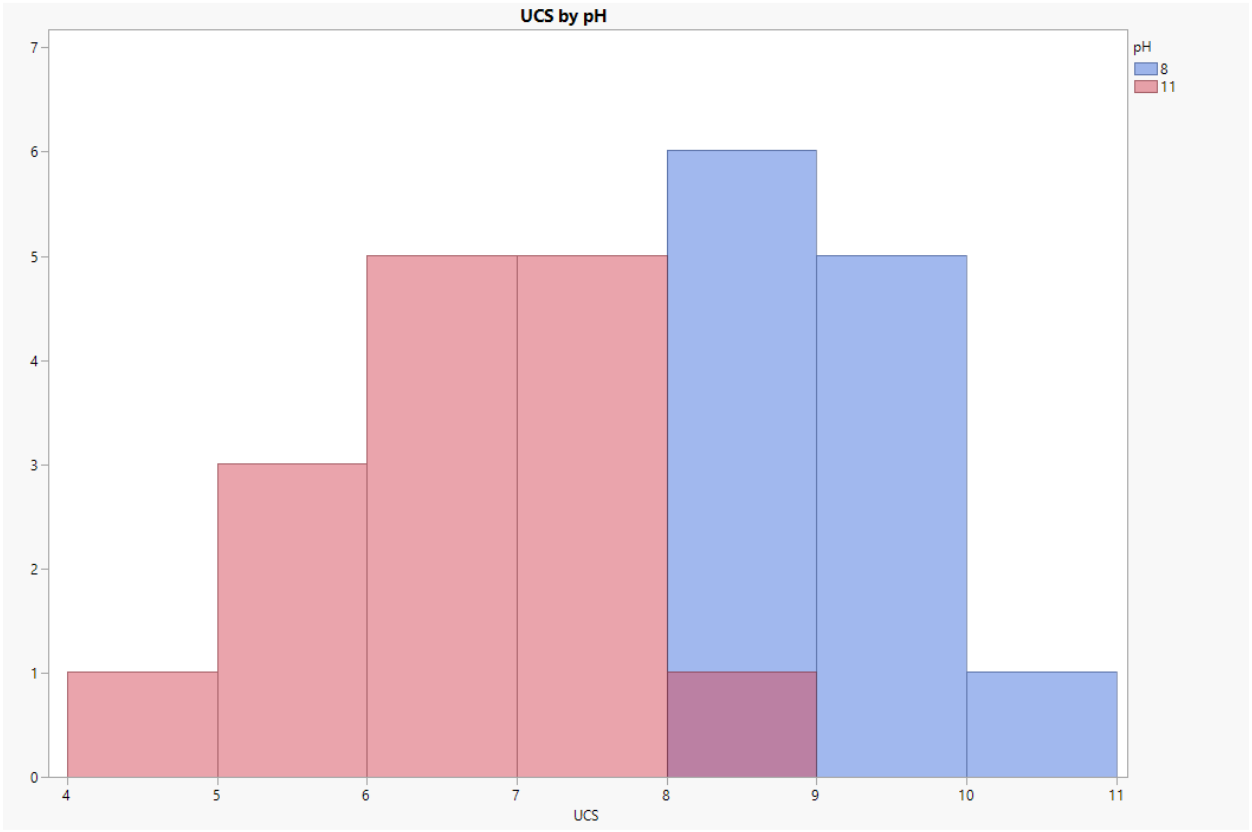

Figure 36 – 3-Day UCS by pH (Devers et al., 2022b)

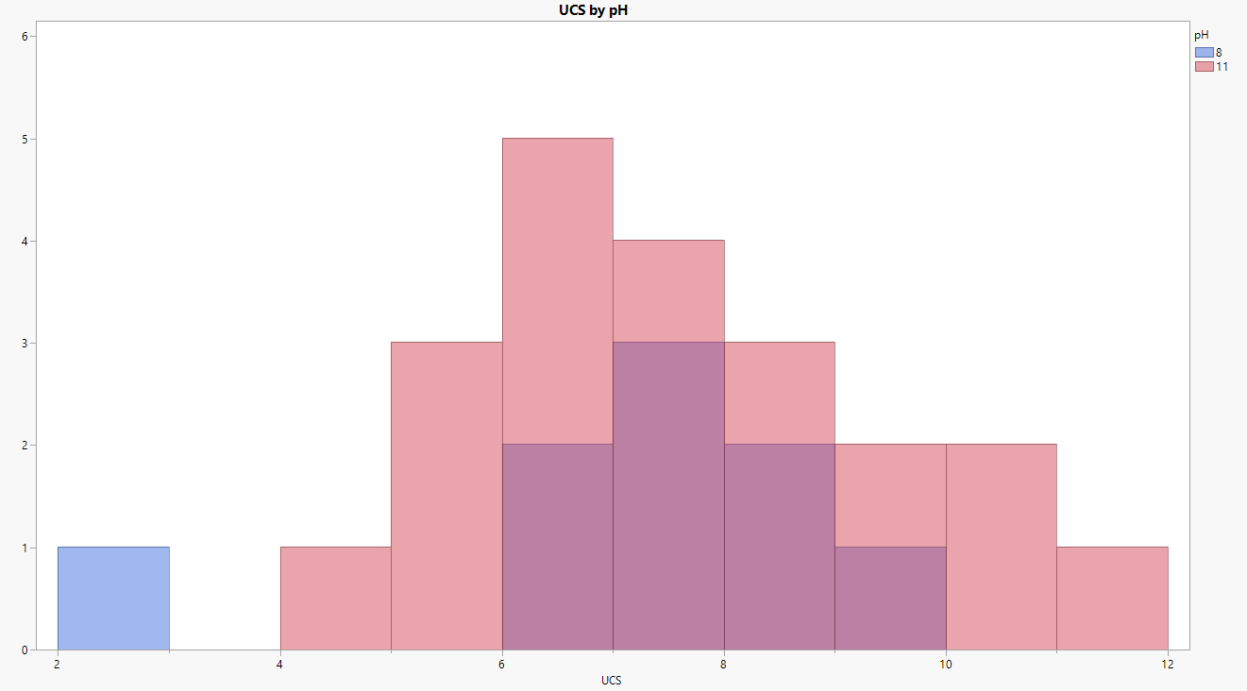

Figure 37 – 7-day UCS testing by pH (Devers et al., 2022b)

In the 3-day testing, samples cured in freshwater showed a significant increase in UCS, although the range of results remained wide, with over a 30% variation in UCS among the freshwater samples. This suggests that while the pH of the curing environment does influence the UCS, other factors also contribute to the observed variability. In the 7-day testing, the difference was even more pronounced, with freshwater samples displaying a much higher concentration of UCS values and a narrower range of results, barring one outlier.

The findings highlight the sensitivity of geopolymer cements to the curing environment's pH, which is a significant concern for practical applications. Water encountered subsurface can be contaminated with various natural compounds, resulting in a wide range of pH values. This variability in environmental pH could lead to inconsistent performance of geopolymer cements, affecting their suitability for wellbore applications.

The interaction between the geopolymer matrix and the curing environment is a complex process that can significantly impact the material's mechanical properties. The alkalinity of the curing solution plays a crucial role in the dissolution of alumino-silicate species from the fly ash and the subsequent polymerization reactions that form the geopolymer network. Variations in pH can alter the rate and extent of these reactions, leading to differences in the microstructure and strength development of the cured geopolymer.

Additionally, the presence of impurities and dissolved ions in the reused water could introduce further complexities in the geopolymerization process. These impurities might interfere with the formation of the alumino-silicate network or create weak points within the structure, contributing to the observed variability in UCS results. Therefore, maintaining a consistent and controlled curing environment is essential for achieving reliable and reproducible properties in geopolymer cements.

Further research is needed to systematically investigate the influence of different pH levels and the presence of various ions in the curing solution on the mechanical properties of geopolymer cements. Such studies could help identify optimal curing conditions and potential additives that can enhance the stability and performance of geopolymers in diverse environmental conditions. Developing standardized protocols for preparing and curing geopolymer samples will also be crucial for ensuring consistency and reliability in their performance.

When looking at the influence of the pH on the testing, the results are fairly improved from earlier analysis. In the 3-day testing, there is a clear improvement in samples tested in freshwater as opposed to the used water. While the UCS is improved, the range of results is not, with over a 30% variation in UCS even among freshwater testing samples. When reviewing the 7-day testing

samples, it is seen that the, baring one outlier, that the freshwater samples have a much higher concentration of UCS. In contrast, the used water had over a 250% sample variation which is highly concerning as natural wellbore conditions have water contaminated by natural compounds and may have a large range of potential pH values.

3.7 Surface Cracking of Geopolymer Samples Cured Under High-Temperature Conditions

The primary objective of this study is to investigate the surface cracking of geopolymer samples cured under high-temperature conditions. Specifically, the research focuses on the onset, progression, and impact of thermal cracking on the structural integrity of geopolymer samples. By doing so, it seeks to offer valuable insights that can inform future research and practical applications of geopolymers in thermally demanding environments. The study also aims to compare the performance of geopolymers in wet and dry curing conditions to understand how moisture influences crack development and material performance.

Understanding thermal cracking in geopolymers is crucial for their application in geothermal, high-temperature industrial processes, and infrastructure exposed to significant thermal variations. The study's findings will help optimize curing protocols, improve material formulations, and ensure the long-term durability of geopolymer-based structures. Additionally, this research will contribute to the broader knowledge of geopolymers, supporting their adoption in diverse environmental conditions.

This research is motivated by the need to verify the applicability of geopolymers in more environmentally challenging applications. As interest in geopolymers grows, additional scrutiny of the material is essential to ensure its reliability and performance under various conditions. The

study's scope includes the preparation of geopolymer samples, their exposure to controlled high temperature curing environments, detailed monitoring of surface cracking, and rigorous mechanical testing to assess the impact of thermal cracking on material strength.

3.7.1 Experimental Procedure

Geopolymer samples were prepared using a standardized mix design to ensure consistency across all test specimens. The mix consisted of Class F Fly Ash, an alkaline activator solution, and additional additives to enhance the material properties. The activator solution was a combination of sodium silicate and sodium hydroxide, which reacts with fly ash to form the geopolymer matrix. The samples were cast into cube molds with dimensions of 50mm x 50mm x 50mm, a common size for uniaxial compressive strength (UCS) testing. The casting process was carefully controlled to minimize air entrapment and ensure uniformity.

The curing conditions were designed to simulate both wet and dry environments at elevated temperatures. Samples were divided into two groups:

1. Wet Curing Environment: Samples were submerged in water and placed in an oven set to a high temperature (e.g., 80°C). The water environment aimed to simulate conditions where the material might be exposed to moisture, such as in geothermal applications. Wet curing helps maintain the hydration process, potentially influencing the development and propagation of cracks.
2. Dry Curing Environment: Samples were placed in the same oven without any water, representing arid or semi-arid conditions. Dry curing exposes the samples to thermal stresses without the mitigating effect of moisture, providing insights into crack behavior under extreme dry conditions.

To capture the full nature of the apparent sample cracking, samples were retrieved from the curing environments at regular intervals. Unlike traditional cement testing, where the intervals of curing grow larger, this study involved pulling samples from the heating environment daily for 14 days. This frequent sampling allowed for a high-resolution analysis of crack propagation over time, providing detailed data on the onset and development of thermal cracks.

To document the progression of surface cracks, each retrieved sample underwent controlled high-resolution photography. The samples were photographed from multiple angles using a digital camera equipped with a macro lens. This setup enabled the capture of fine details in the cracking patterns, which were later analyzed to determine the onset and progression of thermal cracking. The images were taken under consistent lighting conditions to ensure comparability across different samples and time points.

The photographs were analyzed using image processing software to quantify crack dimensions, density, and distribution. Parameters such as crack length, width, and depth were measured, providing a comprehensive dataset for understanding the cracking behavior. The visual documentation was complemented by qualitative observations, noting any distinctive features or anomalies in the crack patterns.

Following photographic documentation, the samples were subjected to UCS testing per API testing standards. The UCS tests were conducted using a universal testing machine, with the loading axis aligned with the direction of the apparent cracks. This alignment was crucial for assessing whether the observed cracks influenced the failure plane during compressive loading. The UCS tests provided quantitative data on the mechanical strength of the samples, which was then correlated

with the photographic evidence of cracking. This dual approach allowed for a comprehensive analysis of how thermal cracking impacts the structural integrity of geopolymers.

The UCS testing involved applying a uniaxial load to the samples until failure, recording the peak load and corresponding stress values. The stress-strain behavior was also monitored, providing insights into the material's deformation characteristics. The UCS values were analyzed statistically to identify trends and variations related to the curing conditions and crack development.

3.7.2 Experimental Results

The results of this study are presented in two main categories: qualitative observations from the photographic documentation and quantitative data from the UCS tests. The findings provide a comprehensive understanding of thermal cracking in geopolymers, highlighting the effects of curing conditions and the implications for material performance.

3.7.2.1. Photographic Observations

The high-resolution images captured during the experiment revealed distinct patterns of crack propagation in the geopolymer samples. In the high-temperature environments, cracks were observed to form as early as the first day of curing. The cracks typically initiated at the surface and gradually extended deeper into the sample over time. The images provided a visual record of the crack development, allowing for detailed analysis of the onset and progression of thermal cracks. **Figure 38** and **Figure 39** (Romero, et al., 2023) depict images of example samples used to investigate surface cracking.

Figure 38 – Class F Fly Ash -Neat Geopolymer (Romero, et al., 2023)

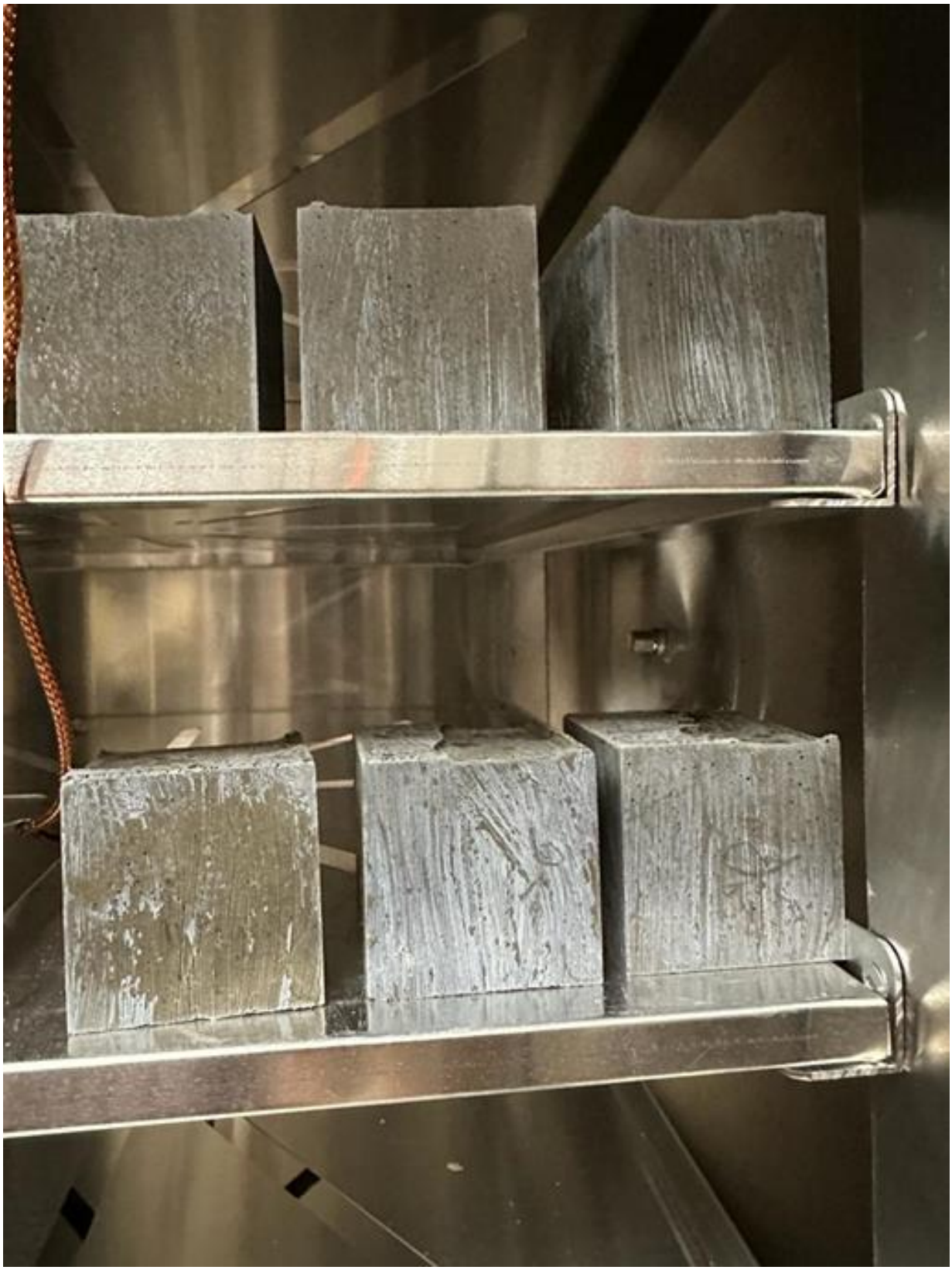

Figure 39 – Class F Fly Ash Sodium Silicate Geopolymer (Romero, et al., 2023)

In the wet curing environment, the presence of moisture appeared to mitigate the severity of cracking to some extent. However, significant cracking still occurred, particularly at higher temperatures. The cracks in wet-cured samples were generally less pronounced than those in dry-cured samples, suggesting that moisture plays a role in influencing the cracking behavior. The wet-cured samples exhibited a more gradual progression of cracks, with smaller crack widths and less extensive crack networks compared to the dry-cured samples.

In contrast, samples cured in the dry environment exhibited more extensive and severe cracking. The lack of moisture likely exacerbated the thermal stresses within the material, leading to more rapid and extensive crack propagation. By the end of the 14-day curing period, many of the dry-cured samples had developed deep, interconnected crack networks. The dry-cured samples showed larger crack widths, higher crack densities, and more extensive crack networks, indicating a greater susceptibility to thermal cracking.

3.7.2.2. UCS Testing Results

The UCS test results provided valuable insights into the mechanical implications of thermal cracking. The UCS values of the samples showed a clear trend of decreasing strength with increasing curing time, particularly in the dry environment. The presence of surface cracks correlated with a significant reduction in UCS, indicating that the cracks were not merely superficial but affected the internal structure of the samples. The reduction in UCS values was more pronounced in the dry-cured samples, highlighting the detrimental impact of thermal cracking on mechanical strength.

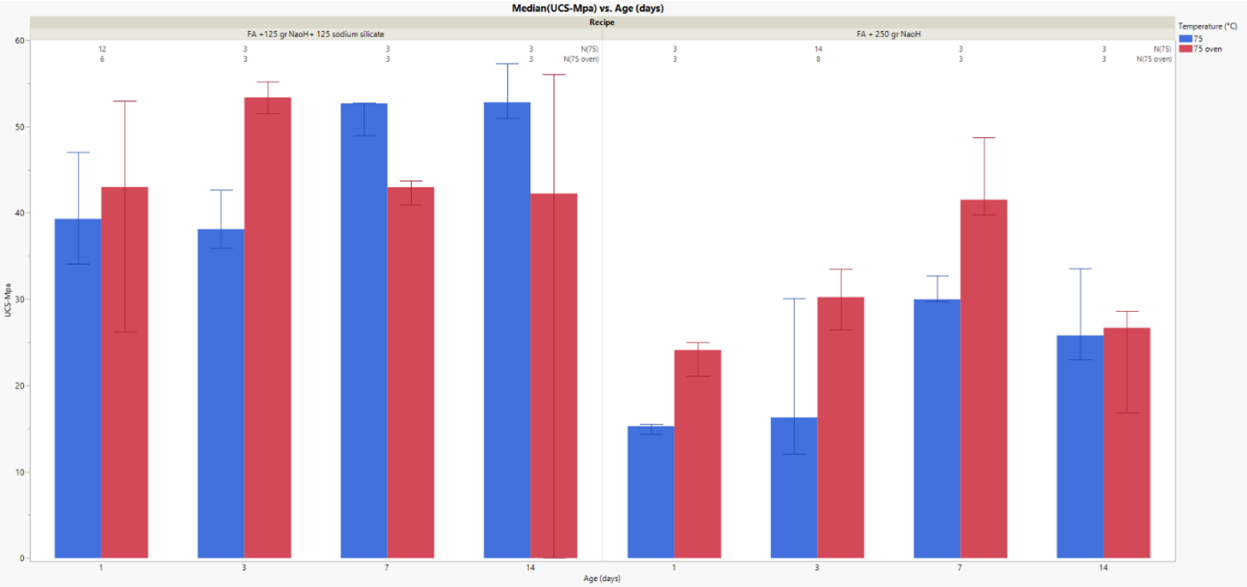

Figure 40 – Side by side UCS comparison of the impact of sodium silicate on geopolymer curing

For wet-cured samples, the UCS values also decreased over time, but the reduction was less severe compared to the dry-cured samples. This suggests that while thermal cracking does occur in wet environments, its impact on the mechanical strength is somewhat mitigated by the presence of moisture. The UCS values for wet-cured samples remained relatively higher, indicating better structural integrity and resistance to thermal cracking.

The comparison of UCS values and photographic evidence allowed for the identification of critical points where cracking significantly affected the structural integrity of the samples. For both wet and dry environments, there were distinct moments when the UCS values deviated sharply from the expected trend, coinciding with the onset of visible crack networks. This deviation typically occurred after several days of curing, indicating a threshold beyond which the cracks significantly compromise the material's strength.

The statistical analysis of UCS values revealed significant differences between the wet and dry curing conditions. The dry-cured samples exhibited a more rapid decline in UCS values, with a higher degree of variability, suggesting greater susceptibility to thermal cracking. The wet-cured

samples showed a more gradual decline, with less variability, indicating a more stable mechanical performance under high-temperature conditions.

Chapter 4 Enhanced Investigation Techniques

This chapter aims to introduce enhanced investigation techniques for studying geopolymer samples and advanced analysis techniques for processing new and existing geopolymer data. The aim of this is to present options for future sample testing as well as potentially interpolating information from existing literature. Much of the previous discussion in this document focuses on elements of mechanical performance relative to either the quality of the fly ash or the environment in which the reaction occurs in. Arguably the most dominant and important question underlying those discussions is that of the consistency of the reaction. Mechanical tests focus on the macroscopic behavior, or more specifically, the nature of multiple cured samples. The focus of the tests in this section are to more closely investigate the more individualized aspects of cured samples, such as porosity and material distributions.

4.1 Application of Nuclear Magnetic Resonance

Nuclear Magnetic Resonance (NMR) is an analytical technique which measures the interaction between atomic nuclei and an external magnetic field. Specifically, the method observes the magnetic properties of certain atomic nuclei that possess a property referred to as spin. Spin is the effect that arises when the nuclei contain unpaired protons or neutrons (Kleinberg et al., 1993). The most studied nuclei are that of hydrogen. While other nuclei, such as carbon, nitrogen and phosphorus can be studied, the observation of hydrogen is the most useful when discussing wellbore cementing materials and binders. NMR is a widely used method in a multitude of oilfield and geophysical applications. The method has been utilized extensively to study porosity and pore size distribution, as well as fluid saturation, composition, density, and wettability. When specifically discussing the application of NMR on studying cement, the method can be applied in

many of the same ways as has been applied in understanding geological formations. Cement is generally regarded as an impermeable solid with relatively high porosity. This means, in theory, many of the same observation targets NMR is used to study in reservoir rock can be done in cement.

4.1.1 Applications of NMR in Cement Studies

Saleh provides a comprehensive review of NMR work specifically targeting cement studies (Saleh et al., 2021). Additionally, authors such as Li establish that very little literature is focused on studying hydration, but rather the silica content of the sample (Li et al., 2019). The review conducted by Saleh had a few key findings, including that pore radius can be determined and the influence of thermal effects on hydration. Overall, the study also showed differences in mixing conditions were reflected on NMR determined porosity, shown in **Figure 41**.

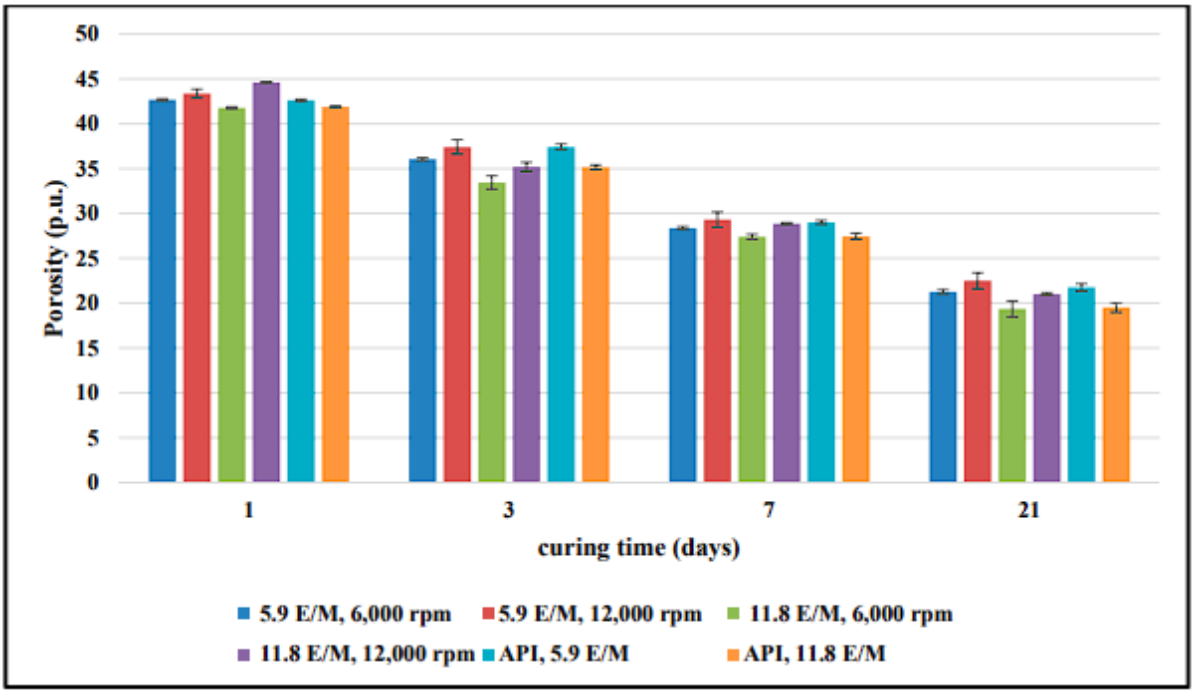

Figure 41 – Analysis conducted from an NMR review, indicating strong porosity difference and a function of time and minor variance as a function of mixing of cement (Saleh et al., 2021)

While the use of NMR is well studied on cement, it is far less so regarding geopolymer material. The under-utilization of NMR could partly be explained due to NMR not being a heavily deployed tool in civil engineering or the relative newness of the geopolymer in oil and gas considerations. This again results in the majority of information available focused on non-generalized geopolymer reactions. Additionally, as NMR is not limited to capturing information about the hydrogen nuclei, some NMR investigations focus instead on the silica, such as the work by Tsai et al., (2010). The focus of this work is well outside oilfield applications yet is generally representative of the current direction of the NMR review on geopolymer.

If the progression of NMR development for cement, as indicated by Saleh, is a precursor to the progression of geopolymer NMR testing, the next advance will be in H NMR instead of Si NMR. If the observations made in cement review, namely pore structure and relationships to mixing conditions, can be expected to be represented in geopolymer samples, would be very beneficial.

While research indicates small pore structure is beneficial to geopolymer, there is not a quick method of testing this with much detail.

4.1.2 Experimental NMR-Based Geopolymer Investigation

While most proton NMR work relating to cement studies the medium- and long-term curing of the material, this Work investigates the short and medium term of the material. The aim is to investigate the potential presence of key differences during the critical setting of the material between the pouring of the sample into the curing environment and the hardening of the material in its curing environment. This Work establishes a testing matrix for comparing the short-term curing behavior of geopolymer against that of two API cement types, Class G and Class H. Each of the slurries were generated under API conditions using the same approach as previous experimental sections.

Figure 42 – Vials for pouring slurry into for NMR testing

Each of the generated slurries were split into a series of vials such as shown in **Figure 42**. These vials are marked with a non-interactive ink to denote the name of the sample. After being poured, the sample denoted with a '-0' was immediately subjected to NMR while the rest were transferred into a water bath to cure at a temperature of 75°C. Single slurry division into multiple samples ensures controlled curing conditions without constant removal from the curing environment to prolonged NMR testing. It is presumed here that the slurries generated are homogenous in nature.

Tests were conducted on each sample every 45 minutes for the first three hours before transitioning to multi-day curing times. Readings for both NMR – T1 and NMR – T2 peak time and porosity were recorded for each test, as well as the relaxation time vs cumulative relaxation time for both T1 and T2. The results of this can be seen captured in **Table 10**.

Table 10 – Results of NMR testing of Cement and Geopolymer Slurries

Name	Type	Curing Time (min)	T1 (ms)	T1 (% Porosity)	T2 (ms)	T2(% Porosity)
H - 0	API Class H Cement	0	14.125	43	7.94	48.1
H - 30	API Class H Cement	45	11.2	48.6	6.31	53.5
H - 60	API Class H Cement	90	10	48.2	5.62	53.1
H - 90	API Class H Cement	135	7.94	41.2	5.01	44.1
H - 120	API Class H Cement	180	3.55	42.7	2.82	44.9
H - 150	API Class H Cement	225	1.41	36	1.26	41.8
H - 180	API Class H Cement	270	0.89	40.3	0.89	44.9
FAF - 0	Class F Fly Ash Geopolymer	0	5.62	2.1	3.98	10.1
FAF - 30	Class F Fly Ash Geopolymer	45	7.94	0.54	2	11.2
FAF - 60	Class F Fly Ash Geopolymer	90	7.94	0.6	1.59	10.7
FAF - 90	Class F Fly Ash Geopolymer	135	7.08	0.41	1.56	10.7
FAF - 120	Class F Fly Ash Geopolymer	180	1259	1	1.59	10.9
FAF - 150	Class F Fly Ash Geopolymer	225	0.89	0.75	1.59	10.2
FAF - 180	Class F Fly Ash Geopolymer	270	0.11	0.88	1.41	10.2
G - 0	API Class G Cement	0	17.8	57.6	7.08	65.1
G - 30	API Class G Cement	45	5.62	48.1	3.16	55
G - 60	API Class G Cement	90	1.59	38.3	1.26	42.9
G - 90	API Class G Cement	135	1.12	34.8	1	37.6
G - 120	API Class G Cement	180	0.794	35	0.89	38.3
G - 150	API Class G Cement	225	0.89	38.5	0.89	39.6
G - 180	API Class G Cement	270	1	36.6	0.89	37.3

4.1.3 NMR Testing Discussions

To better interpret the test results, both the T1 and T2 relaxation times and the respective porosity values have been plotted in **Figure 43** through **Figure 46**.

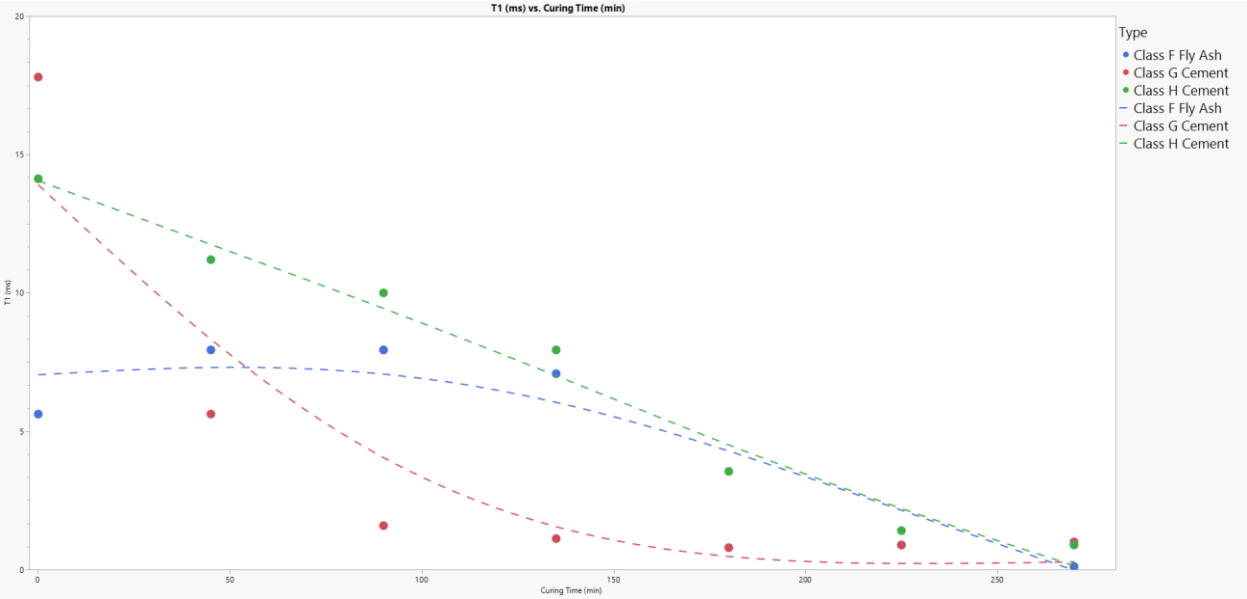

Figure 43 – NMR T1 relaxation time as a function of cure time for tested material – dashed line for visual guidance only

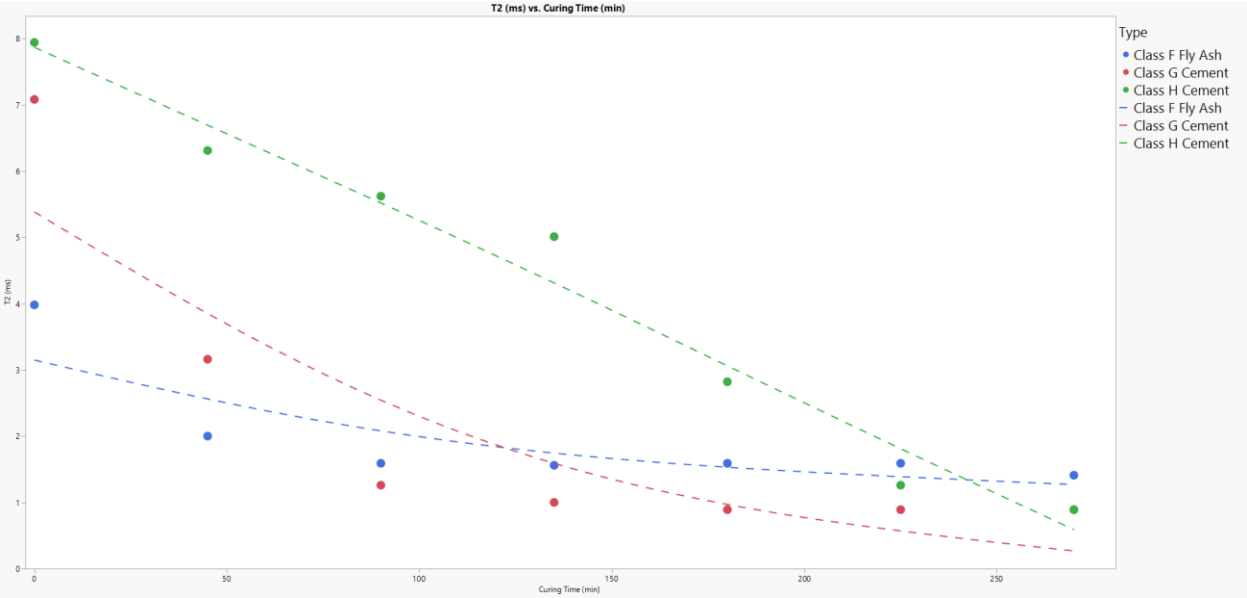

Figure 44 – NMR T2 relaxation time as a function of cure time for tested material – dashed line for visual guidance only

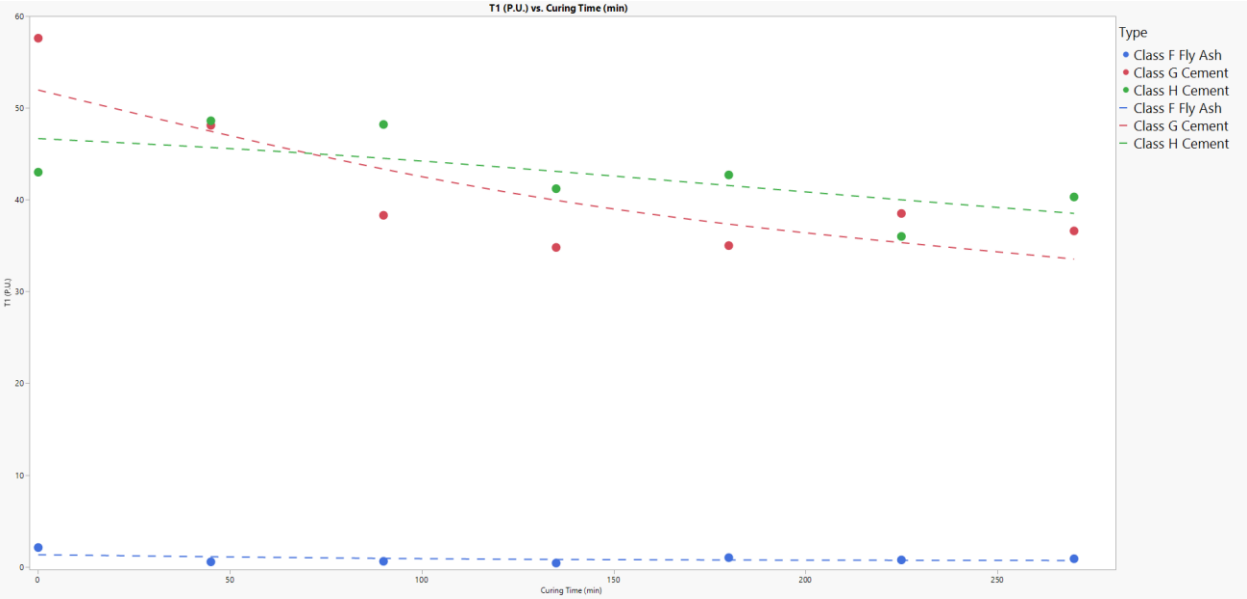

Figure 45 – NMR T1 determined porosity as a function of cure time for tested material – dashed line for visual guidance only

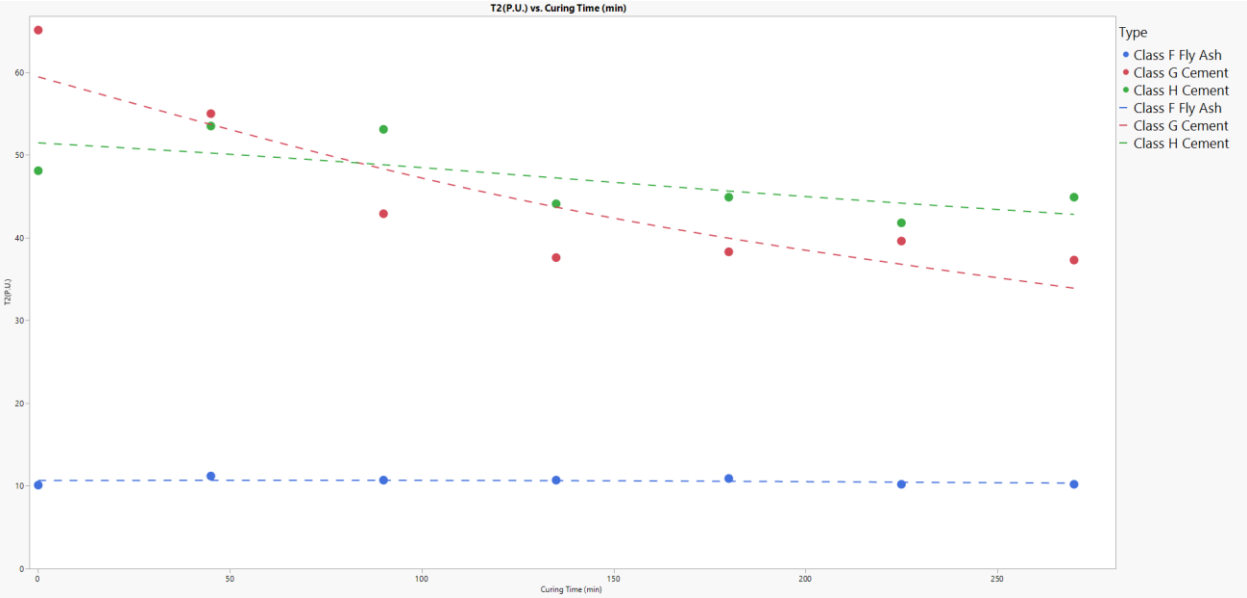

Figure 46 – NMR T2 determined porosity as a function of cure time for tested material – dashed line for visual guidance only

The strong relationship between relaxation time, both T1 and T2, and curing time exhibited by the two cement classes. It is also observed that there is a strong relationship between these relaxation times and cure time with the geopolymer samples. These findings are in line with the work done by Ardelean (2021) discussing all of the influences that drive the relaxation time down; a

phenomenon which is considered generally good in cement. Additionally, the drop in porosity as a function of cure time is also covered by Ardelean (2021), and for many of the same reasons. When looking at the geopolymer porosity as a function of time, however, there is virtually no relationship. The study of the reaction volume and reaction behaviors has been well documented by John and Lothenbach (2023) when it comes to cement. Given that there is virtually no change in porosity as a function of time in geopolymers, and the curing volume of the geopolymers is fixed; this suggests the material reaction volume goes unchanged during the hardening process. Additionally, since there is no evidence that the fluid within geopolymer pores during the curing time do not absorb or otherwise dissipate, it is unclear whether any additional leaching at that pore barrier occurs. As the NMR testing suggests there is still stranded fluid, the unknown nature of that fluid poses risk with regards to practical deployment.

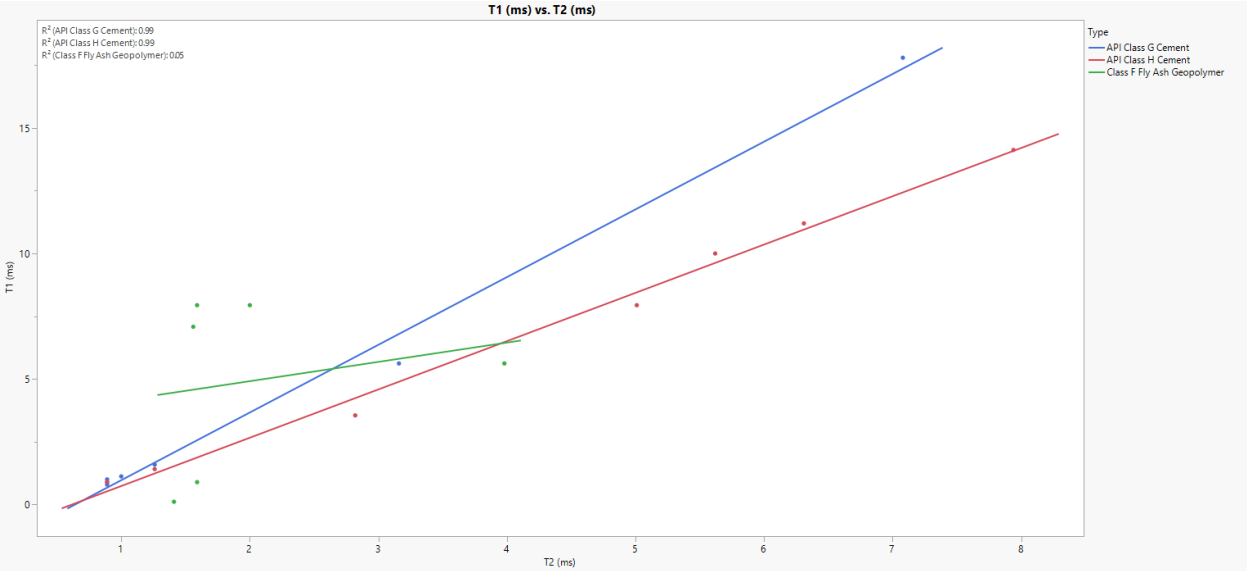

Figure 47 – Trends between relaxation times in cured materials, noting the lack of one on geopolymers

The variation in initial curing behavior is more clearly illustrated by **Figure 47**, indicating the linear relationship between T1 and T2 relaxation times in traditional OPC is strong, while the relationship is again virtually non-existent regarding geopolymers. This again points to critical

differences between the behaviors in OPC and of geopolymers, suggesting that using existing testing and deployment practices for field-level practices is likely to result in large variations between expected and actual performances.

4.2 Scanning Electron Microscopy for Microstructural Analysis

Typically, the maximum resolution of the human eye is roughly .1mm. For scale, the head of a sewing needle is about 1mm across. Fly ash particles, however, are much smaller than the head of a pin, ranging from 10-20 microns in diameter. As fly ash is the primary material used in the formulation of geopolymers, this resolution range establishes an approximation of the range a tool needs to observe and study the substructure of a geopolymer sample. While there are several tools that can achieve resolutions in the magnitude of microns, it is possible for the particle distribution in fly ash to be much finer. Sodium silicate, a primary component of fly ash, can have a particle diameter in the range of a few nanometers when used in detergents and soaps. This particle size is critical, a conclusion derived from the analysis of **Table 11**. While that process typically requires additional refining of the fly ash to achieve that particle size, if the goal is to obtain a better understanding of the geopolymerization process via observation of the substructure of a geopolymer sample, it is appropriate to use what is known to be possible to formulate an experimental workflow.

While there are several observational tools capable of achieving the established resolution, a scanning electron microscope offers a few ideal benefits over other tools such as a Transmission Electron Microscope (TEM) or a Light Microscope (LM). Unlike TEM or LM, Scanning Electron Microscopy (SEM) is not a direct imaging tool, rather an indirect imaging tool. Instead of the transmitted electrons directly creating the image, SEM observes the interactions between the

electron beam and the sample to generate an image. There are a series of interactions that occur when the electron beam hits the sample, and it is the nature of these interactions which result in the creation of a sample image. **Figure 48** gives a generalized depiction of the type of information emitted by a sample subjected to an electron beam.

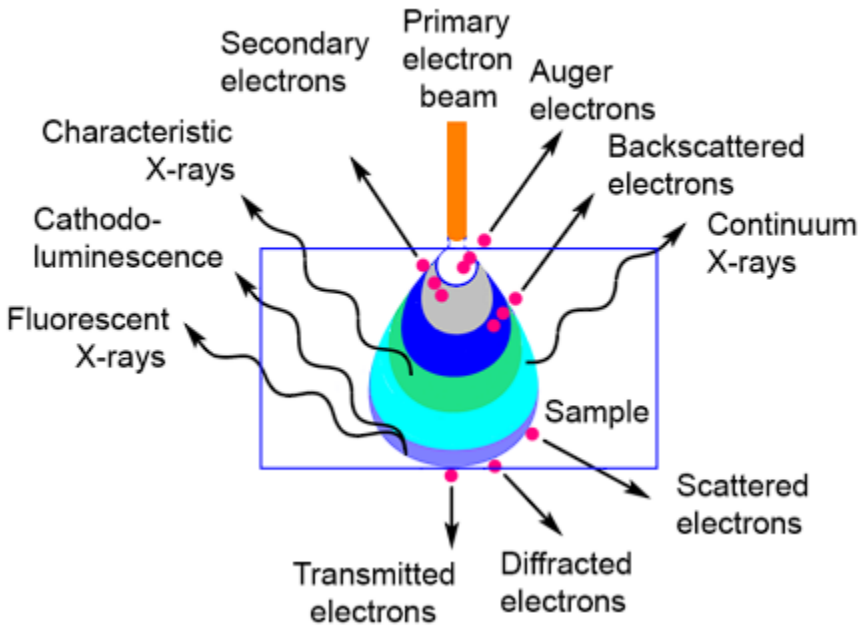

Figure 48 – Representation of the Teardrop interaction volume with emitted signal types (Sharga et al., 2021)

The use of SEM to study characteristics of geopolymers is available in literature, especially to study the influence of additives or specialty curing methods on the geopolymer slurry. **Table 11** provides a brief review of different investigations on geopolymer samples using SEM as part of the experimental procedure.

Table 11 – Review of Geopolymer SEM Research

Author	Sample Type	Additives	Composition Analysis	Resolution Indicator (microns)	Findings
Gonçalves et al., 2023	Metakaolin	Red Mud Residue	Yes	10	No adsorption loss with inclusion of high residue amounts
Wan et al., 2021	BFA-GP	Cd2+ & Pb2+	Yes	20	Experimental adsorption in line with pseudo-second order kinetic models
He et al., 2022	FCC Catalyst and Steel Slag	Waterglass	Yes	100	Stronger Alkaline activators result in improved UCS
Amin et al., 2022	Multiple	Multiple	Yes	20	Specific mixtures with high molar inclusions yielded far better structural development and resultant UCS
Sonal et al., 2022	Fly Ash Class F	Multiple - concrete	Yes	1	Geopolymer beams outperformed OPC beams in every UCS test
Chan & Zhang, 2022	Fly Ash Class F	GGBS	Yes	20	Pore size distribution yielded larger voids at temperatures above 400 Celsius

Table 11 – Review of Geopolymer SEM Research

Author	Sample Type	Additives	Composition Analysis	Resolution Indicator (microns)	Findings
Chindaprasirt et al., 2021	Fly Ash	Limestone	Yes	1	Geopolymer offers requisite mechanical strength needed for current standards for acid leeching while offering key improvements from current solutions
Kovářík et al., 2021	Metakaolin and slag	Ceramic Filler	Yes	5	Material remained geochemically stable at over 1000 Celsius, but issues may arise before 1300 Celsius is achieved
Szabó et al., 2022	Fly Ash	Perlite	Yes	10	While changes in the formation of the material result in the need for additional testing, critical geopolymer structures are present in the lightweight formation
Rodrigue Kaze et al., 2021	Metakaolin and Meta-halloysite	Sodium Silicate	Yes	50	Higher silica modulus results in higher initial yield stress

Table 11 – Review of Geopolymer SEM Research

Author	Sample Type	Additives	Composition Analysis	Resolution Indicator (microns)	Findings
Shee-Ween et al., 2021	Fly Ash Class F	Sodium Silicate	Yes	50	Ideal room temperature samples achieved a UCS value of over 110 MPa at the 28-day mark
Sajan et al., 2021)	Fly Ash Class F	None	Yes	10	While 12M and 14M solutions generated higher UCS at lower curing temperatures, at higher curing temperatures 10M solution performed better
Simão et al., 2021	Metakaolin and Biomass Fly Ash	Stone cutting Waste, Sodium Silicate	Yes	50	Efflorescence can be minimized, but subsequent analysis needs to be conducted on the resultant mixture for additional mechanical insights
Mohsen et al., 2022	GGBFS	RGP	Yes	5	Hydrothermal curing resulted in the formation of hexagonal zeolite structures and high mechanical properties

Table 11 – Review of Geopolymer SEM Research

Author	Sample Type	Additives	Composition Analysis	Resolution Indicator (microns)	Findings
Güngör & Özen, 2021	Clinoptilolite, Mordenite, Analcime	None	Yes	50	Clinoptilolite resulted in the best mechanical properties
Gomes Silveira et al., 2022	Red Mud	Glass waste, Portland Cement	Yes	100	The inclusion of 5% OPC material was twice as beneficial at 0M activator than any other combination of additive and molarity
Mayhoub et al., 2021	Fly Ash	None	Yes	50	Humid curing environments are extremely beneficial to all aspects observed
Zhang et al., 2022	Metakaolin	Magnesium salts	Yes	5	While both salts induced negative effects, MgCl2 was strictly negative while MgSO4 warrants further investigation due to influence on pore structure

Table 11 – Review of Geopolymer SEM Research

Author	Sample Type	Additives	Composition Analysis	Resolution Indicator (microns)	Findings
Osholana et al., 2020	Fluidized Bed Combustion Bottom Ash	Sodium Silicate, Kaolin	Yes	N/A	When reduced to a usable particle size, bottom ash can reach reasonably high strength, 31 MPa, by the 7-day curing mark.
Mendes et al., 2022	Chamotte	Waste Glass	Yes	10	Presence of waste glass promoted the formation of N-A-S-H gel and zeolitic species in the pastes.
Min et al., 2022	GGBFS and Fly Ash	None	Yes	100	Determined that NS activated samples performed better than NH activated under freeze-thaw conditions
Alvee et al., 2022)	Fly Ash	Nano-silicas and CA's	Yes	20	Inclusion of additives resulted in more than a 33% increase in the UCS, and microstructure analysis identified self-healing C-S-H presence.

Table 11 – Review of Geopolymer SEM Research

Author	Sample Type	Additives	Composition Analysis	Resolution Indicator (microns)	Findings
Ahmed et al., 2021	Ferrosilicon slag and Aluminum Slag	None	Yes	200	The industrial slag ingredients utilized can formulate a lightweight construction brick compound with a UCS of 6.1 MPa
Mudgal et al., 2021	Fly Ash	Red Mud	Yes	5	SEM indicated the presence of red mud may be simultaneously causing a closely packing geopolymer gel and acting as filler in generated void space
Hui-Teng et al., 2021	Fly Ash	Ladle furnace slag	Yes	10	While there was an increase in UCS generated from the inclusion of the ladle furnace slag, the improvement was only 4.1% and likely only acted as filler material

Table 11 – Review of Geopolymer SEM Research

Author	Sample Type	Additives	Composition Analysis	Resolution Indicator (microns)	Findings
Pawluczuk et al., 2021	Fly Ash	Multiple - concrete	Yes	1	The strongest samples were generated with an activator molarity of 10M. Additionally, at lower temperatures the inclusion of recycles aggregates improved strength at the cost of durability
Reddy Bellum, 2022	Fly Ash	GGBFS	Yes	N/A	Indications of bond quality from UPV testing suggest GPC is of sufficient quality to be utilized in construct pavement
Tan et al., 2022	Fly Ash and Calcined Kaolin	None	Yes	1000	Foamed geopolymer sphere indicate outstanding potential as a Cu(II) adsorbent for wastewater remediation
Carvalheiras et al., 2023)	Metakaolin	Red Mud	Yes	5	Indications that the lead uptake of this geopolymer type is comparable to previously studied powdered materials

Table 11 – Review of Geopolymer SEM Research

Author	Sample Type	Additives	Composition Analysis	Resolution Indicator (microns)	Findings
Kanagaraj et al., 2022	Fly Ash and GGBFS	Multiple - concrete	Yes	10	Inclusion of sodium silicate waste at high amounts resulted in the highest recorded UCS value, over 40 MPa
Rodrigue Kaze et al., 2022	Metakaolin or Halloysite	Sodium Silicate	Yes	50	Microstructural analysis indicated homogenous geopolymer network, but silica content notably impacts formation
Tahwia et al., 2022	GGBS	Waste Glass, Silica Fume, Sand	Yes	10	The application of heat on the UCS development was large, improving the best performing sample from 126 MPa to 152 MPa

When researchers image geopolymer samples with an SEM, most of time, the research also experimentally determines the composition of the source material. This is important, as while the basics of the geopolymer reaction are understood, the constant pursuit for understanding the impact of additives or contaminants often results in formulating the geopolymer and studying the subsequent substructure. The benefit of this trend is that most well documented SEM images are

coupled with very accurate compositional breakdowns. These breakdowns are critical for traditional understanding of cementing material and for new and developing data driven methods.

4.2.1 Machine Learning Integration of SEM

The widespread development of machine learning algorithms has made image analysis a much faster process. Historically, when analyzing SEM images for example, a subject matter expert would review the image at a fine enough resolution to identify characteristics of interest, a time-consuming endeavor, especially when there is a large quantity of images. Image analysis can be especially problematic for investigating substructure heterogeneity, a topic of interest in geopolymer research. In theory, a homogeneously mixed slurry generated from a homogeneous source, i.e. fly ash or API cement bags, should produce statistically similar samples. Experimental results highlighting large variances in geopolymer performance, however, introduce questions on the homogeneity of the slurry under API mixing conditions. Discussed by Devers et al., (2022a, 2022b) in the investigation of large UCS variance across like-curing conditions of same source geopolymer samples. By using SEM, it is possible to prepare and generate a set of images across multiple samples for analysis. But, as SEM only images a fraction of a sample, determining how much of a sample must be imaged to get a representative amount is necessary.

Once a large and sufficient data set of quality images is collected, the time it traditionally takes to analyze all the images can be greatly reduced by use of a trained machine learning algorithm. The most common method for identification of images or image features is a neural network. The concept of a neural network was to create a computer algorithm that interpreted information in a manner similar to the way a human brain perceives information. To illustrate this concept by example, a house is comprised of features such as windows, doors, a lawn, a roof, and maybe a

chimney. A neural network can be trained to identify these features, and depending on how many of these features the algorithm can detect, attempt to identify if the image is or is not a house. Developing this idea, the model can be trained on house-adjacent images as well, such as mobile homes, office buildings, and maybe even cars. So, while a house and a car both have doors, a car has wheels. A car and a mobile home might both have doors and wheels, but a mobile home might have lawn space. This idea can be developed and refined to a near-infinite degree. The exact manner by which neural network models make decisions is unknown because neural networks are essentially black box decision processes. **Figure 49** shows a detailed diagram for a convolutional neural network.

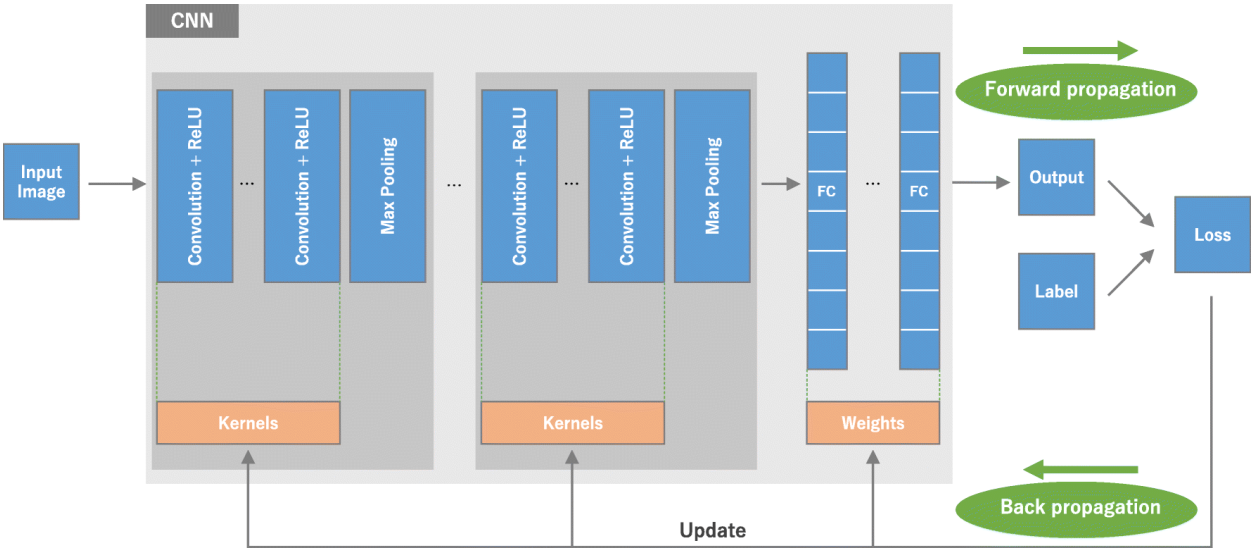

Figure 49 – Detailed breakdown of a potential Convolutional Neural Network design (Yamashita et al., 2018)

The layers between the input and output are called hidden layers and are the ‘black box’ portion of the model (Wei Koh & Liang, 2017). For understanding how the process can be adapted to SEM images, the understanding of how hidden layers work is not critical. What is important, however, is to acknowledge that while the user may define the features of interest on an image, how that information is extrapolated out to a dataset is hidden.

Tools have been specifically developed to build models to quickly analyze features in large SEM data sets. One such tool, 'ilastik', works by allowing the user to trace regions of interest with a particular color (Berg et al., 2019). The more a particular feature is traced, the more confident and accurate the model becomes at identifying untraced sections of the image. Part of why this method is effective on SEM images is that SEM images do not have color. Additionally, features of varying atomic numbers will show up as distinct greyscale values. These SEM image traits tend to enable the models to train faster at an accurate level. This approach is beneficial, as a full image analysis at high resolution can be done at a quicker pace and at a more comprehensive pace.

To study variance of the substructure of samples cured at identical conditions, there are potential experimental procedure obstacles to manage. The first is SEM sample preparation time relative to the sample age. If geopolymers do change substructure as a function of time, samples being placed under the microscope in the first 24 hours will be the most sensitive. Second, samples undergoing SEM are typically polished and subject to ion milling to generate the most refined image. These processes take time to execute. To image three different samples from the same mold, the sample preparation process should occur in parallel for all samples.

If a process which allows the samples to undergo parallel preparation is adopted, the images should be imaged in quick succession. The time in which a sample spends in the SEM is mostly dependent on how long it takes the system to pull the vacuum combined with the time it takes to align the sample and optimize the image. Most likely, for early cure time investigations, executing this process successfully would be incredibly challenging, but less so at cure times of 3 days or more. In addition to the challenges of sample preparation and image acquisition, the problem of image scope is not resolved.

Assume the resolution required to capture the scope of information desired from an SEM image of a geopolymer sample is known. Then assume that image is only .1% of the area of the already reduced sample in the microscope chamber. A .1% representation may not generate confidence to establish structural consistency. To manage this, a special SEM process to programmatically take several images in a grid formation can be used. A 10 by 10 grid of images, each comprised of .1% surface area captures 10% of the surface area of the sample. The benefit of this method is it allows the SEM to set the resolution desired of an image and then construct a large map of the sample at the desired resolution. Downsides of this method include increased time under the microscope and 100 times the amount of information to process.

This is where the real benefit of machine learning models becomes evident. Since the images are greyscale, the image greyscale is relative to the atomic value of the substructure, and the question of study is consistency not composition, it would be possible to deploy the machine learning to determine the number of specified features on each image from the grid and the location on the grid. This process can then, in turn, be used to generate a surface feature map to further investigate if there are any patterns in feature occurrences. This process can then be expanded to observe not only samples from the same slurry cured for the sample time and in the same environments, but generally to all samples using the sample source material and activating material. The construction of this model using a control data set, a set of images collected from samples explicitly for this purpose, could be used as the foundational information for the model. The data collected and model constructed could then branch out, incorporating similar enough SEM images from literature to investigate differences between the control set and the literature. If the control samples are investigated for additional characteristics, such as composition, UCS, and UPV, it may then be

possible to use the differences in feature analysis from the model and other characteristics to build additional models.

This concept was first presented by Devers (2023) as a conference presentation at the 2023 American Association of Drilling Engineers National convention. The work, primarily a proof-of-concept, suggested if a broken sample quality geopolymer sample could be systematically imaged and the resultant images trained a neural network, would work as systematic approach in future SEM testing. The workflow for this process can be seen in **Figure 50**.

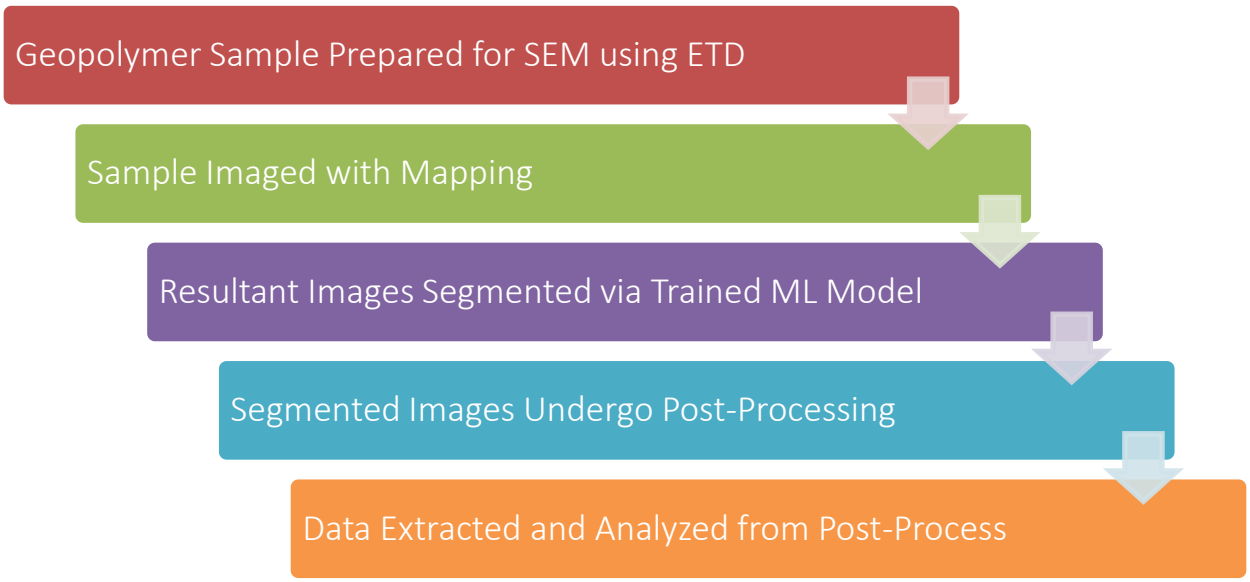

Figure 50 – Workflow for adopting SEM images into a feature identification neural network

While the limitations of the SEM process used were image resolution, the determination was that most critical formation information was available at relatively lower resolution. This greatly reduced not only the negative effects of charging which occur at higher resolution but reduced the amount of sample preparation needed. This in turn greatly reduces the amount of time between the sample being extracted from the curing environment to getting the sample under the SEM.

The idea is more straightforward than some of the literature on this topic. Prime examples of this include the works of Moro et al., (2021) and Sheiati et al., (2022). Both recent works focus on the difficulty of both generating and processing the information generated from SEM images and discussing factors from charging to simply breadth of information. The work by Sheiati discusses a method similar to the proposed machine learning method, not just identifying features, but also upscaling. By use of SegNet, a neural network model for semantic image segmentation, the schematic for which can be seen in **Figure 51**, is much more complex than the method proposed for large-scale analysis.

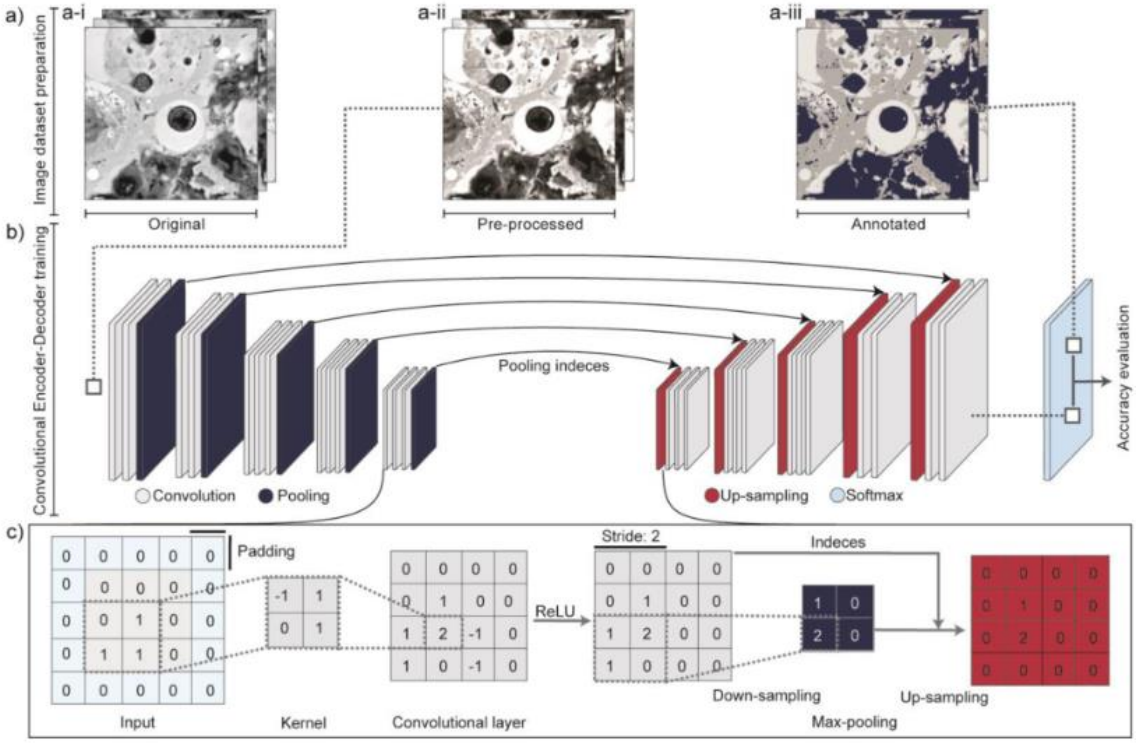

Figure 51 – SegNet schematic for processing backscatter images of geopolymers from SEM (Sheiati et al., 2022)

Complexity considerations aside, the results show the Convolutional Neural Network (CNN) approach is generally very successful. The work reports only a small number of training images were required to see valid models across the image set. The work also indicates more images would be beneficial, as the work shows an increase in the image results in an increase in image clarity at

magnification. The results of this work are a strong indicator that a large-scale generalized model for feature classification is possible. The second work, by Moro et al., (2021) focuses more on predicting the issues potentially associated with SEM and Scanning Electron Microscopy-Energy Dispersive Spectroscopy (SEM-EDS) style investigations, especially nano-micro pore shapes. While this work is focused almost entirely on simulated data from Monte-Carlo simulations, the considerations brought forward by the work indicate considerations for the issues addressed in large-scale image acquisition (Moro et al., 2021). This Work will take two approaches for the application of machine learning image analysis. The first of the methods will use supervised image segmentation as discussed above to segment the images for subsequent analysis. The second of the methods will deploy entirely unsupervised methods.

4.3 SEM Images

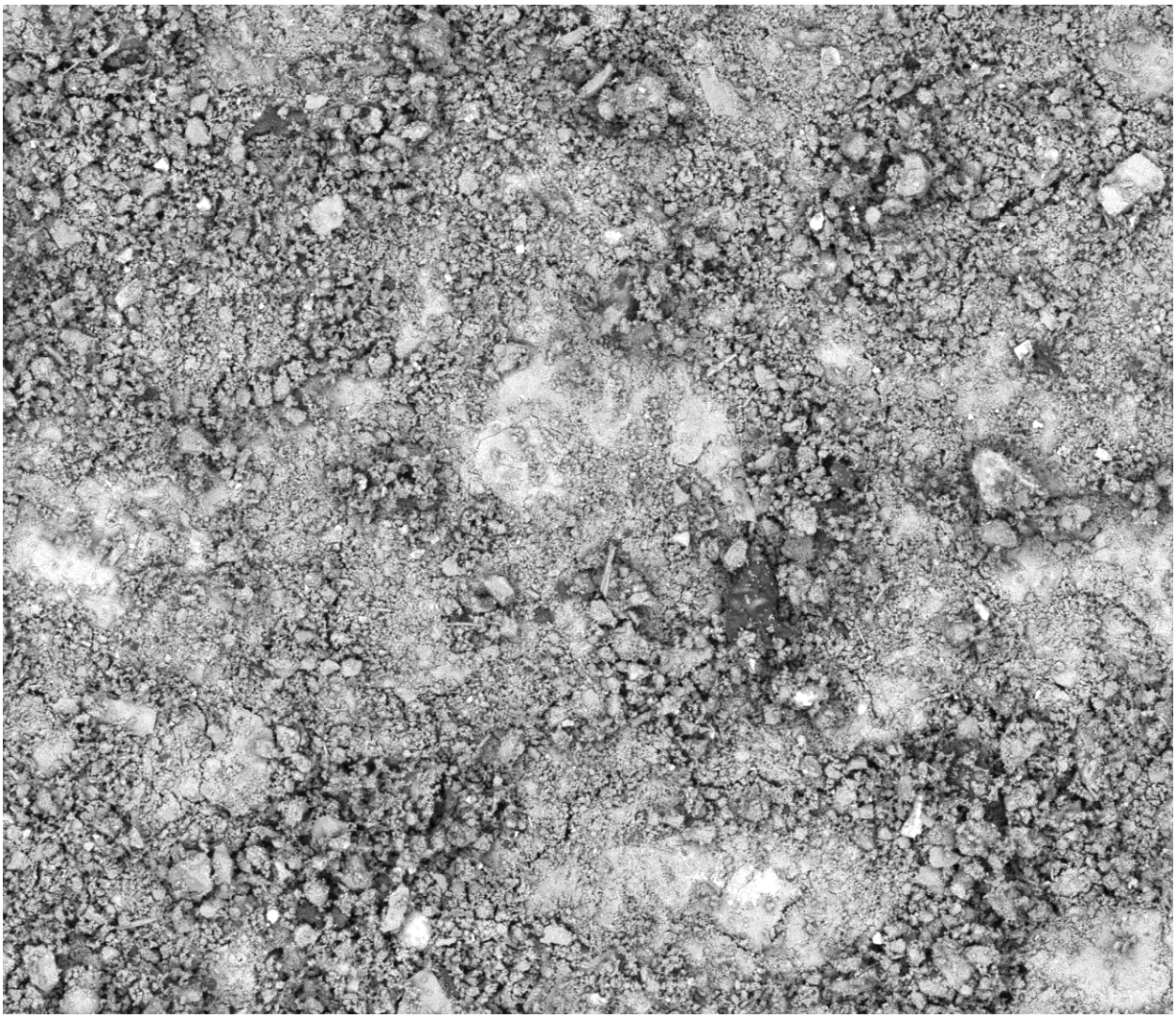

Figure 52 – The first of the 169 SEM images, grid location 1,1

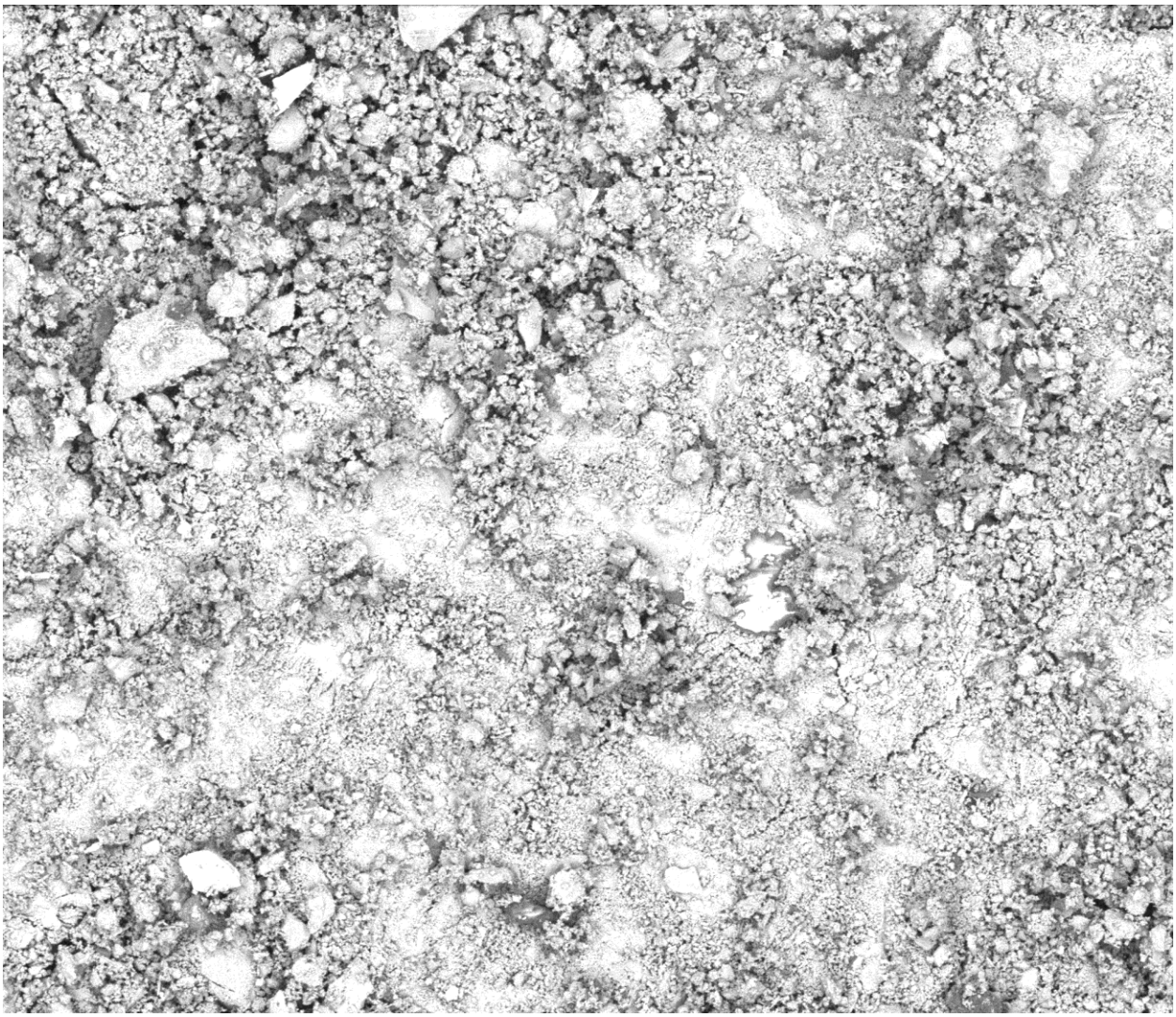

Figure 53 – Last of the 169 SEM images, grid location 13,13

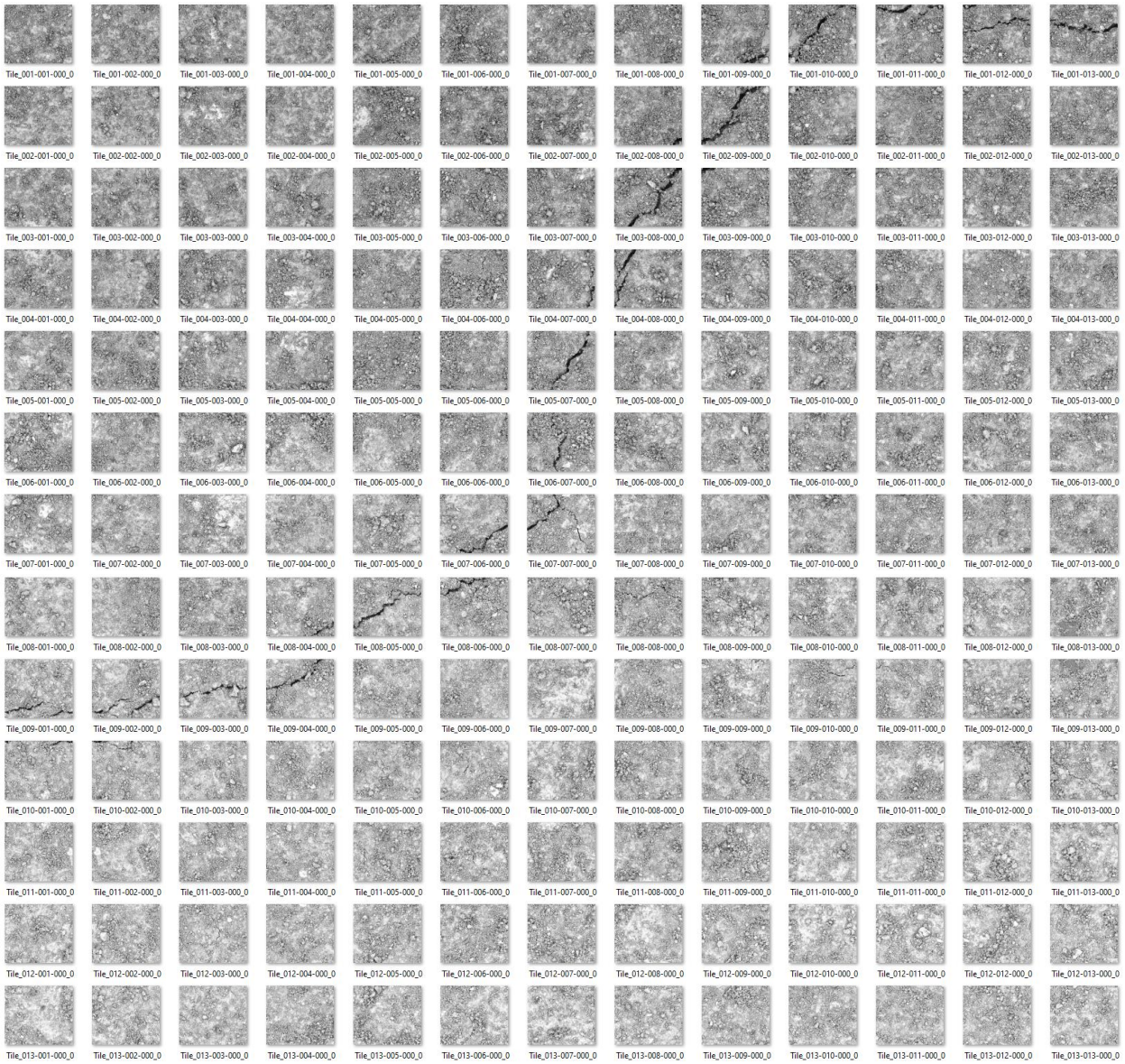

Figure 54 – SEM Image grid, noting the fracture propagated from the top right to the mid left

4.4 Supervised Image Segmentation

Following the workflow from **Figure 50**, the collection of images needed to undergo a segmentation process. **Figure 55** showcases some of how the manual segmentation process works. In this case, the image was manually split into a series of black and white filters targeting different regions of the original SEM image. In this case, **Figure 52** is the original image.

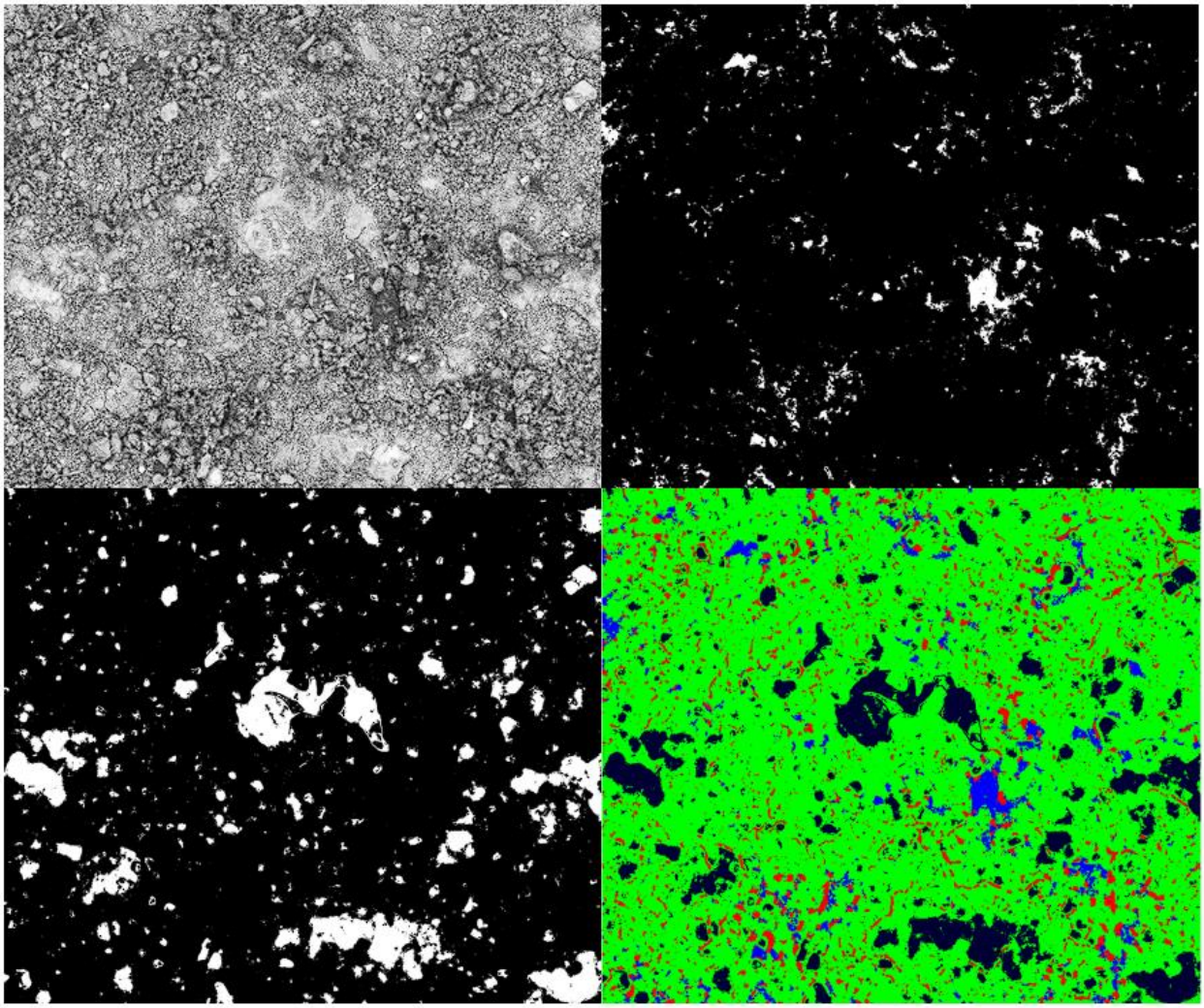

Figure 55 – An example of how the ilastik segmentation tool helps isolate target regions and highlight variance for investigation

The process continues by first determining how many segments, or groupings of information, are wanted. In this case, the target areas of interest were regions of visible compaction or consolidation, regions of poor consolidation, regions of impurities, and pores and fractures. Due to the lack of available target literature to use as a foundation for targeting specifically either aluminum or silicate contributions visibly, this was the only remaining supervised approach. Using the bottom right segment of **Figure 55** as training data, the remaining 168 images were segmented using neural net tools. The resultant segments were the converted to area data and plotted spatially to generate

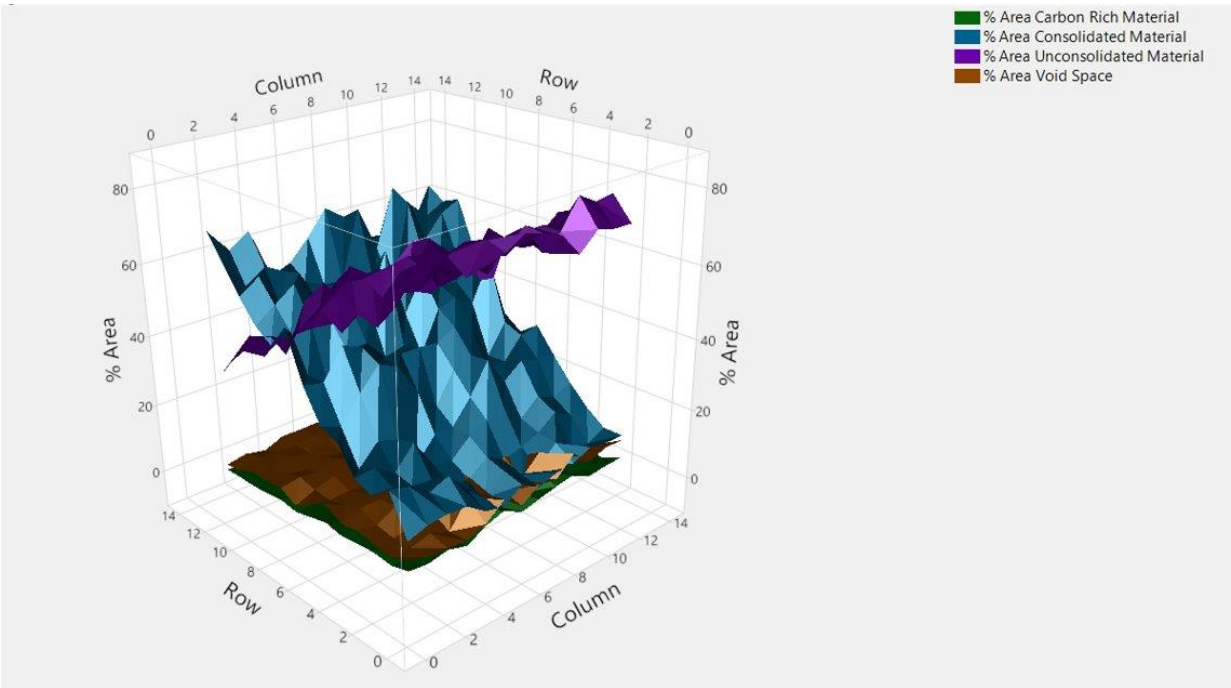

Figure 56 – 3D plot of the contributions of area of each image tile for the composite 2D image

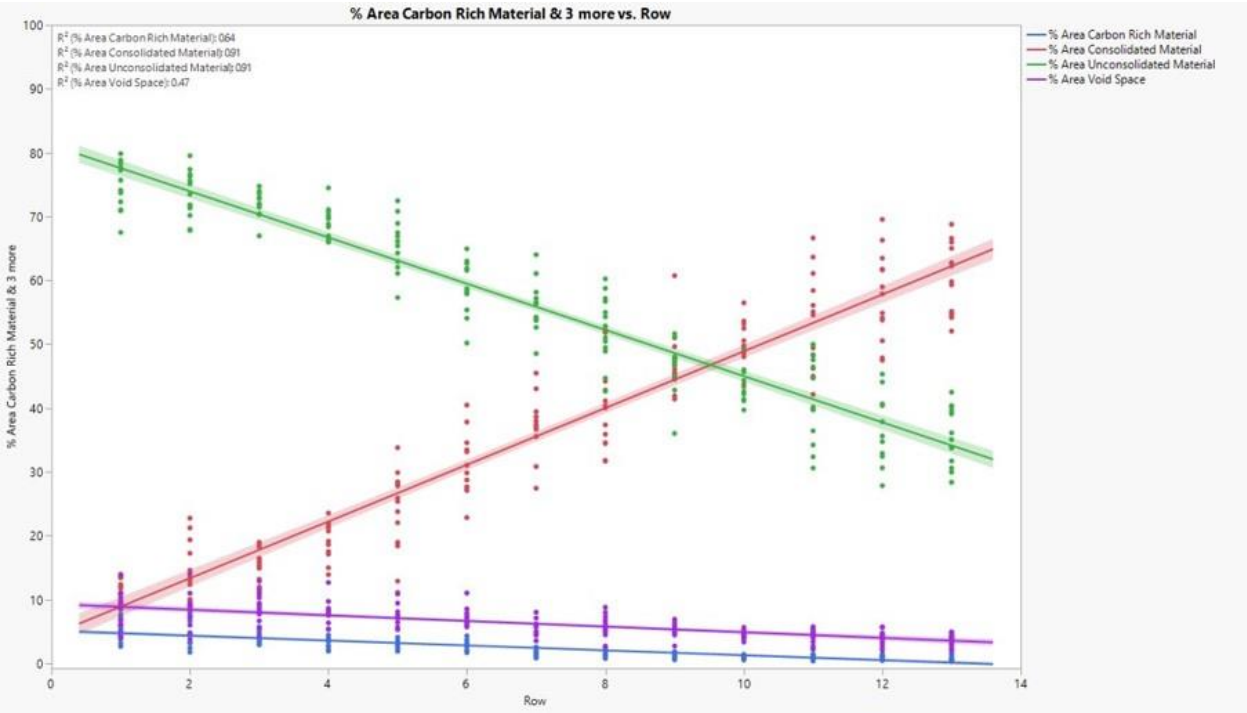

Figure 57 – Strong relation between both consolidated and unconsolidated material as a function of row

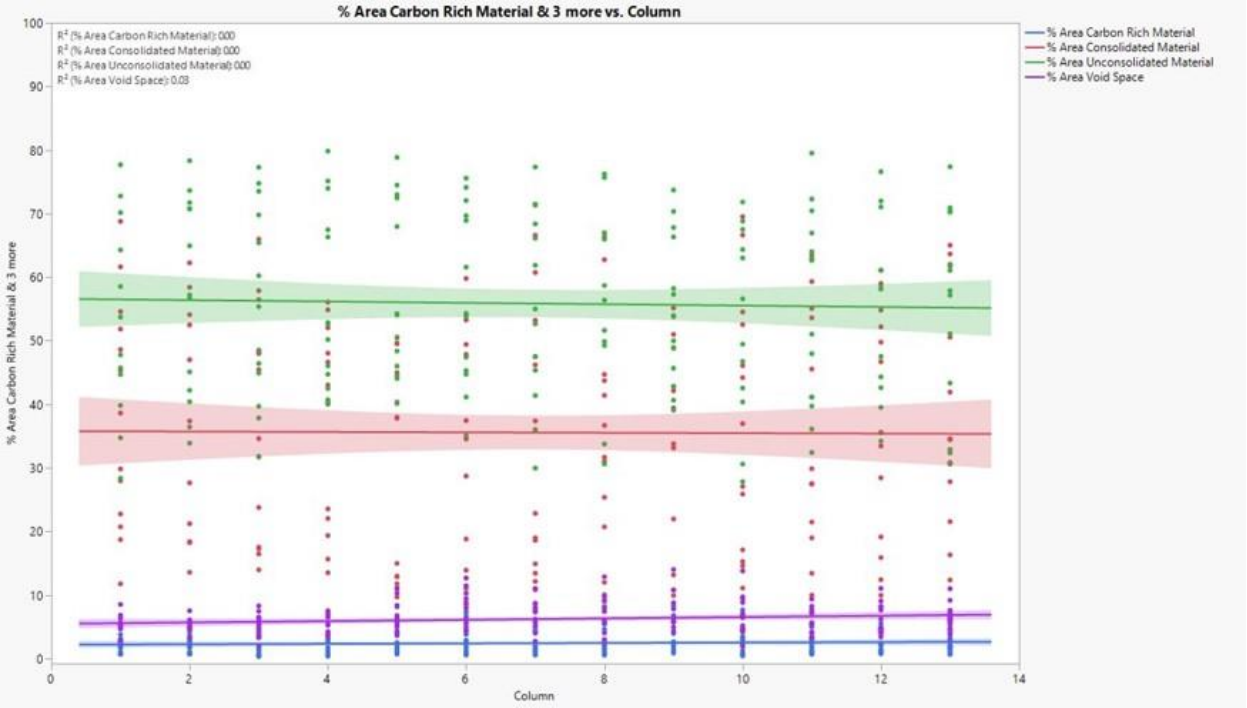

Figure 58 – No trend among any of the factors as a function of column

Immediately the trend between consolidated and unconsolidated material as a function of row is visible. Isolating this into a 2D view in **Figure 57** and plotting for trend, both factors have above a .9 R^2. This is contrasted strongly by the total lack of any correlation among factors in **Figure 58**. Upong reviewing **Figure 52** and **Figure 53**, it is clear trend in the data could skew in this was. Upon reviewing SEM literature, the phenomenon of ion beam drift came up. Ion beam drift is an occurrence that can occur during SEM imaging due to any number of external and internal factors, from thermal to vibrations, and that some SEM machines come equipped with internal methods for mitigating this (Stephensen et al., 2018). In this methodology, the drift of the beam is likely due to a combination of factors. The first is due to materials like cement and geopolymer having a combination of very low permeability while having decent to high porosity. Combined with the need for SEM to operate under a vacuum, it can take a long time for the vacuum to be pulled and the images to be captured. Additionally, the mapping process takes individual images, not one

large image, and breaks them apart. This means the beam is running for a long time, and the image taken longest after the first would be susceptible to the most amount of beam drift.

As the trend is strongly linear, investigations were made to see if it were possible to correct the interference of ion beam drift. Two key approaches were selected. The first is histogram matching. Histogram matching is the simple process by which all of the images in the data set are adjusted to as closely as possible match the histogram of a selected image, as shown in **Figure 59** and showcasing the image in **Figure 60**. This process, while not perfect, almost completely mitigated the trend as a function of column.

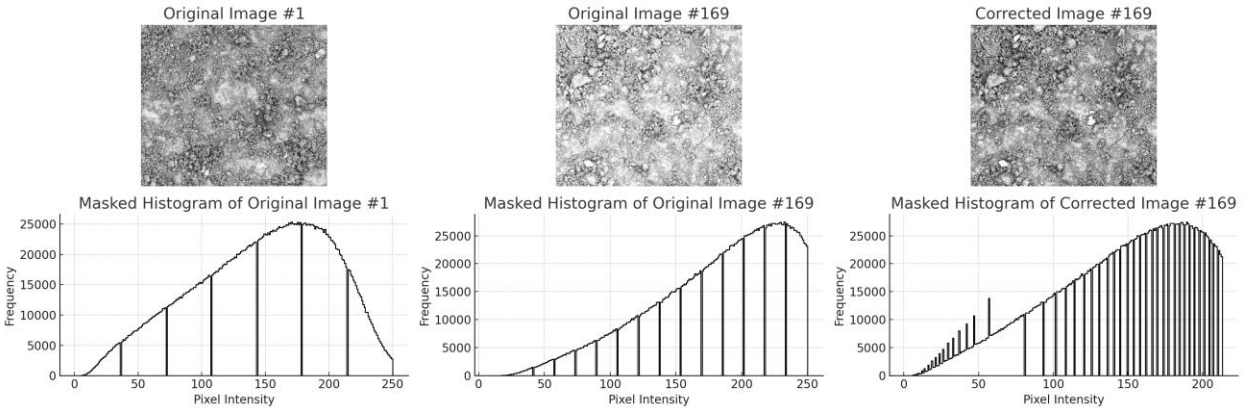

Figure 59 – Histogram matching image 169 to image 1

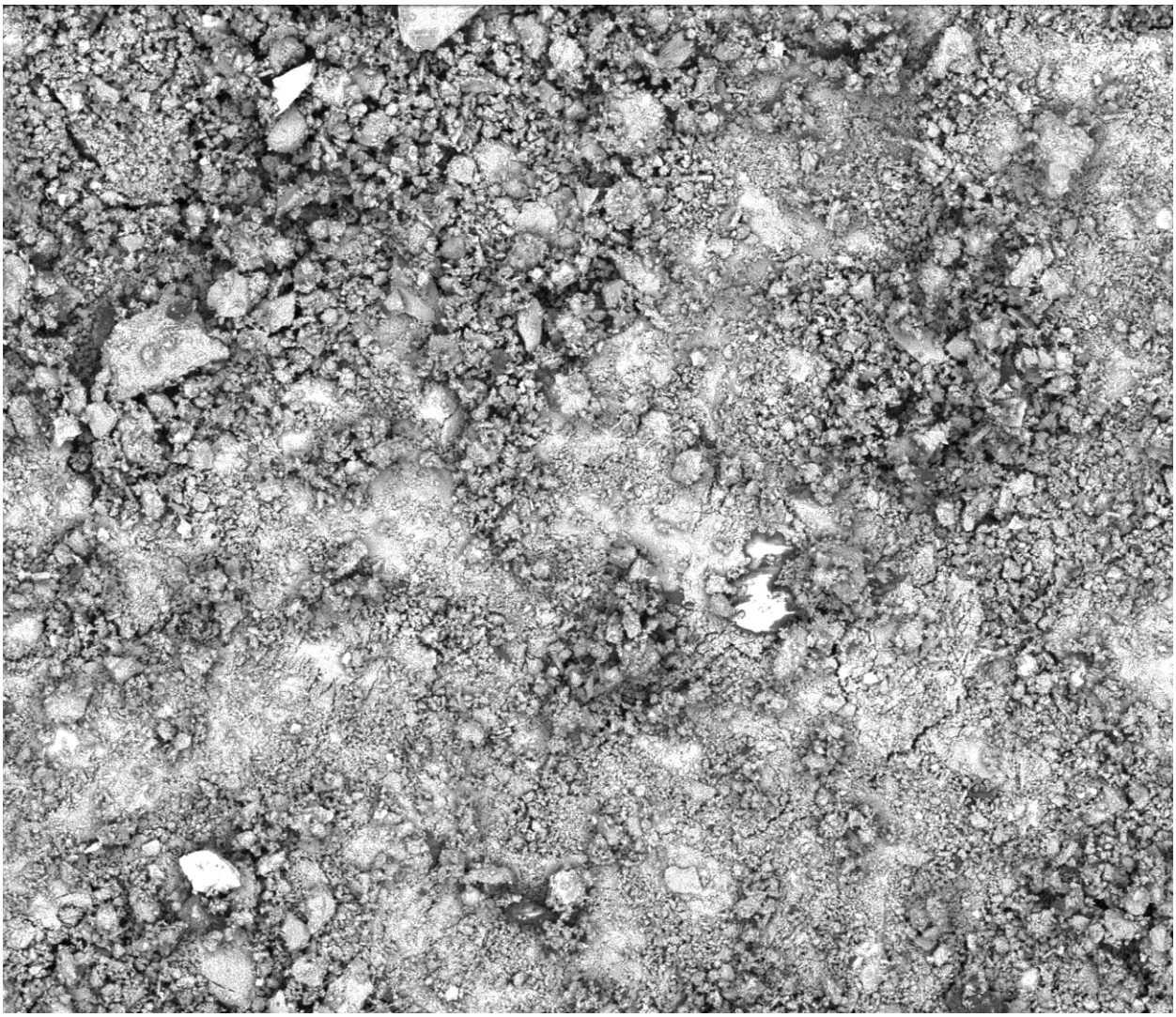

Figure 60 – Histogram correct image 169 from the SEM dataset

The second approach investigated is Contrast Limited Adaptive Histogram Equalization (CLAHE). This method of image analysis is growing in popularity among facial recognition and automated driving, namely for its ability to handle topographic or uneven features on a 2D image (Yang et al., 2019, Musa et al., 2018). This approach aims primarily to reduce the oversimplification of noise that can occur during traditional adaptive histogram equalization. Unlike the previous method of histogram correction, CLAHE is applied wholistically to the entire dataset. **Figure 61** and **Figure 62** showcase the results of this approach.

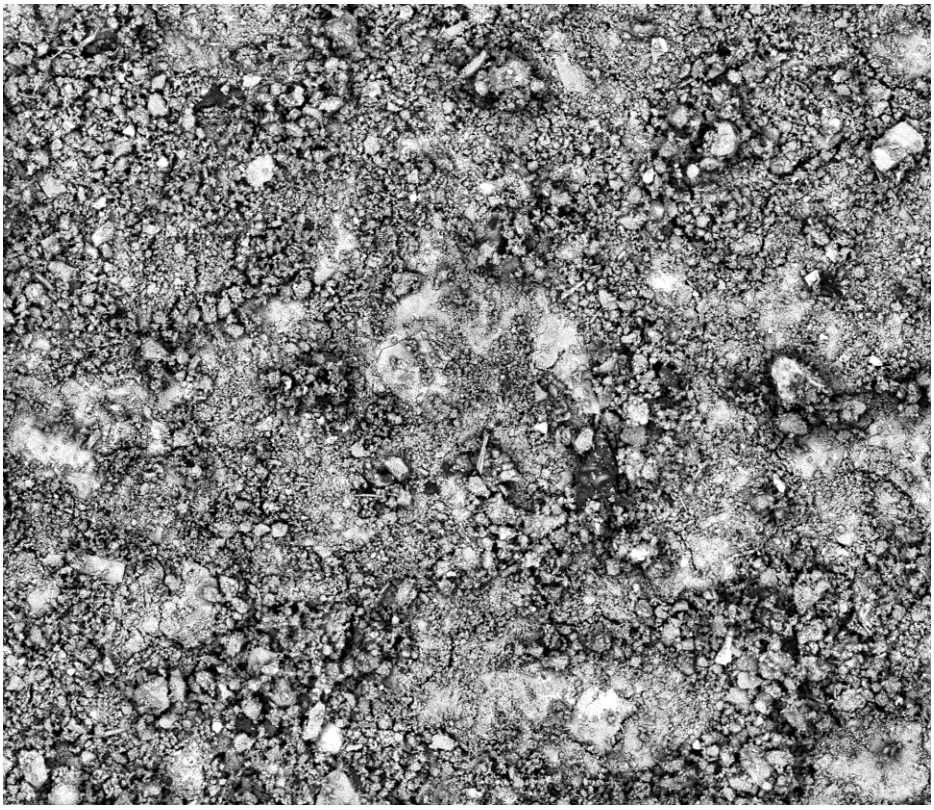

Figure 61 – Image 1 of 169 post CLAHE

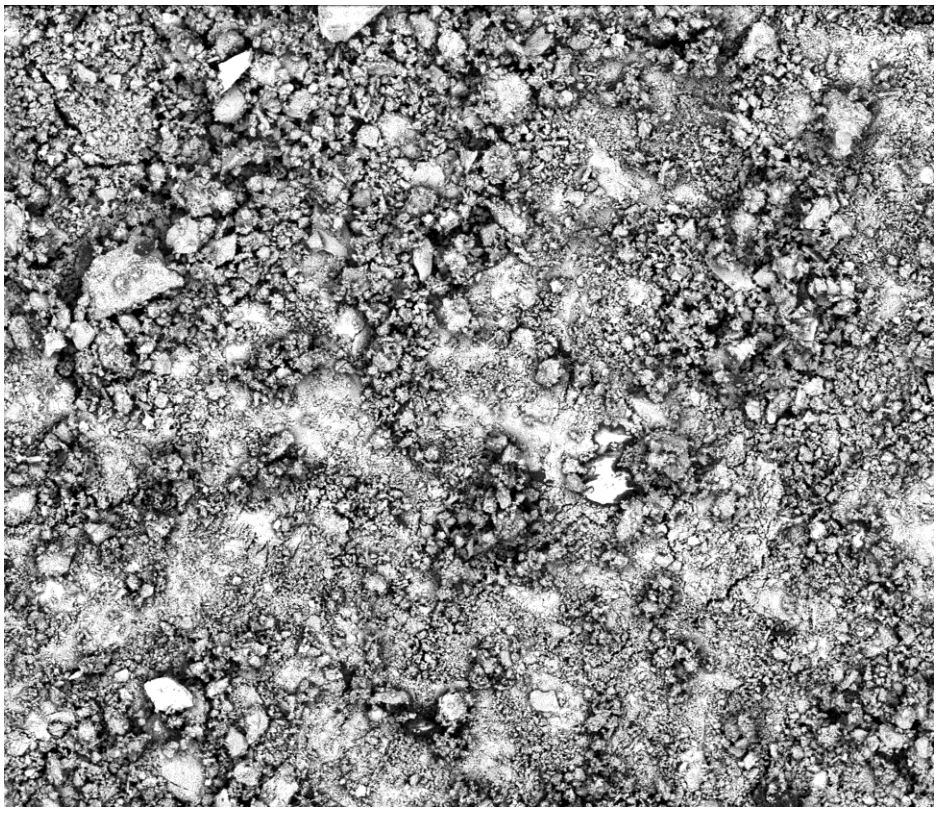

Figure 62 – Image 169 of 169 post CLAHE

Due to the nature of CLAHE altering the entire dataset, thus requiring a completely new segmenting and retraining of the initial model, the CLAHE images were instead used as the training body for an investigation into unsupervised approach.

4.5 Unsupervised Image Segmentation

Gaussian Mixture Models (GMMs) are a probabilistic framework that assumes data points are generated from a combination of multiple Gaussian distributions, each with unknown parameters. This assumption suits GMMs for handling the complex and heterogeneous nature of SEM images. The flexibility of a GMM to model intricate distributions effectively captures the diverse shapes and sizes of structures inherent in SEM images (Bishop, 2006), enabling a precise representation of the underlying data distribution. GMMs manage overlapping clusters by probabilistically assigning data points, accommodating the coexistence of different materials or phases within overlapping regions of SEM images (Reynolds, 2009). This probabilistic approach is crucial for accurately segmenting SEM images with overlapping features.

A significant benefit of GMMs is their capability for unsupervised learning, which does not require labeled training data. This attribute is advantageous in scenarios where labeled data is scarce or costly to obtain (Dempster et al., 1977), particularly for SEM image analysis where manual labeling can be subjective and labor-intensive. In SEM image segmentation, pixels are often represented by multiple features such as intensity, texture, and location. GMMs can incorporate these features into a multivariate Gaussian distribution, enhancing segmentation accuracy (McLachlan & Peel, 2000), thus improving the model's capacity to capture the intricate characteristics of SEM images. The robustness of parameter estimation in GMMs is another critical advantage. The Expectation-Maximization algorithm, employed to estimate the parameters

of a GMM, iteratively refines these parameters to maximize the likelihood of the observed data, ensuring a precise fit (Dempster et al., 1977). This process results in accurate and reliable segmentation outcomes.

In practical applications, GMMs have demonstrated success in identifying different material phases in SEM images, offering detailed insights into microstructural compositions (Liu et al., 2019). They facilitate precise measurement of porosity and grain size in geological samples, essential for characterizing material properties (Gonzalez & Woods, 2002). Additionally, GMMs detect defects in materials by segmenting regions that deviate from the expected Gaussian distribution, identifying potential weak points (Zhou et al., 2014). Much like in the supervised method, segmentations are still generated. An example of this can be seen in **Figure 63**

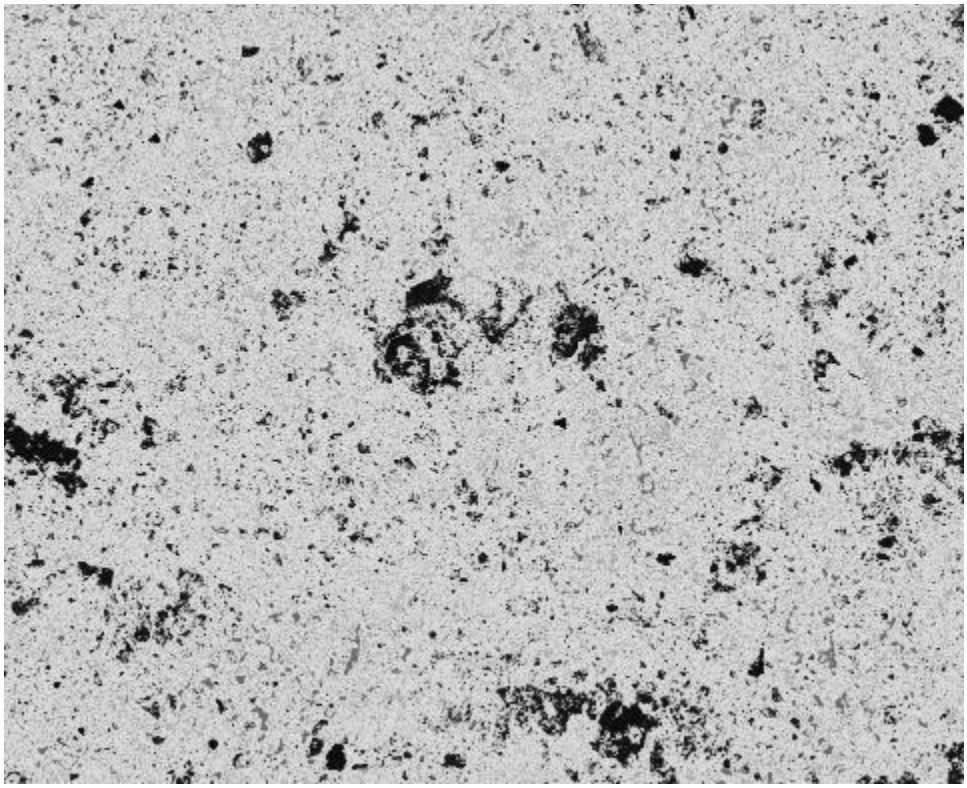

Figure 63 – Image 1 post CLAHE post GMM segmentation

While this segment does not have a color map applied it like previously, this image represents several segments not all of which are distinguishable by the human eye. Additionally, since the purpose of this is an unsupervised approach, the analysis of statistical insights from processing the model are more important than reviewing resultant images, but **Figure 64** applies a color map to help give an idea of the detail.

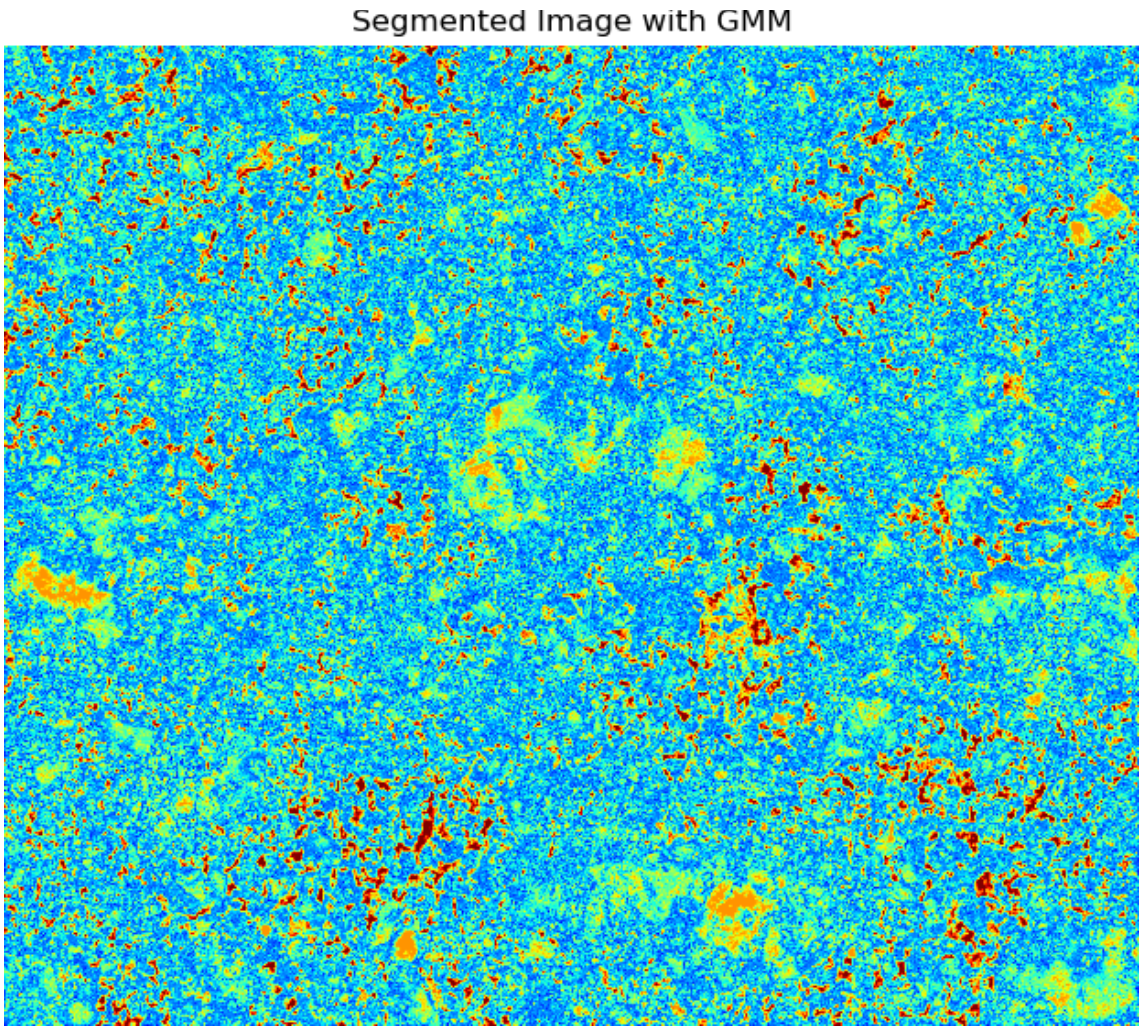

Figure 64 – Color map applied to image one of the GMM approach

4.5.1 Distribution of Segment Areas

The distribution of segment areas provides essential insights into the size variability of segments within an image. The segment area, defined by the number of pixels constituting that segment,

allows the identification of features of varying sizes. This metric is particularly relevant in materials science and geological imaging, where the size of different features can indicate crucial properties and conditions.

In materials science, the size distribution of particles can reveal different material phases, which is vital for quality control and understanding material properties. For instance, in composite materials, the distribution of reinforcing particles significantly influences the composite's mechanical properties. Detailed analysis of segment areas can identify defects, inhomogeneities, or variations in material composition, thereby impacting the material's performance and durability (Deng et al., 2016). In geological imaging, the size distribution of mineral grains provides information about the formation processes and history of the rock, essential for geological mapping and resource exploration. For example, in shale imaging, the distribution of pore sizes significantly impacts the permeability and porosity of the shale, influencing its suitability for hydraulic fracturing operations. By analyzing size distribution, researchers can identify regions with different porosity and permeability characteristics (Liu et al., 2019).

For geopolymers used in oil and gas well cementing, understanding the size distribution of various phases (e.g., unreacted fly ash particles, gel phases) can indicate the effectiveness of the geopolymerization process. A uniform distribution of small segment areas might suggest a well-reacted material with fewer defects and better mechanical properties. Conversely, large variations might indicate inhomogeneities that could compromise material performance under high pressure and temperature conditions typical of well environments.

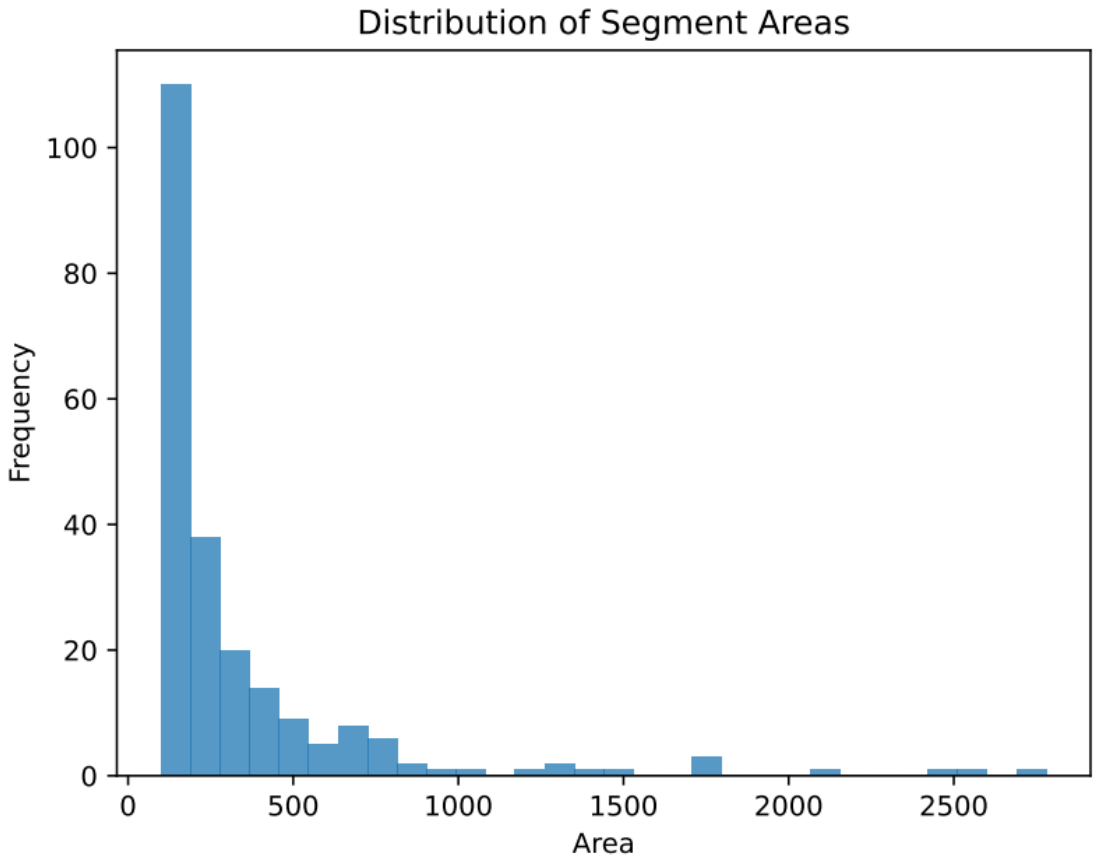

Figure 65 – Right-skewed distribution of GMM determined segments from the SEM dataset

First reactions are that the presence of a strong peak with a relatively small area suggests that the majority of the segments determined by the GMM represent areas of uniform reaction. Duxson et al., (2007) found that the presence of a uniform segment size distribution, such as the one suggested in **Figure 65**, lead to more reliable mechanical properties throughout the material. The tail section of the size distribution suggests there are at least some levels of inhomogeneity. This claim is supported by Provis & Van Deventer (2009) when they highlighted the variability in particle sizes within geopolymer matrixes can cause heterogeneous mechanical properties. This conclusion is only one of two likely contributions from these results, as the previously mentioned fracture propagating through the same will also contribute to some level of analytic influence.

4.5.2 Centroid Distributions

The centroid of a segment represents its geometric center. Analyzing the distribution of centroids within an image provides valuable information on how segments are spatially arranged. This metric is essential for identifying patterns and clustering within the image, revealing significant insights into the structure and organization of the sample. In geological imaging, the spatial distribution of mineral grain centroids can reveal clustering of grains, indicating different depositional environments or diagenetic processes. For example, in shale formations, the clustering of clay minerals can influence the mechanical properties and fracture behavior of the rock (Zou et al., 2010). Haralick et al., (1973) demonstrated how centroid distributions can classify textures in images, providing a framework for using spatial distribution metrics to differentiate between various textures and patterns.

In materials science, understanding the spatial arrangement of particles helps characterize the material's microstructure and predict its properties. For instance, the distribution of centroids in a composite material can indicate the effectiveness of the mixing process and the uniformity of the material. A uniform centroid distribution might suggest a well-mixed material with consistent properties, while clustering might indicate areas of agglomeration or defects (Jain et al., 2000). For geopolymers used in well cementing, understanding the spatial arrangement of phases is crucial. Clustering of certain phases, such as unreacted particles or voids, can lead to weak points in the material, potentially causing failures under the mechanical stresses encountered in wellbore environments. Analyzing centroid distributions helps in identifying and mitigating such clustering, thereby improving the material's integrity and reliability.

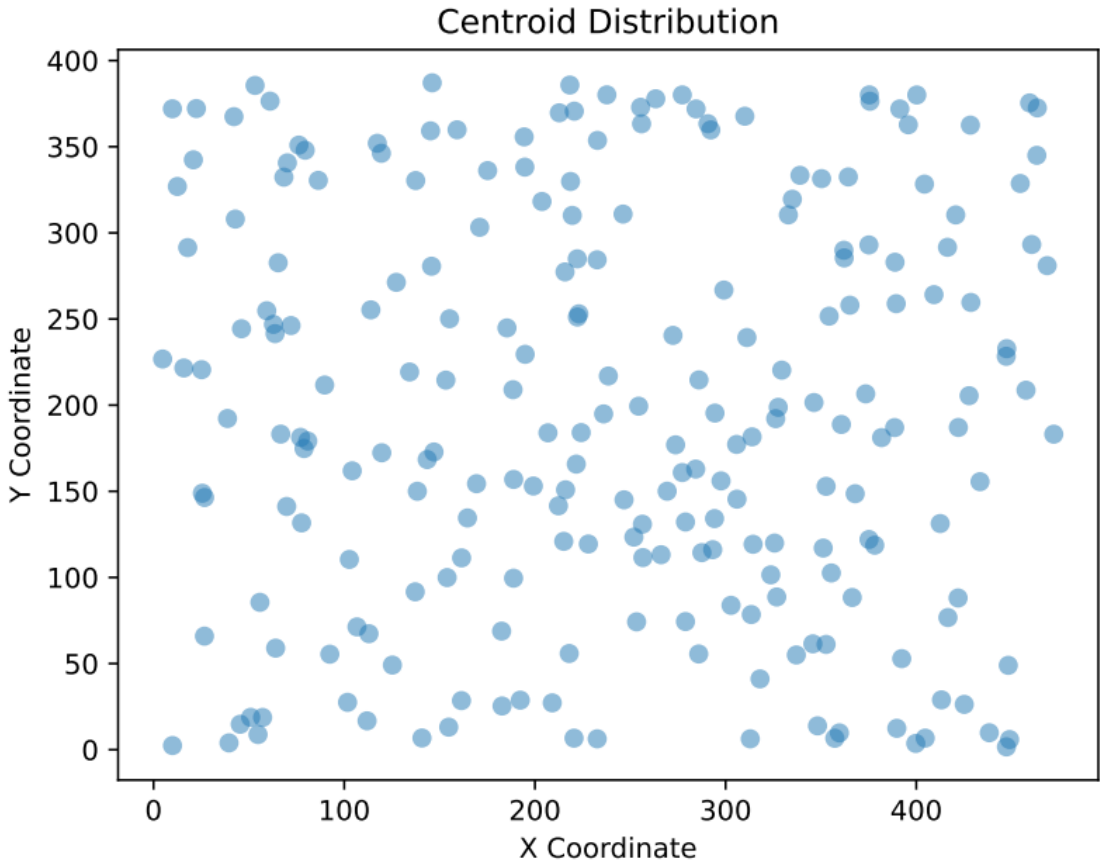

Figure 66 – Even spread and uniform centroid distribution as determined by GMM analysis

In line with the segment area analysis, the uniform scattering of segment centroids across the image set suggests the material is consistently reacted throughout the image set, a critical finding, as the image set tiles of a composite 2D section. Consistent and uniform distribution of geopolymer phases was determined by Fernández-Jimenez et al., (2006) to lead to improved mechanical performance. Also, Davidovits (2008) suggests that overly-centralized clustering could lead to points of stress concentration. These points drive to one of the primary goals of the image analysis, determining if the distribution of the reaction was leading to a bias in failure propagation. **Figure 66** suggests that is not the case, as the points are seemingly random and evenly spread across the chart.

4.5.3 Nearest Neighbor Distances

The nearest neighbor distance measures the distance between the centroids of adjacent segments. This metric helps understand the spatial relationships between segments, providing insights into the degree of clustering and dispersion within the image. Analyzing nearest neighbor distances is vital in materials science and geological imaging. In materials science, this metric helps characterize particle distributions, influencing the material's mechanical properties and behavior under stress. For instance, closely packed particles might result in higher material strength but lower ductility, whereas dispersed particles might improve toughness but reduce strength (Dong et al., 2017). Duda et al., (2000) demonstrated the use of nearest neighbor distances in identifying clusters and analyzing spatial patterns, providing a comprehensive overview of how spatial relationships can classify and understand different patterns in images.

In geological imaging, nearest neighbor distances can reveal the spatial organization of mineral grains within a rock sample, helping identify depositional environments and diagenetic processes. For example, in cemented sandstone, the distances between grains can indicate the degree of cementation and porosity, crucial for understanding the rock's reservoir quality (Guo et al., 2024). Gonzales & Woods (2008) emphasized the importance of spatial relationships in diagnosing material properties based on imaging techniques. For geopolymers in well cementing, closely packed reactive phases can enhance the overall strength and cohesiveness of the material. However, excessive clustering of voids or unreacted particles can lead to weak points. By analyzing nearest neighbor distances, researchers can optimize the mix to ensure a balanced distribution that maximizes strength and durability while minimizing potential failure points.

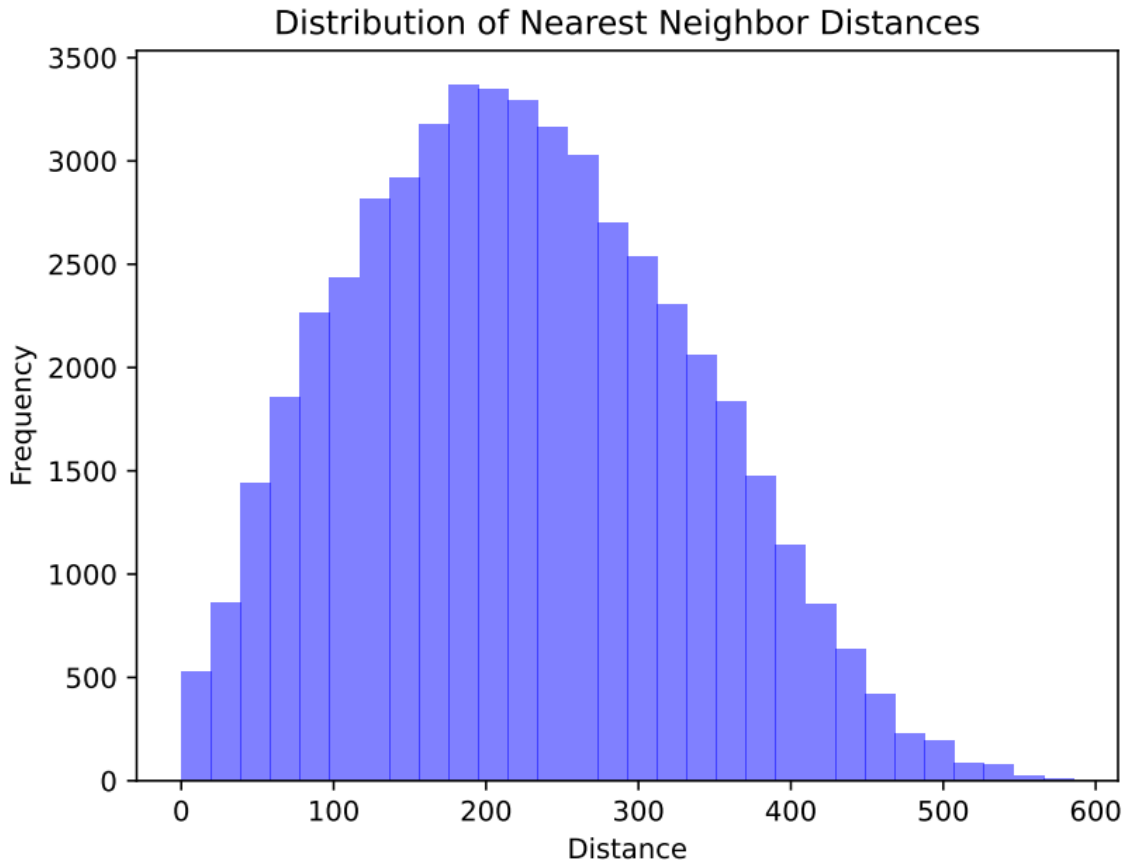

Figure 67 – The fairly uniform and normal distribution of distances between centroids by frequency, determined by GMM analysis

Figure 67 suggests the spacing of the centroids across the sample set is normally distributed with slightly longer tail on the right side of the distribution. While spacing distribution width ranges are relative, the work of Duxson et al., (2007) suggests the wider or more variant the particle sizes are the more heterogeneous the mechanical properties. This suggestion is supported by the work of Chen et al., (2020) discussing how the more closely packed particles or phases are the more likelihood there is of structural weakness. The normalness of the distribution suggests that no segment or segments are overly centralized and packed. This normal distribution is too present for a few select images or segments to be increasing the width, so this is likely indication of some level of inhomogeneity.

4.5.4 Segment Perimeters

The perimeter of a segment is the length of its boundary. This metric helps understand the shape and edge complexity of segments, providing insights into the roughness or smoothness of segment boundaries. In geological imaging, irregular grain boundaries might indicate complex depositional environments or diagenetic processes. For instance, irregular grain boundaries in shale can suggest a high degree of compaction and pressure solution, indicative of the rock's burial history (Loucks et al., 2009). In materials science, the roughness of particle boundaries can influence the mechanical interlocking between particles, affecting the material's strength and durability. Curtis et al., (2012) provided insights into how the development of organic porosity in shale impacts the mechanical properties of the rock.

In SEM images of geopolymers, the shape and complexity of segment boundaries can indicate the nature of the reaction products and the degree of crystallinity. For example, smoother boundaries might suggest well-formed amorphous phases, whereas rough, irregular boundaries could indicate partially reacted or crystalline phases. Understanding these characteristics is vital for optimizing the geopolymer’s mechanical properties and ensuring its suitability for high-stress applications like well cementing.

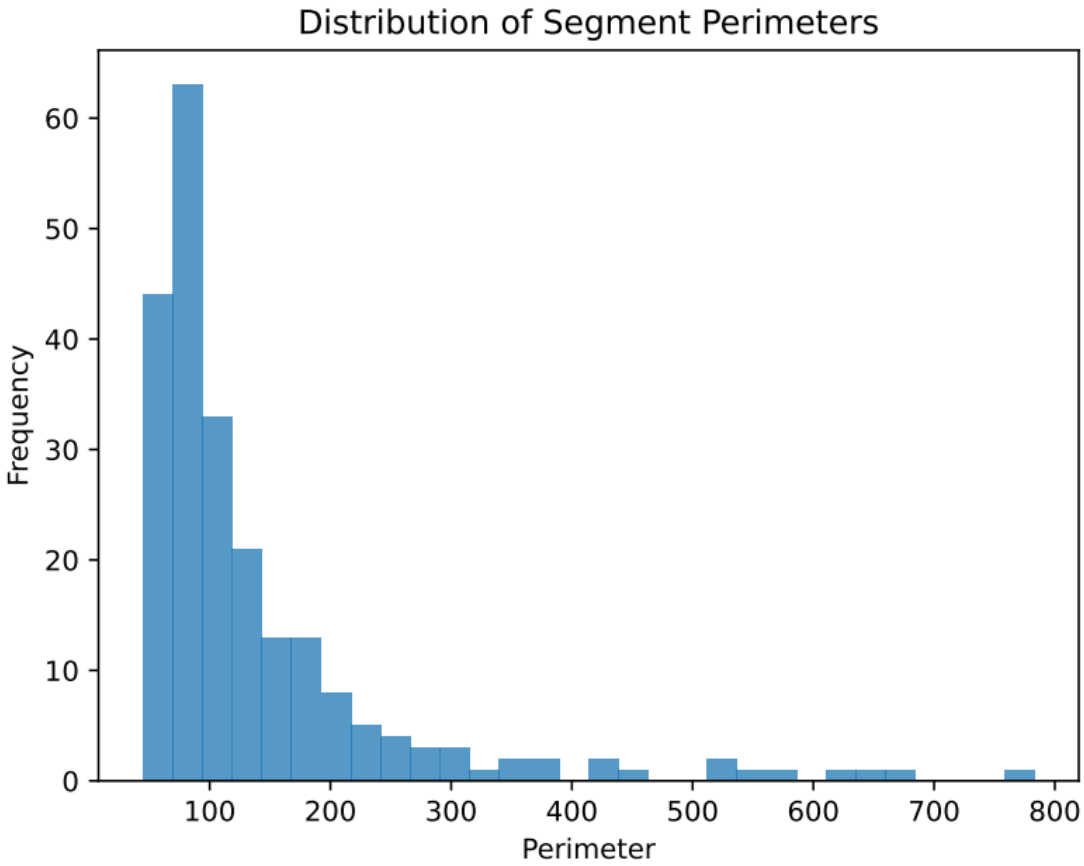

Figure 68 – The GMM determined parameter of the segments plotted with the frequency of the perimeter

The perimeter of the segments is important, as when viewed in conjunction with the area of the segments one gets an idea of the general segment shapes. Large perimeters with smaller areas would suggest irregular or elongated segments that could lead to diminished mechanical properties or the inclusion of stress concentrations (Bernal et al., 2012). If the majority of the perimeters are small, such as they are in **Figure 68**, the segments are likely more uniform in shape. The uniformity of particle shapes in geopolymerization is noted to directly contribute to improvements in mechanical properties (Rattanasak and Chindaprasirt, 2009). The long tail does indicate the presence of the presence of a small number of highly irregular shapes, but there is a known presence of a major fracture propagating through the image set, likely contributing to the larger-perimeter segments.

4.5.5 Segment Compactness

Compactness measures how closely packed a segment is: a perfect circle has a compactness of 1, with less compact shapes having values less than 1. Analyzing segment compactness is essential for differentiating between regular and irregular shapes. In geological imaging, this can help identify different mineral types or detect abnormalities in grain shapes, which might indicate different depositional environments or diagenetic processes. For example, well-rounded grains might suggest a high-energy depositional environment, while irregular grains might indicate low-energy conditions or post-depositional alterations (Curtis et al., 2012). Haralick et al., (1973) discussed how compactness can be used as a texture feature for image classification.

In materials science, particle shape affects how they pack together and interact, influencing the material's mechanical properties. High compactness values (close to 1) suggest regular circular shapes, which might indicate well-formed particles with consistent properties. Lower values indicate irregular or elongated shapes, which might suggest particles with defects or variations in material composition (Gonzales & Woods, 2008). In geopolymers, high compactness values suggest well-formed, regular phases that are likely to contribute to a stronger, more durable material. Low compactness values might indicate irregularly shaped phases, which could be a sign of incomplete reaction or the presence of defects. By analyzing compactness, researchers can gain insights into the quality of the geopolymerization process and make necessary adjustments to improve material properties.

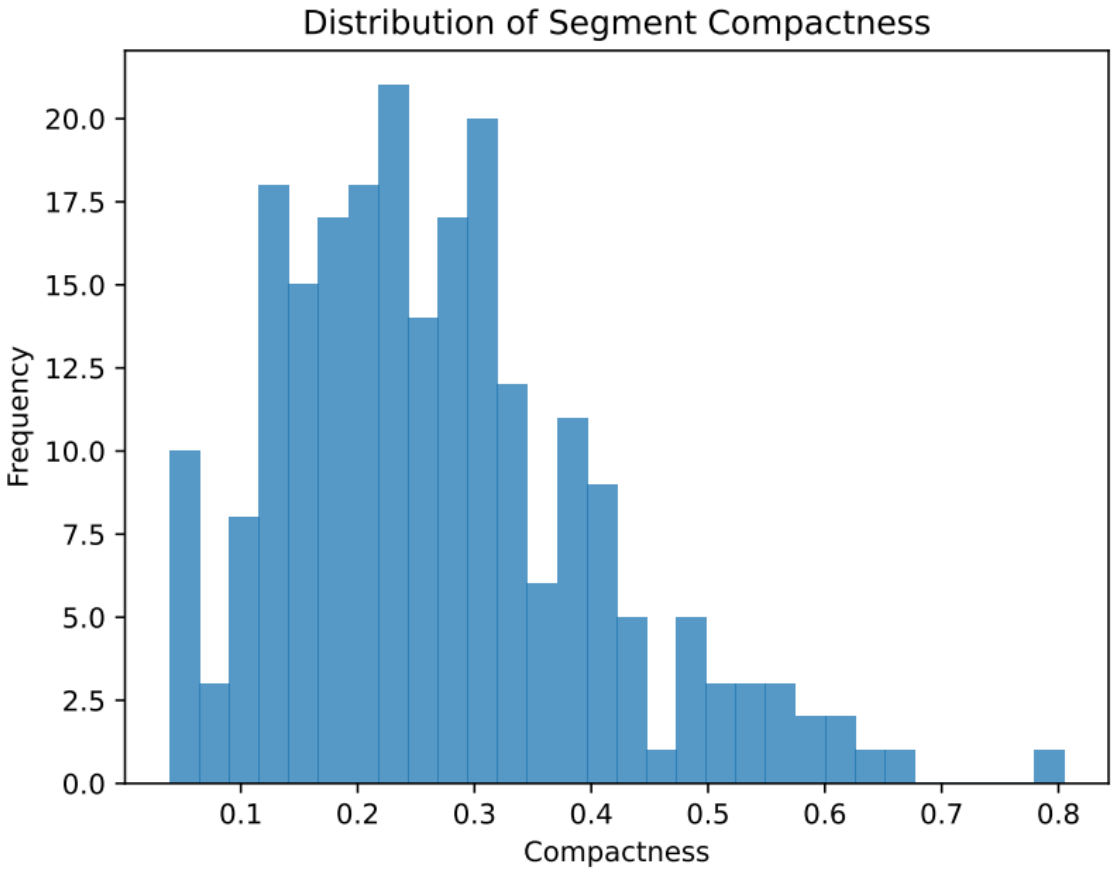

Figure 69 – GMM determination of compactness by frequency, highlighting poor compaction

Figure 69, at first glance, seems contradictory to the previous sections. The majority of the data falls well below .5, suggesting most of the segments exhibit irregular shapes. The presence of this would suggest the there is an increased likelihood of premature failure due to weak points within the material (Xu et al., 2022). This claim, however, is not actually contradictory to the statements made previously as irregularity of shapes and uniformity of the shapes as a whole are not the same. The low compactness simply suggests that the segments are mostly the same area and perimeter, just not round.

4.5.6 Mean Intensities

The mean intensity of a segment is the average pixel value within that segment, indicating the average brightness or density of the segment. In geological imaging, different mineral types or rock phases might have distinct mean intensities, allowing for the identification and characterization of different rock types or alterations. For example, in SEM imaging of cement samples, the mean intensity can indicate different hydration products or the presence of unreacted materials (Zargari et al., 2015). By measuring the mean intensity of different segments, researchers can identify regions of interest that might require further investigation or analysis. Pizer et al., (1987) discussed adaptive histogram equalization techniques and their applications in enhancing contrast and improving the visibility of different structures based on intensity variations.

In materials science, mean intensity can provide information about the composition and density of different regions within a material. For example, in a composite material, regions with different mean intensities might correspond to different phases or components. By analyzing the mean intensity of different segments, researchers can understand the distribution and composition of materials, which is essential for quality control and material optimization (Milliken et al., 2013). In SEM images of geopolymers, mean intensity can provide information about the composition and density of different phases. For example, higher mean intensities might indicate denser, more crystalline phases, while lower intensities could suggest amorphous or porous regions. Understanding these variations is crucial for tailoring the material properties to meet specific requirements in well cementing, such as achieving optimal strength and durability under varying temperature and pressure conditions.

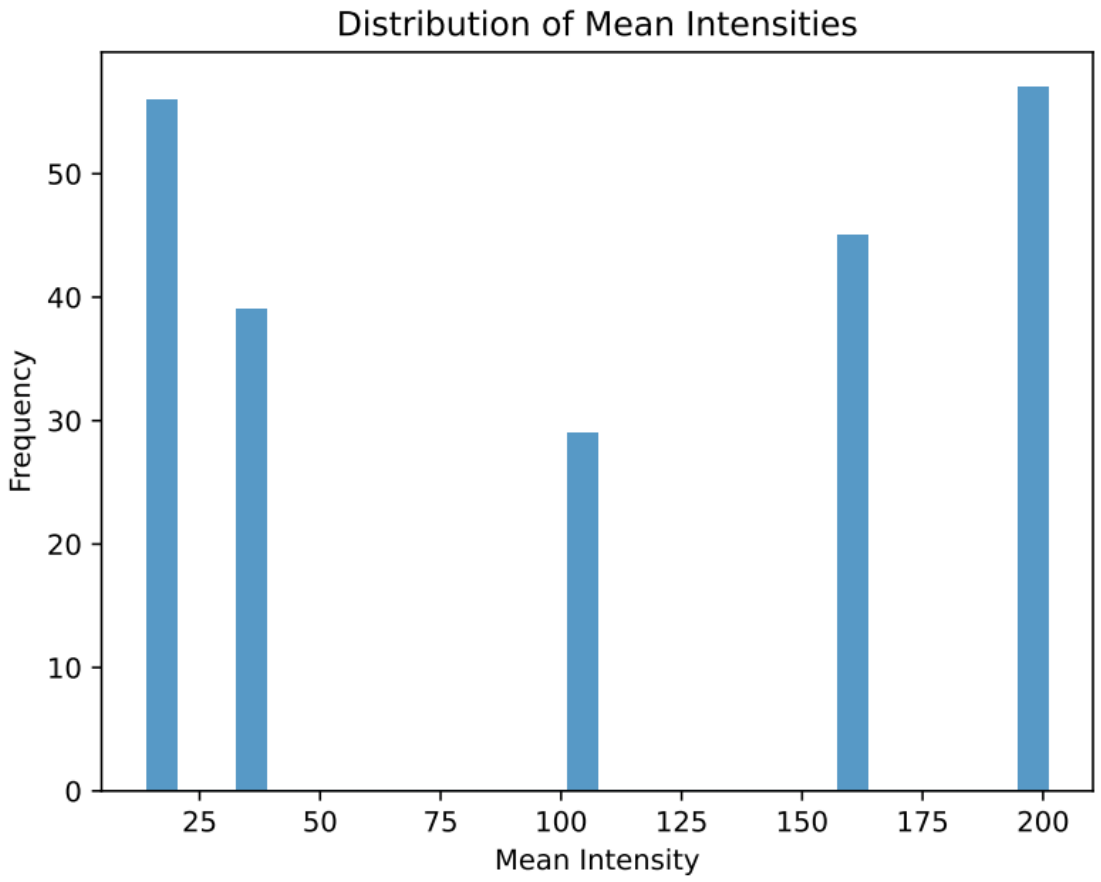

Figure 70 – 5 distinct mean intensities determined by GMM analysis

Figure 70 is the first of the analytics figures in this section that gives insights to the possible composition of the different segments. While the previous figures suggest large numbers of segments and segment characteristics, the distinct values of **Figure 70** could correspond to either different phases of the material (Shi et al., 2012) or to the varied material composition (De Silva et al., 2007). These are not mutually exclusive conclusions. It seems the most reasonable conclusion here is that the model has generally identified five distinct features the image segments may have. It could be that these are reacted geopolymer, partially reacted geopolymer, unreacted powder, impurities such as carbon, and the propagated fractures. While this is speculative based on the composite analysis of the work, the unsupervised nature of the model makes this hard to verify practically.

4.5.7 Intensity Standard Deviations

The intensity standard deviation within a segment measures the variability of pixel values, indicating how much the pixel values within a segment differ from the mean intensity. The standard deviation of intensity helps identify regions with uniform or varying density. High variability might indicate heterogeneous materials or geological samples, while low variability suggests homogeneity. In geological imaging, regions with high intensity variability might correspond to areas with mixed mineral compositions or different diagenetic histories (Passey et al., 2010). By measuring the intensity standard deviation of different segments, researchers can identify regions with abnormal variability that might suggest the presence of different mineral phases or alterations. Haralick et al., (1973) emphasized the importance of texture features, including intensity variability, in image classification.

In materials science, variability in intensity can indicate differences in material composition or the presence of defects. For example, a material with uniform composition might have low intensity variability, while a material with varying composition or defects might have high intensity variability. By analyzing the intensity standard deviation of different segments, researchers can identify regions with potential defects or variations in material composition, which is essential for quality control and material optimization. Milliken et al., (2013) discussed how intensity measurements, including standard deviations, can be used to characterize different materials and identify regions of interest within images. In SEM images of geopolymers, high variability in intensity within segments can indicate heterogeneous regions within the geopolymer, which might compromise its mechanical integrity. Low variability suggests a more homogeneous material, which is desirable for consistent performance. By analyzing intensity standard deviations,

researchers can identify regions of potential weakness and refine the processing techniques to produce a more uniform and reliable material for well cementing applications.

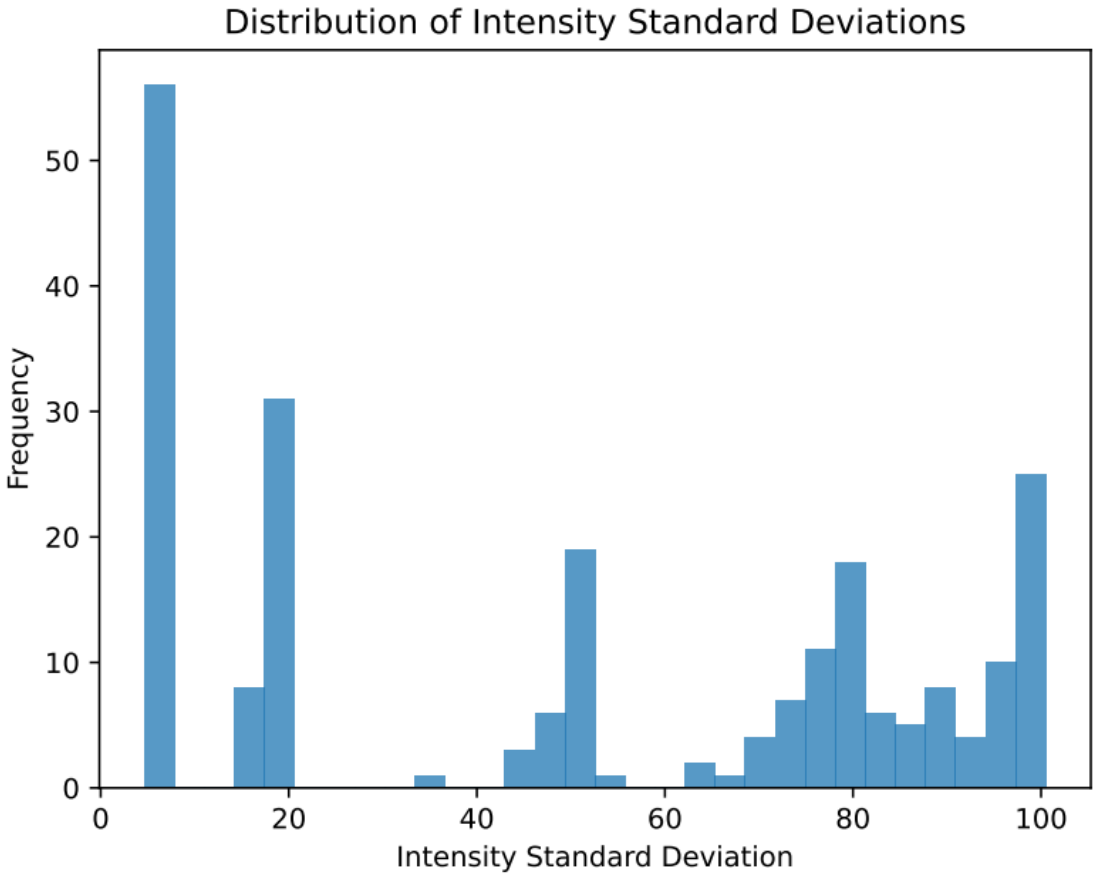

Figure 71 – Fairly variate distribution of intensity standard distributions

The majority of the data in **Figure 71** is really split into two groups, groupings lower than 25 and groups larger than 75. This distribution typically suggests one of two non-mutually exclusive behaviors. The first is that there is still too noticeable of a brightness variance across the images. The other is that while sections of the images display highly idealized geopolymerization, there exists meaningful imaged regions of heterogeneity that previous results in this section did not as strongly indicate.

Chapter 5 Generalized Comparison of API Cement to Geopolymers

Discussion and detailing of the differences between established Portland Cement and geopolymer is not novel. Since the inception of geopolymer technologies, Portland Cement has been held as the comparative analog for discussion due to geopolymers as a possible replacement of Portland Cement. Geopolymers are intended to be a functional 'use-case' replacement to cement – especially within the civil engineering industry.

Experimental data presented demonstrates API Class C cement outperforms Class F Fly Ash geopolymers by approximately 200%. This substantial disparity in mechanical performance highlights a significant challenge in substituting traditional Portland cement with geopolymers within the context of current API testing standards. However, there are promising signs that geopolymers can be an alternative to API cements for oil and gas applications, and for geothermal applications.

5.1 Standards Comparison

Portland cement, the current standard for wellbore cementing operations, is highly scrutinized by published API cement standards, ensuring consistent and predictable material properties.

Currently, there are no published geopolymer standards. Further, literature review reveals significant variability in the UCS of tested geopolymer samples, even when tested under identical conditions. This lack of consistency is a major concern for the adoption of geopolymers as an alternative to traditional cements in wellbore applications.

5.2 Chemical Composition and Microstructure Comparison

The inherent difference in the chemical composition and microstructure between API Class C cement and Class F Fly Ash geopolymers is a fundamental factor contributing to the observed mechanical disparities. API Class C cement, primarily composed of calcium silicates and aluminates, undergoes hydration reactions that form a dense, interconnected matrix of calcium silicate hydrate (C-S-H) gel and calcium hydroxide ($Ca(OH)_2$), imparting high early strength and durability. Conversely, geopolymers, synthesized through the alkali-activation of alumino-silicate materials, form a three-dimensional network of alumino-silicate gel. The presence of unreacted fly ash particles and variability in the degree of geopolymerization can lead to inconsistencies in the mechanical properties of geopolymer samples.

5.3 Chemical Reactions Comparison

Portland cement undergoes a complex set of chemical reactions, or hydration, involving the formation of calcium-silicate-hydrate (C-S-H) gel, which contributes to its logarithmic strength development over time. Geopolymers chemically react to form an alumino-silicate network (polymerization), the kinetics of which may be influenced by various factors such as the source of fly ash, activator solution concentration, and curing conditions. The observed linear strength development over time suggests a steady, but less pronounced, increase in strength, which may be due to the continuous dissolution and re-polymerization processes occurring within the geopolymer matrix.

5.4 Mechanical Properties Comparison

The large range of UCS results observed suggests that the properties of geopolymers are highly sensitive to variations in the composition of the fly ash used, the curing environment, and the mixing process. Unlike Portland cement, which is highly standardized, the composition of fly ash can vary significantly depending on the source and production process. This variability in raw materials contributes to the observed inconsistencies in the performance of geopolymer cements.

The inclusion of sodium silicate in geopolymer formulations enhances mechanical properties. Sodium silicate acts as an additional source of silicate ions, promoting the formation of a denser and more cohesive matrix. This additive accelerates the dissolution of fly ash particles, resulting in a stronger material. In contrast, OPC relies on the hydration of clinker minerals, which can be slower and less efficient in achieving high strength.

Furthermore, the inclusion of potentially hazardous materials, such as liquid glass, in the geopolymer mixture raises additional concerns regarding the safety and practicality of using geopolymers in downhole applications. While liquid glass can improve the UCS of geopolymer cements, its use introduces additional complexities in the mixing and handling processes, which need to be carefully managed to ensure safe and effective application.

5.5 Curing Environment Comparison

In water-rich environments, UCS results of fly ash-based geopolymers indicate superior mechanical properties compared to OPC. The presence of water enhances the geopolymerization process, leading to improved strength and durability. In contrast, OPC is prone to degradation in water-rich environments due to the formation of hydration products that can compromise integrity.

This observation highlights the advantage of geopolymers in downhole applications where water presence is inevitable.

In elevated temperature environments, UCS results of fly ash-based geopolymers show that fly ash-based geopolymers retain their strength, whereas OPC is susceptible to thermal degradation. This observation highlights the advantage of geopolymers in downhole applications where high temperature subterranean formations are increasingly encountered in both oil and gas, and geothermal operations.

5.6 Environmental Impact Comparison

The production of API cement is energy-intensive and generates significant carbon emissions. In contrast, geopolymers utilize industrial byproducts, such as fly ash, which reduces the demand for raw materials and lowers carbon emissions. This environmental benefit aligns with global efforts to reduce carbon footprints and promote sustainable construction practices. Cements cannot harden without water.

5.7 Summary

The comparison between OPC and fly ash-based geopolymers underscores the potential of geopolymer as a viable alternative for well cementing. Geopolymers can offer superior mechanical properties, enhanced thermal stability, and environmental sustainability compared to OPC. The ability to maintain strength and integrity in water-rich and high-temperature environments makes geopolymers a promising alternative for well cementing, especially in wells that encounter high temperature subterranean environments such as those increasingly encountered in geothermal and deep hydrocarbon-bearing subterranean environments.

However, it is important to note that further research is needed to optimize geopolymer formulations and curing conditions. The potential thermal stability issues observed at higher temperatures warrant additional investigation to ensure the long-term performance of geopolymers. Future studies should also explore the effects of other additives and formulations, and the influence of continuous thermal cycling and high-pressure conditions.

Chapter 6 The Case for Geopolymer Standards

API nor ASTM have published standards regarding the manufacturing, use or testing of geopolymer materials in subterranean applications. While no published standards exist from either of these two entities, ASTM has acknowledged geopolymers in published books, papers, and symposia; and many of the inclusions discuss the testing and formulation of geopolymer materials.

The comparison with Portland cement highlights the need for rigorous standardization and quality control in the production, application and testing of geopolymer cements. The well-established API standards for Portland cement ensure that the material's properties are well understood and predictable, providing a reliable basis for designing and implementing wellbore cementing operations. For geopolymers to be considered a viable alternative, similar standards must be developed to ensure consistent performance and reliability.

6.1 Standards Literature Review

A review of geopolymer testing literature revealed no clear standard or protocol has been uniformly used for testing. Further, UCS testing results exhibit significant variability, primarily due to differences in fly ash composition, alkali activator concentration, material formulations, and curing conditions. This variability impedes meaningful comparisons, scalability and reproducibility of results.

Both ‘regular use’ case and ‘high-risk use’ case potential of geopolymers in the oil and gas industry suggests that an examination of the current API cement testing standards for adoption to geopolymer testing is appropriate.

6.2 Standards Benefits

Benefits of standards for the manufacturing, use or testing of geopolymer include:

- Supporting the comparability, reproducibility and scalability of geopolymer research, fostering collaboration and innovation within the scientific community
- Enabling meaningful comparisons between geopolymer systems and traditional API cement, providing a robust basis for evaluating the feasibility of geopolymers as sustainable alternatives
- Promoting a broader understanding of geopolymer long-term performance and durability under field conditions
- Paving the way for their successful integration into oil and gas applications, contributing to the industry's sustainability goals and reducing its environmental footprint
- Facilitating the identification of optimal material formulations and curing environments
- Promoting further research both UPV and UCS testing of geopolymer as researchers would have a reference to compare information, resulting in subsequent larger-scale tailored research

6.3 Standards Development Recommendations

Consideration should be given to developing geopolymer standards similar to API 10B. And the manner in which API 10B includes pozzolans should be considered.

Geopolymer standards should account for the unique characteristics of geopolymers regarding composition, preparation, chemical reactions, curing regimes, mechanical behavior and testing. For example, the inclusion of additional pre-curing steps to ensure complete dissolution of

alumino-silicate precursors, or adjustments to curing temperatures and durations to optimize the geopolymerization process, could significantly enhance the mechanical properties of geopolymer samples. Moreover, the incorporation of supplementary materials, such as nano-silica or slag, could be explored to improve the mechanical performance and consistency of geopolymers. Additionally, early slurry tests need to be adopted to account for the core functional differences between geopolymers and cements during that window.

Chapter 7 Implications for Geothermal Well Construction

The findings of this study have important implications for geothermal well construction. Geothermal wells are subjected to extreme conditions, including high temperatures and the presence of water. The performance of cementitious materials in these conditions is critical to ensure the integrity and stability of the wellbore. This study demonstrates that fly ash-based geopolymers offer significant advantages over traditional OPC in geothermal applications.

The superior mechanical properties of geopolymers, particularly in water-abundant environments, make them well-suited for geothermal wells. The presence of water enhances the geopolymerization process, leading to improved strength and durability. This characteristic is crucial in geothermal applications, where water is often present in the wellbore. Geopolymers' ability to maintain their integrity and strength in water-rich environments ensures the stability and longevity of the wellbore.

The potential enhanced thermal stability of geopolymers is another significant advantage for geothermal well completions. Geothermal wells are subjected to high temperatures, which can degrade traditional OPC. In contrast, geopolymers demonstrate superior performance at elevated temperatures, maintaining their strength and integrity. This thermal stability is critical to withstand the harsh conditions of geothermal wells and ensure the long-term performance of the cementitious material.

The environmental benefits of geopolymers also have important implications for geothermal well completions. The production of OPC is energy-intensive and generates significant carbon emissions. Geopolymers, on the other hand, utilize industrial byproducts, such as fly ash, reducing the demand for raw materials and lowering carbon emissions. This environmental sustainability

aligns with the goals of reducing the carbon footprint and promoting sustainable practices in geothermal well completions.

The findings of this study suggest that geopolymers can be used as viable alternatives to OPC in geothermal well completions. Superior mechanical properties, enhanced thermal stability, and environmental benefits of geopolymers make them well-suited for the extreme conditions of geothermal wells. The ability to maintain strength and integrity in water-abundant and high-temperature environments ensures the stability and longevity of the wellbore.

However, it is important to note that further research is needed to optimize geopolymer formulations and curing conditions. The potential thermal stability issues observed at higher temperatures warrant additional investigation to ensure the long-term performance of geopolymers. Future studies should also explore the effects of other additives and the influence of continuous thermal cycling and high-pressure conditions. This is especially true given that there is evidence that fluid remains trapped in geopolymer slurries as the porosity remains fixed post-pour.

In summary, the implications for geothermal well completions highlight the advantages of fly ash-based geopolymers in terms of mechanical properties, thermal stability, and environmental sustainability. Geopolymers demonstrate superior performance in downhole applications, making them promising alternatives for well cementing in geothermal wells. Further research is needed to address potential thermal stability issues and optimize formulations for long-term performance.

Chapter 8 Conclusions

This work has reviewed both cement hydration and geopolymer polycondensation, also known as geopolymerization. Once defining the purpose of cement in the oil and gas industry, the growing challenges faced by cement are established and a potential replacement alternative, geopolymers, are established. In this review, the cement hydration reaction and the geopolymer reaction were characterized, first by focusing on how the reactions behaved and what the major components of the reaction are. From there, testing of the geopolymer material as it pertains to potential oil and gas development was analyzed, and found great inconsistency among testing parameters. An in-depth review of traditional cement testing was conducted which was analyzed for generalized geopolymer compatibility. In cases where the geopolymer material is considered incompatible with existing testing conditions, reason is given for this conclusion. Finally, additional testing and analysis options for studying the material are provided. NMR and SEM are determined to be two of the most expansive potential investigative methods for further gaining insight into the critical reaction of geopolymerization. Additionally, insights gathered from those experimental methods were collected and compiled to help formulate opinions and findings on key differences between geopolymers and OPC.

The conclusions, best summarized, are as follows.

1. Over 400 unique geopolymer samples generated across 9 unique experimental approaches,
2. Multiple aspects of both cement and geopolymer literature has been reviewed,
3. Most practical geopolymer research seems to be focused on civil and environmental engineering applications,

4. The primary reaction of cement, hydration, is more comprehensively understood than geopolymerization, which is much more subject to its source material for its reaction,
5. Geopolymer data, specifically reporting on testing practices, is severely under-standardized,
6. ASTM and API both provide comprehensive cement testing procedure, but both lack any regulation on real geopolymer sample testing,
7. Geopolymer literature does suggest, by aggregation, a general recipe comprising of Class F Fly Ash and 10M NaOH in 2 parts to 1 ratio,
8. Testing geopolymers made with the aggregated recipe under traditional API considerations yield inconsistent and poor overall results
9. Several factors such as curing environment, pH, and temperature, all play a role in the achieved UCS and UPV of the geopolymer sample,
10. The distribution of material within the fly ash plays a significant role in achievable UCS,
11. Geopolymers tend to prematurely fail without the presence of free water when no beneficial additives are used,
12. Geopolymer NMR testing seems to be following the same general experimental path of cement, where Si NMR is currently being conducted but there is little literature relating to H NMR,
13. Relaxation times trend strongly with cure time with regards to NMR but porosity remains stagnant,
14. It is possible to undertake large-scale SEM investigations on unpolished geopolymer samples,

15. Supervised and unsupervised segmentation and machine learning models can be used to generate information regarding geopolymer SEM, each with their own benefits,
16. Reproducible and distributable methodology generated for the unsupervised analysis via machine learning using SEM images of geopolymer samples developed
17. While geopolymers possess the potential to supplement or even replace OPC, field testing practices need to be created from scratch for both safety and material understanding.

References

American Association of State Highway and Transportation Officials. (2023). Standard Specification for Coal Fly Ash and Raw or Calcined Natural Pozzolan for Use in Concrete (AASHTO M295).

Abid, K., Gholami, R., Elochukwu, H., Mostofi, M., Bing, C. H., & Muktadir, G. (2018). A methodology to improve nanosilica based cements used in CO2 sequestration sites. *Petroleum*, *4*(2), 198–208. https://doi.org/10.1016/j.petlm.2017.10.005

Adams N, & Charrier T. (1985). Drilling Engineering: A Complete Well Planning Approach. Penn Well Pub. Co.

Adjei, S., Elkatatny, S., Wilberforce Aggrey, N., Abdelraouf, Y. (2022). Geopolymer as the future oil-well cement: A review. *Journal of Petroleum Science and Engineering, Volume 208, Part B.* 109485. ISSN 0920-4105. https://doi.org/10.1016/j.petrol.2021.109485.

Ahdaya, M., & Imqam, A. (2019a). Investigating geopolymer cement performance in presence of water based drilling fluid. *Journal of Petroleum Science and Engineering*, *176*, 934–942. https://doi.org/10.1016/j.petrol.2019.02.010

Ahdaya, M., & Imqam, A. (2019b). Fly ash Class C based geopolymer for oil well cementing. *Journal of Petroleum Science and Engineering*, *179*, 750–757. https://doi.org/10.1016/j.petrol.2019.04.106

Ahmaruzzaman, M. (2010). A review on the utilization of fly ash. In *Progress in Energy and Combustion Science* (Vol. 36, Issue 3, pp. 327–363). https://doi.org/10.1016/j.pecs.2009.11.003

Ahmed, M. M., El-Naggar, K. A. M., Tarek, D., Ragab, A., Sameh, H., Zeyad, A. M., Tayeh, B. A., Maafa, I. M., & Yousef, A. (2021). Fabrication of thermal insulation geopolymer bricks using ferrosilicon slag and alumina waste. *Case Studies in Construction Materials*, *15*. https://doi.org/10.1016/j.cscm.2021.e00737

Aliabdo, A. A., Abd Elmoaty, A. E. M., & Salem, H. A. (2016). Effect of cement addition, solution resting time and curing characteristics on fly ash based geopolymer concrete performance. *Construction and Building Materials*, *123*, 581–593. https://doi.org/10.1016/j.conbuildmat.2016.07.043

Alterary, S. S., & Marei, N. H. (2021). Fly ash properties, characterization, and applications: A review. In *Journal of King Saud University - Science* (Vol. 33, Issue 6). Elsevier B.V. https://doi.org/10.1016/j.jksus.2021.101536

Alvee, A. R., Malinda, R., Akbar, A. M., Ashar, R. D., Rahmawati, C., Alomayri, T., Raza, A., & Shaikh, F. U. A. (2022). Experimental study of the mechanical properties and microstructure of geopolymer paste containing nano-silica from agricultural waste and crystalline admixtures. *Case Studies in Construction Materials*, *16*. https://doi.org/10.1016/j.cscm.2021.e00792

Amin, M., Elsakhawy, Y., Abu el-hassan, K., & Abdelsalam, B. A. (2022). Behavior evaluation of sustainable high strength geopolymer concrete based on fly ash, metakaolin, and slag. *Case Studies in Construction Materials, 16*. https://doi.org/10.1016/j.cscm.2022.e00976

American Petroleum Institute. (2019). Cements and Materials for Well Cementing (API 10A).

American Petroleum Institute. (2013). Recommended Practice for Testing Well Cements (API 10B).

Ardelean, Ioan. (2021). The Effect of an Accelerator on Cement Paste Capillary Pores: NMR Relaxometry Investigations. Molecules. 26. 5328. 10.3390/molecules26175328.

Argos USA (2022). Mill Test Report Newberry Plant. https://www.argos-us.com/wp-content/uploads/2021/03/Argos-NBR-Type-IL-10-Mill-Test-Report-January-2022.pdf.

American Society for Testing and Materials. (2020). Standard Test Method for Comprehensive Strength of Hydraulic Cement Mortars (ASTM C109/C109M).

American Society for Testing and Materials. (2021). Standard Terminology Relating to Concrete and Concrete Aggregates (ASTM C125-21a).

American Society for Testing and Materials. (2007). Standard Specification for Portland Cement (ASTM C150-07).

American Society for Testing and Materials. (1995). Standard Test Method for Density of Hydraulic Cement (ASTM C188-95).

American Society for Testing and Materials. (2022). Standard Specification for Coal Fly Ash and Raw or Calcined Natural Pozzolan for Use in Concrete (ASTM C618-22).

American Society for Testing and Materials. (2021). Standard Test Method for Major and Minor Elements in Coal Ash By X-Ray Fluorescence (ASTM D4326-21).

Bellabarba, M., Bulte-Loyer, H., Froelich, B., Le Roy-Delage, S., Van Kuijk, R., Zeroug, S., Guillot, D., Moroni, N., Pastor, S., & Zanchi, A. (2008). Ensuring zonal isolation beyond the life of the well. *Oilfield Review*, *20*(1), 18–31.

Berg, S., Kutra, D., Kroeger, T., Straehle, C. N., Kausler, B. X., Haubold, C., Schiegg, M., Ales, J., Beier, T., Rudy, M., Eren, K., Cervantes, J. I., Xu, B., Beuttenmueller, F., Wolny, A., Zhang, C., Koethe, U., Hamprecht, F. A., & Kreshuk, A. (2019). ilastik: interactive machine learning for (bio)image analysis. *Nature Methods*, *16*(12), 1226–1232. https://doi.org/10.1038/s41592-019-0582-9

Bernal, S. A., Mejía de Gutiérrez, R., & Provis, J. L. (2012). Engineering and durability properties of concretes based on alkali-activated granulated blast furnace slag/metakaolin blends. Construction and Building Materials, 33, 99-108. doi:10.1016/j.conbuildmat.2012.01.017

Bishop, C. M., & Nasrabadi, N. M. (2006). Pattern recognition and machine learning (Vol. 4, No. 4, p. 738). New York: springer.

Brandl, A., Cutler, J., Seholm, A., Sansil, M., & Braun, G. (2011). *Cementing Solutions for Corrosive Well Environments*. http://onepetro.org/DC/article-pdf/26/02/208/2092236/spe-132228-pa.pdf/1

Bu, Y., Ma, R., Du, J., Guo, S., Liu, H., & Zhao, L. (2020). Utilization of metakaolin-based geopolymer as a mud-cake solidification agent to enhance the bonding strength of oil well cement-formation interface. *Royal Society Open Science*, *7*(2). https://doi.org/10.1098/rsos.191230

C. MacLaren, D., & Anne White, M. (2003). Cement: Its Chemistry and Properties. *Journal of Chemical Education*, *80*(6). https://doi.org/10.1021/ed080p623

Carvalheiras, J., Novais, R. M., & Labrincha, J. A. (2023). Metakaolin/red mud-derived geopolymer monoliths: Novel bulk-type sorbents for lead removal from wastewaters. *Applied Clay Science*, *232*. https://doi.org/10.1016/j.clay.2022.106770

Chan, C. L., & Zhang, M. (2022). Behaviour of strain hardening geopolymer composites at elevated temperatures. *Cement and Concrete Composites*, *132*. https://doi.org/10.1016/j.cemconcomp.2022.104634

Chen, X., Kim, E., Suraneni, P., & Struble, L. (2020). Quantitative Correlation between the Degree of Reaction and Compressive Strength of Metakaolin-Based Geopolymers. Materials, 13, 5784. doi:10.3390/ma13245784

Chindaprasirt, P., Jitsangiam, P., Chalee, W., & Rattanasak, U. (2021). Case study of the application of pervious fly ash geopolymer concrete for neutralization of acidic wastewater. *Case Studies in Construction Materials*, *15*. https://doi.org/10.1016/j.cscm.2021.e00770

Curtis, M. E., Cardott, B. J., Sondergeld, C. H., & Rai, C. S. (2012). Development of organic porosity in the Woodford Shale with increasing thermal maturity. International Journal of Coal Geology, 103, 26-31. https://doi.org/10.1016/j.coal.2012.04.004

Davidovits, J. (2008). *Geopolymer Chemistry and Applications*. Geopolymer Institute, Saint-Quentin.

Dempster, A., Laird, N., Rubin, D. (1977). *Journal of the Royal Statistical Society. Series B (Methodological), Vol. 39, No. 1*. pp. 1-38.

De Silva, P., Sagoe-Crentsil, K., & Sirivivatnanon, V. (2007). Geopolymer cements: A review of developments and opportunities. Journal of Materials Science, 42(9), 2917-2933. doi:10.1007/s10853-006-0637-z

Deng, H., Hu, X., Li, H. A., Luo, B., & Wang, W. (2016). Improved pore-structure characterization in shale formations with FESEM technique. Journal of Natural Gas Science and Engineering, 36, 168-177. https://doi.org/10.1016/j.jngse.2016.08.063

Devers, C.; Teodoriu, C.; Amani, M. (2022a). "Influence of Abundant Water on Geopolymer Curing at Elevated Temperatures", Paper ID: 267 presented at the 2022 Geothermal Rising Conference (GRC 2022), Reno, Nevada, August 28-31, 2022.

Devers, C.; Teodoriu, C.; Salehi, S.; Amani, M. (2022b) "Geopolymers, Are They Consistent Enough for Geothermal", PROCEEDINGS, 47th Workshop on Geothermal Reservoir Engineering, Stanford University, Stanford, California, February 7-9, 2022, SGP-TR 223, https://pangea.stanford.edu/ERE/db/GeoConf/papers/SGW/2022/Devers.pdf

Devers, C. (2023). Machine Learning Feature Classification of Geopolymers with Scanning Electron Microscopy. Presentation given at the April 4, 2023, American Association of Drilling Engineers National Technical Conference. www.aade.org.

Dong, T., Harris, N.B., Ayranci, K., Twemlow, C.E., & Nassichuk, B.R. (2017). The impact of composition on pore throat size and permeability in high maturity shales: Middle and Upper Devonian Horn River Group, northeastern British Columbia, Canada. Marine and Petroleum Geology, 81, 220-236. https://doi.org/10.1016/j.marpetgeo.2017.01.020

Duda, R. O., Hart, P. E., & Stork, D. G. (2000). Pattern Classification. Wiley-Interscience. https://doi.org/10.1002/9780470317442

Duxson, P., Fernández-Jiménez, A., Provis, J. L., Lukey, G. C., Palomo, A., & Van Deventer, J. S. J. (2007). Geopolymer technology: The current state of the art. *Journal of Materials Science*, *42*(9), 2917–2933. https://doi.org/10.1007/S10853-006-0637-Z

Duxson, P., Mallicoat, S. W., Lukey, G. C., Kriven, W. M., & Van Deventer, J. S. J. (2007). The effect of alkali and Si/Al ratio on the development of mechanical properties of metakaolin-based geopolymers. *Colloids and Surfaces A: Physicochemical and Engineering Aspects*, *292*(1), 8–20. https://doi.org/10.1016/j.colsurfa.2006.05.044

Fernández-Jiménez, A., Palomo, A., & Criado, M. (2005). Microstructure development of alkali-activated fly ash cement: A descriptive model. *Cement and Concrete Research*, *35*(6), 1204–1209. https://doi.org/10.1016/j.cemconres.2004.08.021

Fernández-Jimenez, A., de la Torre, A., Palomo, A., López-Olmo, G. Alonso, M., Aranda, M. (2006). Quantitative determination of phases in the alkali activation of fly ash. Part I. Potential ash reactivity. *Fuel, Volume 85, Issues 5–6.* Pages 625-634, ISSN 0016-2361, https://doi.org/10.1016/j.fuel.2005.08.014.

Fu, Y. F., Wong, Y. L., Tang, C. A., & Poon, C. S. (2004). Thermal induced stress and associated cracking in cement-based composite at elevated temperatures—Part I: Thermal cracking around single inclusion. *Cement and Concrete Composites*, *26*(2), 99–111. https://doi.org/10.1016/S0958-9465(03)00086-6

Giasuddin, H. M., Sanjayan, J. G., & Ranjith, P. G. (2013). Strength of geopolymer cured in saline water in ambient conditions. *Fuel*, *107*, 34–39. https://doi.org/10.1016/j.fuel.2013.01.035

Gomes Silveira, N. C., Figueiredo Martins, M. L., Bezerra, A. C. da S., & Gabriel da Silva Araújo, F. (2022). Ecological geopolymer produced with a ternary system of red mud, glass waste, and Portland Cement. *Cleaner Engineering and Technology*, *6*. https://doi.org/10.1016/j.clet.2021.100379

Gonçalves, N. P. F., Olhero, S. M., Labrincha, J. A., & Novais, R. M. (2023). 3D-printed red mud/metakaolin-based geopolymers as water pollutant sorbents of methylene blue. *Journal of Cleaner Production*, *383*. https://doi.org/10.1016/j.jclepro.2022.135315

Gonzales, R. C., & Woods, R. E. (2008). Digital Image Processing. Prentice Hall. https://doi.org/10.1117/1.3588021

Gu, J., & Chen, X. (2009). Research and Practice on Cement Slurry of Oil and Gas Reservoir Protection. *Petroleum Science and Technology*, *27*(16), 1845–1853. https://doi.org/10.1080/10916460802626364

Güngör, D., & Özen, S. (2021). Development and characterization of clinoptilolite-, mordenite-, and analcime-based geopolymers: A comparative study. *Case Studies in Construction Materials*, *15*. https://doi.org/10.1016/j.cscm.2021.e00576

Guo, R., Yang, W., Deng, X., Shi, S., Li, S., Qiu, J., Zhang, J., Chen, J., Hao, L., Ma, X., Ma, D., & Liu, P. (2024). Dynamic coupling between cementation and porosity evolution of the Chang 8 tight sandstone reservoir, Ordos Basin: Insights from in-situ microanalysis. Marine and Petroleum Geology, 106840. https://doi.org/10.1016/j.marpetgeo.2024.106840

Haralick, R. M., Shanmugam, K., & Dinstein, I. (1973). Textural features for image classification. IEEE Transactions on Systems, Man, and Cybernetics, SMC-3(6), 610-621. https://doi.org/10.1109/TSMC.1973.4309314

He, H., Liu, H., Guo, Y., Li, Y., Li, P., Zhang, H., Hu, T., & Ni, H. (2022). Alkali-excited gel structure and compositions evolution in geopolymers synthesized from the spent FCC catalyst and steel slag. *Journal of Materials Research and Technology*, *21*, 2663–2671. https://doi.org/10.1016/j.jmrt.2022.10.057

Heah, C. Y., Kamarudin, H., Mustafa Al Bakri, A. M., Binhussain, M., Luqman, M., Khairul Nizar, I., Ruzaidi, C. M., & Liew, Y. M. (2011). Effect of curing profile on kaolin-based geopolymers. *Physics Procedia*, *22*, 305–311. https://doi.org/10.1016/j.phpro.2011.11.048

Hui-Teng, N., Cheng-Yong, H., Yun-Ming, L., Abdullah, M. M. A. B., Ern Hun, K., Razi, H. M., & Yong-Sing, N. (2021). Formulation, mechanical properties and phase analysis of fly ash geopolymer with ladle furnace slag replacement. *Journal of Materials Research and Technology*, *12*, 1212–1226. https://doi.org/10.1016/j.jmrt.2021.03.065

International Energy Agency (2021). Statistics Report Key World Energy Statistics 2021.

Jain, A. K., Duin, R. P. W., & Mao, J. (2000). Statistical pattern recognition: A review. IEEE Transactions on Pattern Analysis and Machine Intelligence, 22(1), 4-37. https://doi.org/10.1109/34.824779

Jani, P., & Imqam, A. (2021). Class C fly ash-based alkali activated cement as a potential alternative cement for CO2 storage applications. *Journal of Petroleum Science and Engineering*, *201*. https://doi.org/10.1016/j.petrol.2021.108408

John, E., Lothenbach, B. (2023). Cement hydration mechanisms through time – a review. *Journal of Material Science 58, 9805–9833.* https://doi.org/10.1007/s10853-023-08651-9

Kabir, S. M. Alamgir, Alengaram, U. Johnson, Jumaat, Mohd Zamin, Sharmin, Afia, Islam, Azizul. (2015). Influence of Molarity and Chemical Composition on the Development of Compressive Strength in POFA Based Geopolymer Mortar. *Advances in Materials Science and Engineering*. https://doi.org/10.1155/2015/647071.

Kanagaraj, B., Anand, N., Raj R, S., & Lubloy, E. (2022). Performance evaluation of sodium silicate waste as a replacement for conventional sand in geopolymer concrete. *Journal of Cleaner Production*, *375*. https://doi.org/10.1016/j.jclepro.2022.134172

Kleinberg, R. L., Farooqui, S. A., & Horsfield, M. A. (1993). T1/T2 Ratio and Frequency Dependence of NMR Relaxation in Porous Sedimentary Rocks. *Journal of Colloid and Interface Science, 158*(1), 195–198. https://doi.org/10.1006/JCIS.1993.1247

Kovářík, T., Hájek, J., Pola, M., Rieger, D., Svoboda, M., Beneš, J., Šutta, P., Deshmukh, K., & Jandová, V. (2021). Cellular ceramic foam derived from potassium-based geopolymer composite: Thermal, mechanical and structural properties. *Materials and Design, 198*. https://doi.org/10.1016/j.matdes.2020.109355

Lee, W. K. W., & Van Deventer, J. S. J. (2002). The effects of inorganic salt contamination on the strength and durability of geopolymers. www.elsevier.com/locate/colsurfa

Li, Q., Hurt, A. P., & Coleman, N. J. (2019). The application of 29Si NMR spectroscopy to the analysis of calcium silicate-based cement using Biodentine™ as an example. *Journal of Functional Biomaterials, 10*(2). https://doi.org/10.3390/jfb10020025

Liu, M., Xie, R., Guo, J., & Jin, G. (2019). Characterization of Pore Structures of Tight Sandstone Reservoirs by Multifractal Analysis of the NMR T2 Distribution. *Energy & Fuels, 33(11), 11061-11070*. https://doi.org/10.1021/acs.energyfuels.8b02869

Loucks, R. G., Reed, R. M., Ruppel, S. C., & Jarvie, D. M. (2009). Morphology, genesis, and distribution of nanometer-scale pores in siliceous mudstones of the Mississippian Barnett Shale. Journal of Sedimentary Research, 79(12), 848-861. https://doi.org/10.2110/jsr.2009.092

MacLaren, C., D., and White, A., M. (2003). Cement: Its Chemistry and Properties. *Journal of Chemical Education, 80(6).* https://doi.org/10.1021/ed080p623

Mahima Kumar, M., Senthilvadivu, R., Brahmaji Rao, J. S., Neelamegam, M., Ashok Kumar, G. V. S., Kumar, R., & Jena, H. (2020). Characterization of fly ash by ED-XRF and INAA for the synthesis of low silica zeolites. *Journal of Radioanalytical and Nuclear Chemistry*, *325*(3), 941–947. https://doi.org/10.1007/s10967-020-07243-0

Mayhoub, O. A., Mohsen, A., Alharbi, Y. R., Abadel, A. A., Habib, A. O., & Kohail, M. (2021). Effect of curing regimes on chloride binding capacity of geopolymer. *Ain Shams Engineering Journal*, *12*(4), 3659–3668. https://doi.org/10.1016/j.asej.2021.04.032

McLachlan, G. and Peel, D. (2000) Finite Mixture Models. Wiley Series in Probability and Statistics, John Wiley & Sons, Inc. http://dx.doi.org/10.1002/0471721182

Mehta, A., & Siddique, R. (2017). Strength, permeability and micro-structural characteristics of low-calcium fly ash based geopolymers. *Construction and Building Materials*, *141*, 325–334. https://doi.org/10.1016/j.conbuildmat.2017.03.031

Mendes, B. C., Pedroti, L. G., Vieira, C. M. F., Carvalho, J. M. F., Ribeiro, J. C. L., Albuini-Oliveira, N. M., & Andrade, I. K. R. (2022). Evaluation of eco-efficient geopolymer using chamotte and waste glass-based alkaline solutions. *Case Studies in Construction Materials*, *16*. https://doi.org/10.1016/j.cscm.2021.e00847

Milliken, K. L., Rudnicki, M., Awwiller, D. N., & Zhang, T. (2013). Organic matter–hosted pore system, Marcellus Formation (Devonian), Pennsylvania. AAPG Bulletin, 97(2), 177-200. https://doi.org/10.1306/07231212011

Min, Y., Wu, J., Li, B., Zhang, M., & Zhang, J. (2022). Experimental study of freeze–thaw resistance of a one-part geopolymer paste. *Case Studies in Construction Materials*, *17*. https://doi.org/10.1016/j.cscm.2022.e01269

Mohd Ali, A. Z., Jalaluddin N. A., Zulkiflee, N. (2020). The Effect of Dry Mix Sodium Hydroxide onto Workability and Compressive Strength of Geopolymer Paste. *International Journal of Integrated Engineering Vol.12 no.9 114-120.* https://doi.org/10.30880/ijie.2020.12.09.014.

Mohsen, A., Kohail, M., Abadel, A. A., Alharbi, Y. R., Nehdi, M. L., & Ramadan, M. (2022). Correlation between porous structure analysis, mechanical efficiency and gamma-ray attenuation power for hydrothermally treated slag-glass waste-based geopolymer. *Case Studies in Construction Materials*, *17*. https://doi.org/10.1016/j.cscm.2022.e01505

Moro, D., Ulian, G., & Valdrè, G. (2021). Monte Carlo strategy for SEM-EDS micro-nanoanalysis of geopolymer composites. *Composites Part C: Open Access*, *6*. https://doi.org/10.1016/j.jcomc.2021.100183

Mudgal, M., Singh, A., Chouhan, R. K., Acharya, A., & Srivastava, A. K. (2021). Fly ash red mud geopolymer with improved mechanical strength. *Cleaner Engineering and Technology*, *4*. https://doi.org/10.1016/j.clet.2021.100215

Musa, Purnawarman, Rafi, Farid and Lamsani, Missa. (2018). A Review: Contrast-Limited Adaptive Histogram Equalization (CLAHE) methods to help the application of face recognition. 1-6. 10.1109/IAC.2018.8780492.

Nasvi, M. C. M., Ranjith, P. G., & Sanjayan, J. (2014). Effect of different mix compositions on apparent carbon dioxide (CO2) permeability of geopolymer: Suitability as well cement for CO2 sequestration wells. *Applied Energy*, *114*, 939–948. https://doi.org/10.1016/j.apenergy.2013.05.050

Nath, S. K., Maitra, S., Mukherjee, S., & Kumar, S. (2016). Microstructural and morphological evolution of fly ash based geopolymers. *Construction and Building Materials*, *111*, 758–765. https://doi.org/10.1016/j.conbuildmat.2016.02.106

Nelson, E. B. (n.d.). Well Cementing Fundamentals.

Osholana, T. S., Dludlu, M. K., Oboirien, B., & Sadiku, R. (2020). Enhanced reactivity of geopolymers produced from fluidized bed combustion bottom ash. *South African Journal of Chemical Engineering*, *34*, 72–77. https://doi.org/10.1016/j.sajce.2020.06.006

Paiva, M. D. M., Silva, E. C. C. M., Melo, D. M. A., Martinelli, A. E., & Schneider, J. F. (2018). A geopolymer cementing system for oil wells subject to steam injection. *Journal of Petroleum Science and Engineering*, *169*, 748–759. https://doi.org/10.1016/j.petrol.2018.06.022

Palomo, A., Blanco-Varela, M. T., Granizo, M. L., Puertas, F., Vazquez, T., & Grutzeck, M. W. (1999). Chemical stability of cementitious materials based on metakaolin. In *Cement and Concrete Research* (Vol. 29).

Passey, Q. R., Bohacs, K. M., Esch, W. L., Klimentidis, R., & Sinha, S. (2010). From oil-prone source rock to gas-producing shale reservoir—Geologic and petrophysical characterization of unconventional shale-gas reservoirs. SPE Reservoir Evaluation & Engineering, 13(01), 108-122. https://doi.org/10.2118/131350-PA

Patel, Y. J., & Shah, N. (2018). Enhancement of the properties of Ground Granulated Blast Furnace Slag based Self Compacting Geopolymer Concrete by incorporating Rice Husk Ash. *Construction and Building Materials*, *171*, 654–662. https://doi.org/10.1016/j.conbuildmat.2018.03.166

Pawluczuk, E., Kalinowska-Wichrowska, K., Jiménez, J. R., Fernández-Rodríguez, J. M., & Suescum-Morales, D. (2021). Geopolymer concrete with treated recycled aggregates: Macro and microstructural behavior. *Journal of Building Engineering*, *44*. https://doi.org/10.1016/j.jobe.2021.103317

Pizer, S. M., Amburn, E. P., Austin, J. D., Cromartie, R., Geselowitz, A., Greer, T., ... & Zimmerman, J. B. (1987). Adaptive histogram equalization and its variations. Computer Vision, Graphics, and Image Processing, 39(3), 355-368. https://doi.org/10.1016/S0734-189X(87)80186-X

Provis, J. L., & Van Deventer, J. S. J. (2009). Geopolymers: Structure, Processing, Properties and Industrial Applications. Woodhead Publishing.

Rahman, S. H. B. A., Irawan, S., Shafiq, N., & Rajeswary, R. (2020). Investigating the expansion characteristics of geopolymer cement samples in a water bath and compared with the expansion of ASTM Class-G cement. *Heliyon*, *6*(2). https://doi.org/10.1016/j.heliyon.2020.e03478

Rattanasak, U., & Chindaprasirt, P. (2009). Influence of NaOH solution on the synthesis of fly ash geopolymer. Materials Science and Engineering: A, 527(3), 707-712. doi:10.1016/j.msea.2009.08.074

Reddy Bellum, R. (2022). Investigation on the accelerated pavement test track (APTT) in the development of road network using geopolymer concrete. *Cleaner Materials*, *4*. https://doi.org/10.1016/j.clema.2022.100074

Reynolds, D. (2009). Gaussian Mixture Models. In: Li, S.Z., Jain, A. (eds) *Encyclopedia of Biometrics* (pp. 659–663). Springer, Boston, MA. https://doi.org/10.1007/978-0-387-73003-5_196

Rickard, W. D. A., Gluth, G. J. G., & Pistol, K. (2016). In-situ thermo-mechanical testing of fly ash geopolymer concretes made with quartz and expanded clay aggregates. *Cement and Concrete Research*, *80*, 33–43. https://doi.org/10.1016/j.cemconres.2015.11.006

Rincon, F., Abid, K., Arbad, N., & Teodoriu, C. (2022). A comprehensive analysis of class H cement Unconfined Compressive Strength using cubical and cylindrical samples. *Journal of Petroleum Science and Engineering*, *215* (Part B), 110692. https://doi.org/10.1016/j.petrol.2022.110692

Rodrigue Kaze, C., Adesina, A., Alomayri, T., Assaedi, H., Kamseu, E., Chinje Melo, U., & Leonelli, C. (2021). Characterization, reactivity and rheological behaviour of metakaolin and Meta-halloysite based geopolymer binders. *Cleaner Materials*, *2*. https://doi.org/10.1016/j.clema.2021.100025

Rodrigue Kaze, C., Adesina, A., Laure Lecomte-Nana, G., Assaedi, H., Alomayri, T., Kamseu, E., & Chinje Melo, U. (2022). Physico-mechanical and microstructural properties of geopolymer binders synthesized with metakaolin and meta-halloysite as precursors. *Cleaner Materials*, *4*. https://doi.org/10.1016/j.clema.2022.100070

Romero Tellez, M. L. (2023). Study On The Mechanical And Thermal Properties Of Class G Cement Composites. https://shareok.org/handle/11244/340042

Sajan, P., Jiang, T., Lau, C. K., Tan, G., & Ng, K. (2021). Combined effect of curing temperature, curing period and alkaline concentration on the mechanical properties of fly ash-based geopolymer. *Cleaner Materials*, *1*. https://doi.org/10.1016/j.clema.2021.100002

Saleh, F. K., Teodoriu, C., & Sondergeld, C. (2021). Review of nmr studies for oilwell cements and their importance. In *ChemEngineering* (Vol. 5, Issue 2). MDPI AG. https://doi.org/10.3390/chemengineering5020018

Salehi, S., Khattak, M. J., Ali, N., Ezeakacha, C., & Saleh, F. K. (2018). Study and Use of Geopolymer Mixtures for Oil and Gas Well Cementing Applications. *Journal of Energy Resources Technology, Transactions of the ASME*, *140*(1). https://doi.org/10.1115/1.4037713

Salehi, S., Khattak, M. J., Rizvi, H., Karbalaei, S. F., & Kiran, R. (2017a). Sensitivity analysis of fly ash geopolymer cement slurries: Implications for oil and gas wells cementing applications. *Journal of Natural Gas Science and Engineering*, *37*, 116–125. https://doi.org/10.1016/j.jngse.2016.11.025

Salehi, S., Khattak, M.J., & Bwala, A.H. (2017b). Characterization, morphology and shear bond strength analysis of geopolymers: Implications for oil and gas well cementing applications. *Journal of Natural Gas Science and Engineering*, 38, 323-332.

Sharga, B. M., Pylypiv, D. B., & Feketa, V. (2021). Medical Biology Practicals. Cytology. Practical 2. Electron microscopy. Pesticides determination View project radiation protection view project. https://www.researchgate.net/publication/349226453

Shee-Ween, O., Cheng-Yong, H., Yun-Ming, L., Abdullah, M. M. A. B., Li Ngee, H., Chan, L. W. L., Wan-En, O., Jaya, N. A., & Yong-Sing, N. (2021). Cold-pressed fly ash geopolymers: effect of formulation on mechanical and morphological characteristics. *Journal of Materials Research and Technology*, *15*, 3028–3046. https://doi.org/10.1016/j.jmrt.2021.09.084

Sheiati, S., Behboodi, S., & Ranjbar, N. (2022). Segmentation of backscattered electron images of geopolymers using convolutional autoencoder network. *Expert Systems with Applications*, *206*. https://doi.org/10.1016/j.eswa.2022.117846

Shi, C., Krivenko, P. V., & Roy, D. M. (2012). Alkali-Activated Cements and Concretes. CRC Press.

Simão, L., Fernandes, E., Hotza, D., Ribeiro, M. J., Montedo, O. R. K., & Raupp-Pereira, F. (2021). Controlling efflorescence in geopolymers: A new approach. *Case Studies in Construction Materials*, *15*. https://doi.org/10.1016/j.cscm.2021.e00740

Sonal, T., Urmil, D., & Darshan, B. (2022). Behaviour of ambient cured prestressed and non-prestressed geopolymer concrete beams. *Case Studies in Construction Materials*, *16*. https://doi.org/10.1016/j.cscm.2021.e00798

Soutsos, M., Boyle, A. P., Vinai, R., Hadjierakleous, A., & Barnett, S. J. (2016). Factors influencing the compressive strength of fly ash based geopolymers. *Construction and Building Materials*, *110*, 355–368. https://doi.org/10.1016/j.conbuildmat.2015.11.045

Stanley Igbojekwe, Saeed Salehi, & Mohammad J. Khattak. (2015). Development of a New Geopolymer Based Cement: Laboratory Investigation. *AADE*.

Stephenson LT, Szczepaniak A, Mouton I, Rusitzka KAK, Breen AJ, Tezins U, et al. (2018). The Laplace Project: An integrated suite for preparing and transferring atom probe samples under cryogenic and UHV conditions. PLoS ONE 13(12): e0209211. https://doi.org/10.1371/journal.pone.0209211

Suchorski, D. (n.d.). *The Cement Mill Test Report*. www.concrete.org/

Suraneni, P., Burris, L., Shearer, C. R., & Hooton, R. D. (2021). ASTM C618 fly ash specification: Comparison with other specifications, shortcomings, and solutions. *ACI Materials Journal*, *118*(1), 157–167. https://doi.org/10.14359/51725994

Szabó, R., Dolgos, F., Debreczeni, Á., & Mucsi, G. (2022). Characterization of mechanically activated fly ash-based lightweight geopolymer composite prepared with ultrahigh expanded perlite content. *Ceramics International*, *48*(3), 4261–4269. https://doi.org/10.1016/j.ceramint.2021.10.218

Tahwia, A. M., Heniegal, A. M., Abdellatief, M., Tayeh, B. A., & Elrahman, M. A. (2022). Properties of ultra-high performance geopolymer concrete incorporating recycled waste glass. *Case Studies in Construction Materials*, *17*. https://doi.org/10.1016/j.cscm.2022.e01393

Tan, T. H., Mo, K. H., Lai, S. H., & Ling, T. C. (2022). Investigation on the copper ion removal potential of a facile-fabricated foamed geopolymer sphere for wastewater remediation. *Cleaner Materials*, *4*. https://doi.org/10.1016/j.clema.2022.100088

Thirumakal, P., Nasvi, M. C. M., & Sinthulan, K. (2020). Comparison of mechanical behaviour of geopolymer and OPC-based well cement cured in saline water. *SN Applied Sciences*, *2*(8). https://doi.org/10.1007/s42452-020-3154-9

Tsai, Y. L., Hanna, J. V., Lee, Y. L., Smith, M. E., & Chan, J. C. C. (2010). Solid-state NMR study of geopolymer prepared by sol–gel chemistry. *Journal of Solid State Chemistry*, *183*(12), 3017–3022. https://doi.org/10.1016/J.JSSC.2010.10.008

Wan, J., Zhang, F., Han, Z., Song, L., Zhang, C., & Zhang, J. (2021). Adsorption of Cd2+ and Pb2+ by biofuel ash-based geopolymer synthesized by one-step hydrothermal method. In *Arabian Journal of Chemistry* (Vol. 14, Issue 8). Elsevier B.V. https://doi.org/10.1016/j.arabjc.2021.103234

Wei Koh, P., & Liang, P. (2017). Understanding Black-box Predictions via Influence Functions.

Xie, J., & Kayali, O. (2014). Effect of initial water content and curing moisture conditions on the development of fly ash-based geopolymers in heat and ambient temperature. *Construction and Building Materials*, *67*, 20–28. https://doi.org/10.1016/j.conbuildmat.2013.10.047

Xu, J., Li, M., Zhao, D., Zhong, G., Sun, Y., Hu, X., Sun, J., Li, X., Zhu, W., Li, M., et al., (2022). Research and Application Progress of Geopolymers in Adsorption: A Review. Nanomaterials, 12, 3002. doi:10.3390/nano12173002

Yamashita, R., Nishio, M., Do, R. K. G., & Togashi, K. (2018). Convolutional neural networks: an overview and application in radiology. In *Insights into Imaging* (Vol. 9, Issue 4, pp. 611–629). Springer Verlag. https://doi.org/10.1007/s13244-018-0639-9

Yang, W., and Zhai, X. "Contrast Limited Adaptive Histogram Equalization for an Advanced Stereo Visual SLAM System," 2019 International Conference on Cyber-Enabled Distributed Computing and Knowledge Discovery (CyberC), Guilin, China, 2019, pp. 131-134, doi: 10.1109/CyberC.2019.00030.

Zargari, S., Canter, K. L., & Prasad, M. (2015). Porosity evolution in oil-prone source rocks. Fuel, 153, 110-117. https://doi.org/10.1016/j.fuel.2015.02.072

Zhang, B., Huang, D., Li, L., Lin, M., Liu, Y., Fang, W., Lu, J., Liu, F., Li, Y., Liu, Y., & Xiong, Z. (2022). Effect of magnesium salt contamination on the microstructures and properties of metakaolinite-based geopolymer: the role of MgCl2and MgSO4. *Journal of Materials Research and Technology*, *20*, 4500–4514. https://doi.org/10.1016/j.jmrt.2022.09.019

Zhou, L., Song, Z., Chen, J., Ge, Z., Li, Z. (2014). Process-Quality Monitoring Using Semi-supervised Probability Latent Variable Regression Models. IFAC Proceedings Volumes, Volume 47, Issue 3. Pages 8272-8277. ISSN 1474-6670. ISBN 9783902823625. https://doi.org/10.3182/20140824-6-ZA-1003.01226.

Zou, C., Dong, D., Wang, S., Li, J., Li, X., Huang, J., ... & Lin, W. (2010). Shale gas in China: Characteristics, challenges and prospects (I). Petroleum Exploration and Development, 37(6), 664-672. https://doi.org/10.1016/S1876-3804(11)60001-7

Appendix A – T Test Results

Figure	Age	Comparison	t-Ratio	Prob>|t|
Figure 19	1	API Mixing Conditions	-1.019	0.366
Figure 19	3	API Mixing Conditions	-0.91	0.415
Figure 19	7	API Mixing Conditions	-1.55	0.166
Figure 19	14	API Mixing Conditions	-8.04	0.002
Figure 19	21	API Mixing Conditions	NA	NA
Figure 19	28	API Mixing Conditions	-2.49	0.067
Figure 20	7	Age 3 days	0.85	0.398
Figure 20	14	Age 3 days	3.25	0.0023
Figure 20	21	Age 3 days	2.5	0.0154
Figure 20	31	Age 3 days	0.874	0.288

Figure	Age	Comparison	t-Ratio	Prob>|t|
Figure 20	14	Age 7 days	3.01	0.0045
Figure 20	21	Age 7 days	2.14	0.037
Figure 20	31	Age 7 days	0.347	0.730
Figure 20	21	Age 14 days	0.205	0.838
Figure 20	31	Age 14 days	-2.37	0.0283
Figure 20	31	Age 21 days	-1.11	0.278
Figure 36	1	Curing Temperature	0.984	0.336
Figure 35	1	Curing Environment	-0.274	0.7863
Figure 37	1	Recipe	7.34	0.0001
Figure 36	3	Curing Temperature	3.39	0.0022
Figure 35	3	Curing Environment	-1.42	0.1671

Figure	Age	Comparison	t-Ratio	Prob>|t|
Figure 37	3	Recipe	8.45	0.0001
Figure 36	7	Curing Temperature	2.501	0.0203
Figure 35	7	Curing Environment	-0.671	0.509
Figure 37	7	Recipe	2.9	0.008
Figure 36	14	Curing Temperature	1.28	0.0816
Figure 35	14	Curing Environment	0.711	0.495
Figure 37	14	Recipe	7.491	0.0001

Appendix B – SEM Analysis Code

```
import os
import numpy as np
import matplotlib.pyplot as plt
from matplotlib.backends.backend_pdf import PdfPages
from PIL import Image
from sklearn.mixture import GaussianMixture
from skimage.measure import regionprops, label
from skimage import img_as_ubyte
import pickle

def load_and_preprocess_image(image_path):
    try:
        image = Image.open(image_path).convert('L')
        image_array = np.array(image)
        print(f"Loaded and preprocessed image: {image_path}")
        return image_array
    except Exception as e:
        print(f"Error loading image {image_path}: {e}")
        return None

def apply_gmm(image_array, n_components=5):
    reshaped_image = image_array.reshape(-1, 1)
    gmm = GaussianMixture(n_components=n_components,
random_state=0).fit(reshaped_image)
    segmented_image = gmm.predict(reshaped_image)
    segmented_image = segmented_image.reshape(image_array.shape)
    return segmented_image

def calculate_segment_properties(segmented_image):
    labeled_image = label(segmented_image)
    properties = regionprops(labeled_image, intensity_image=segmented_image)

    if not properties:
        print("No segments found.")

    min_area_threshold = 10  # Example threshold, adjust as needed
    properties = [prop for prop in properties if prop.area >= min_area_threshold]

    segment_areas = [prop.area for prop in properties]
    centroids = [prop.centroid for prop in properties]
    perimeters = [prop.perimeter for prop in properties]
    compactness = [
        4 * np.pi * prop.area / (prop.perimeter ** 2) if prop.perimeter != 0 else 0
        for prop in properties
```

```
    ]
    mean_intensities = [prop.mean_intensity for prop in properties]
    intensity_std_devs = [prop.intensity_image.std() for prop in properties]

    return {
        "areas": segment_areas,
        "centroids": centroids,
        "perimeters": perimeters,
        "compactness": compactness,
        "mean_intensities": mean_intensities,
        "intensity_std_devs": intensity_std_devs
    }

def process_images(input_folder):
    all_properties = {
        "areas": [],
        "centroids": [],
        "perimeters": [],
        "compactness": [],
        "mean_intensities": [],
        "intensity_std_devs": []
    }

    for filename in os.listdir(input_folder):
        if filename.endswith('.tif'):
            print(f"Starting processing: {filename}")
            image_path = os.path.join(input_folder, filename)
            image_array = load_and_preprocess_image(image_path)
            if image_array is None:
                continue
            segmented_image = apply_gmm(image_array)
            props = calculate_segment_properties(segmented_image)

            for key in all_properties.keys():
                all_properties[key].extend(props[key])

            print(f"Completed processing: {filename}")

    return all_properties

def save_properties(properties, file_path):
    with open(file_path, 'wb') as file:
        pickle.dump(properties, file)
    print(f"Properties saved to {file_path}")

def load_properties(file_path):
```

```
    with open(file_path, 'rb') as file:
        properties = pickle.load(file)
    print(f"Properties loaded from {file_path}")
    return properties

def analyze_results(properties, report_path):
    with PdfPages(report_path) as pdf:
        # Analyze Segment Areas
        plt.figure()
        plt.hist(properties["areas"], bins=30, alpha=0.75)
        plt.title('Distribution of Segment Areas')
        plt.xlabel('Area')
        plt.ylabel('Frequency')
        pdf.savefig()
        plt.close()

        # Analyze Centroid Distributions
        centroids = np.array(properties["centroids"])
        if centroids.size > 0:
            plt.figure()
            plt.scatter(centroids[:, 1], centroids[:, 0], alpha=0.5)
            plt.title('Centroid Distribution')
            plt.xlabel('X Coordinate')
            plt.ylabel('Y Coordinate')
            pdf.savefig()
            plt.close()

        # Calculate and plot nearest neighbor distances in chunks to avoid memory errors
        if centroids.size > 0:
            chunk_size = 1000  # Adjust the chunk size based on available memory
            num_chunks = (len(centroids) + chunk_size - 1) // chunk_size
            plt.figure()
            for i in range(num_chunks):
                for j in range(i, num_chunks):
                    chunk1 = centroids[i*chunk_size:(i+1)*chunk_size]
                    chunk2 = centroids[j*chunk_size:(j+1)*chunk_size]
                    if len(chunk1) > 0 and len(chunk2) > 0:
                        chunk_distances = distance.cdist(chunk1, chunk2, 'euclidean').flatten()
                        plt.hist(chunk_distances, bins=30, alpha=0.5, color='blue')
            plt.title('Distribution of Nearest Neighbor Distances')
            plt.xlabel('Distance')
            plt.ylabel('Frequency')
            pdf.savefig()
            plt.close()

        # Analyze Segment Perimeters
```

```
        plt.figure()
        plt.hist(properties["perimeters"], bins=30, alpha=0.75)
        plt.title('Distribution of Segment Perimeters')
        plt.xlabel('Perimeter')
        plt.ylabel('Frequency')
        pdf.savefig()
        plt.close()

        # Analyze Segment Compactness
        plt.figure()
        plt.hist(properties["compactness"], bins=30, alpha=0.75)
        plt.title('Distribution of Segment Compactness')
        plt.xlabel('Compactness')
        plt.ylabel('Frequency')
        pdf.savefig()
        plt.close()

        # Analyze Mean Intensities
        plt.figure()
        plt.hist(properties["mean_intensities"], bins=30, alpha=0.75)
        plt.title('Distribution of Mean Intensities')
        plt.xlabel('Mean Intensity')
        plt.ylabel('Frequency')
        pdf.savefig()
        plt.close()

        # Analyze Intensity Standard Deviations
        plt.figure()
        plt.hist(properties["intensity_std_devs"], bins=30, alpha=0.75)
        plt.title('Distribution of Intensity Standard Deviations')
        plt.xlabel('Intensity Standard Deviation')
        plt.ylabel('Frequency')
        pdf.savefig()
        plt.close()

if __name__ == "__main__":
    input_folder = r"C:\Users\cdevers\Downloads\SEM Project_Prelim PhD Project\CLAHE
Corrected Images v2"
    report_path = r"C:\Users\cdevers\Downloads\SEM Project_Prelim PhD
Project\combined_analysis_report.pdf"

    # Process images and calculate properties
    properties = process_images(input_folder)

    # Analyze results and generate PDF report
    analyze_results(properties, report_path)
```